Design of Cell Adhesive and Angiogenic Titanium Surfaces for Cellular Stimulation

“Dissertation zur Erlangung des Grades eines ‚Doktor rerum naturalium (Dr. rer. nat.)‘ der Fachbereiche:

- 08 Physik, Mathematik und Informatik
- 09 Chemie, Pharmazie und Geowissenschaften
- 010 Biologie
- 04 Universitätsmedizin

der
Johannes Gutenberg-Universität“

vorgelegt von
Dipl. Biol. Martin Heller
geboren am 13.09.81 in Wiesbaden

Datum der mündlichen Prüfung: 10.04.13

Max Planck Graduate Center
mit der Johannes Gutenberg-Universität

Max-Planck-Institut
für Polymerforschung

JG|U UNIVERSITÄTSmedizin.
MAINZ

Die vorliegende Arbeit wurde von Februar 2010 bis Februar 2013 im Rahmen des „Max Planck Graduate Center“ zusammen mit der Johannes Gutenberg-Universität Mainz angefertigt. Die beteiligten Institute waren das Max-Planck-Institut für Polymerforschung, die Hals-, Nasen-, Ohrenklinik und die Klinik für Mund-, Kiefer- und Gesichtschirurgie der Universitätsmedizin in Mainz.

Zusammenfassung

Die Förderung der Zelladhäsion durch sogenannte biomimetische Oberflächen wird in der Medizin als vielversprechender Ansatz gesehen, um Komplikationen wie z. B. Fremdkörperreaktionen nach der Implantation entgegenzuwirken. Neben der Immobilisierung einzelner Biomoleküle wie z. B. dem RGD-Peptid, Proteinen und Wachstumsfaktoren auf verschiedenen Materialien, konzentriert man sich derzeit in der Forschung auf die Co-Immobilisierung zweier Moleküle gleichzeitig. Hierbei werden die funktionellen Gruppen z. B. von Kollagen unter Verwendung von nur einer Kopplungschemie verwendet, wodurch die Kopplungseffizienz der einzelnen Komponenten nur begrenzt kontrollierbar ist. Das Ziel der vorliegenden Arbeit war die Entwicklung eines Immobilisierungsverfahrens, welches die unabhängige Kopplung zweier Faktoren kontrolliert ermöglicht. Dabei sollten exemplarisch das adhäsionsfördernde RGD-Peptid (Arginin-Glycin-Asparaginsäure) zusammen mit dem Wachstumsfaktor VEGF (*Vascular Endothelial Growth Factor*) auf Titan gebunden werden. In weiteren Experimenten sollten dann die pro-adhäsiven Faktoren Fibronektin, Kollagen, Laminin und Osteopontin immobilisiert und untersucht werden.

Die Aminofunktionalisierung von Titan durch plasma polymerisierte Allylaminschichten wurde als Grundlage für die Entwicklung des nasschemischen Co-immobilisierungsverfahren verwendet. Für eine unabhängige und getrennte Anbindung der verschiedenen Biomoleküle stand in diesem Zusammenhang die Entwicklung eines geeigneten Crosslinker Systems im Vordergrund. Die Oberflächencharakterisierung der entwickelten Oberflächen erfolgte mittels Infrarot Spektroskopie, *Surface Plasmon Resonance* Spektroskopie (SPR), Kontaktwinkelmessungen, *Step Profiling* und *X-Ray Photoelectron* Spektroskopie (XPS). Zur Analyse der Anbindungsprozesse in Echtzeit wurden SPR-Kinetik Messungen durchgeführt. Die biologische Funktionalität der modifizierten Oberflächen wurde *in vitro* an Endothelzellen (HUVECs) und Osteoblasten (HOBs) und *in vivo* in einem Tiermodell-System an der *Tibia* von Kaninchen untersucht.

Die Ergebnisse zeigen, dass alle genannten Biomoleküle sowohl einzeln auf Titan kovalent gekoppelt als auch am Bespiel von RGD und VEGF in einem getrennten Zwei-Schritt-Verfahren co-immobilisiert werden können. Des Weiteren

wurde die biologische Funktionalität der gebundenen Faktoren nachgewiesen. Im Falle der RGD modifizierten Oberflächen wurde nach 7 Tagen eine geförderte Zelladhäsion von HUVECs mit einer signifikant erhöhten Zellbesiedlungsdichte von 28,5 % ($p<0,05$) gezeigt, wohingegen auf reinem Titan Werte von nur 13 % beobachtet wurden. Sowohl VEGF als auch RGD/VEGF modifizierte Proben wiesen im Vergleich zu Titan schon nach 24 Stunden eine geförderte Zelladhäsion und eine signifikant erhöhte Zellbesiedlungsdichte auf. Bei einer Besiedlung von 7,4 % auf Titan, zeigten VEGF modifizierte Proben mit 32,3 % ($p<0,001$) eine deutlichere Wirkung auf HUVECs als RGD/VEGF modifizierte Proben mit 13,2 % ($p<0,01$). Die pro-adhäsiven Faktoren zeigten eine deutliche Stimulation der Zelladhäsion von HUVECs und HOBs im Vergleich zu reinem Titan. Die deutlich höchsten Besiedlungsdichten von HUVECs konnten auf Fibronektin mit 44,6 % ($p<0,001$) und Kollagen mit 39,9 % ($p<0,001$) nach 24 Stunden beobachtet werden. Laminin zeigte keine und Osteopontin nur eine sehr geringe Wirkung auf HUVECs. Bei Osteoblasten konnten signifikant erhöhte Besiedlungsdichten im Falle aller pro-adhäsiven Faktoren beobachtet werden, jedoch wurden die höchsten Werte nach 7 Tagen auf Kollagen mit 90,6 % ($p<0,001$) und Laminin mit 86,5 % ($p<0,001$) im Vergleich zu Titan mit 32,3 % beobachtet. Die Auswertung der Tierexperimente ergab, dass die VEGF modifizierten Osteosyntheseplatten, im Vergleich zu den reinen Titankontrollen, eine gesteigerte Knochenneubildung auslösten. Eine solche Wirkung konnte für RGD/VEGF modifizierte Implantate nicht beobachtet werden.

Insgesamt konnte gezeigt werden, dass mittels plasmapolymerisierten Allylamin Schichten die genannten Biomoleküle sowohl einzeln gebunden als auch getrennt und kontrolliert co-immobilisiert werden können. Des Weiteren konnte eine biologische Funktionalität für alle Faktoren nach erfolgter Kopplung *in vitro* gezeigt werden. Wider Erwarten konnte jedoch kein zusätzlicher biologischer Effekt durch die Co-immobilisierung von RGD und VEGF im Vergleich zu den einzeln immobilisierten Faktoren gezeigt werden. Um zu einer klinischen Anwendung zu gelangen, ist es nun notwendig, das entwickelte Verfahren in Bezug auf die immobilisierten Mengen der verschiedenen Faktoren hin zu optimieren.

Abstract

In medicine the enhancement of cell adhesion is regarded as promising approach of research to counteract complications after implantation such as foreign body reactions. Parallel to the single immobilization of biomolecules such as the RGD-peptide, proteins or growth factors onto various materials, current research is focused on the co-immobilization of two different molecules. For example, functional groups of collagen are used for the co-immobilization which, however, utilizes only one type of coupling chemistry. In this case, the coupling efficiency of the single components provides only limited control. The aim of this work was the design of an immobilization procedure for the independent and controllable conjugation of two factors. For this purpose, the adhesion enhancing RGD-peptide (arginine-glycine-aspartate) and the vascular endothelial growth factor (VEGF) were to be conjugated exemplarily onto titanium. Furthermore, pro-adhesive factors such as fibronectin, collagen, laminin and osteopontin were to be investigated after immobilization.

The amino-functionalization of titanium via plasma polymerized allylamine was used as base for the wet chemical co-immobilization procedure. In this context, the development of a suitable cross-linker system for an independent and separated biomolecule conjugation was prioritized. For the surface characterization infrared spectroscopy, surface plasmon resonance spectroscopy (SPR), contact angle measurements, step profiling and x-ray photoelectron spectroscopy (XPS) were utilized. Real-time analysis of the conjugation processes were performed via SPR kinetic measurements. The biological functionality of the modified surfaces was investigated *in vitro* with endothelial cells (HUVECs) and osteoblasts (HOBs) and *in vivo* in an animal model system at the *tibia* of rabbits.

The results reveal that all mentioned biomolecules could be conjugated independently onto titanium and co-immobilized in a separated two-step procedure, as shown by the example of RGD and VEGF. Furthermore, the biological functionality of the conjugated factors could be proven. In the case of RGD modified surfaces, an enhanced cell adhesion and a significantly increased cell coverage ($p<0,05$) of HUVECs was observed after 7 days with 28,5 % compared to titanium with 13 %. VEGF as well as RGD/VEGF modified samples

exhibited a promoted cell adhesion and significantly increased values for the cell coverage already after 24 hours. In comparison to pure titanium with a cell coverage of 7,4 %, a more distinct effect on HUVECs was observed for VEGF modified surfaces with 32,3 % ($p<0,001$) compared to RGD/VEGF modified samples with 13,2 % ($p<0,01$). The pro-adhesive factors led to a distinct stimulation of cell adhesion of HUVECs and HOBs in comparison to pure titanium. By far the highest cell coverage of HUVECs was observed on fibronectin modified surfaces with 44,6 % ($p<0,001$) and on collagen with 39,9 % ($p<0,001$) after 24 hours. For laminin no effect was observed, and for osteopontin only a slight enhancement of cell adhesion on HUVECs was found. In the case of osteoblasts, significantly increased cell coverage on all samples with pro-adhesive factors was observed, but the highest values were observed on collagen with 90,6 % ($p< 0,001$) and laminin with 86,5 % ($p<0,001$) compared to titanium with 32,3 % after 7 days. The analysis of the animal experiments revealed that VEGF modified osteosynthesis plates triggered new bone formation, compared to the non-modified titanium controls. Such effects were not observed in the case of RGD/VEGF modified implants.

Altogether, it was found that plasma polymerized allylamine is suitable for the conjugation of the mentioned biomolecules as well as for a separated and controlled co-immobilization. Furthermore, the biological functionality of all used factors could be demonstrated *in vitro* after immobilization. Against expectation, no additional biological effect as result of the RGD and VEGF co-immobilization could be demonstrated. In order to transfer the developed surfaces to clinical applications, it will be necessary to optimize the developed procedures concerning the amounts of the immobilized factors.

Table of Contents

Figures

Tables

Table of Abbreviations

a.u.	arbitrary unit
°C	degrees celsius
CRGD	cysteine-arginin-glycin-aspartate
DMSO	dimethyl sulfoxide
∆θ	delta theta
ECM	extra cellular matrix
EtOH	ethanol
FITC	fluoresceine isothiocyanate
h	hour
HOBs	human osteoblasts
HUVECs	human umbilical vein endothelial cells
M	molarity of a solution (mol/l)
µg	microgram
min	minute
µl	microliter
ng	nanograms
nm	nanometer
OD	optical density
PBS	phospate buffered saline
pp-AA	plasma polymerized allylamine
rpm	rounds per minute
RT	room temperature
Sccm	standard cubic centimeter per minute
SD	standard deviation
sulfo-SDTB	sulfo-succinimidyl-4-*O*-(4,4´-dimethoxytrityl) butyrate
UV	ultraviolet
UV/VIS	ultraviolet/visible light
VEGF	vascular endothelial growth factor

1 Introduction

1.1 Titanium as Implant Material: Historical Overview

Titanium was first found in Cornwall, by William Gregor 1798 (Barksdale, 1966). It is the ninth most abundant element in the lithosphere, has a low density and is a strong, lustrous and corrosion resistant transition metal (Van Noort, 1987).

As reviewed by Van Noort in 1987, titanium was introduced in the medical field in 1940 by Bothe and coworkers (Bothe et al., 1940). In the 1950s and 1960s first animal experiments with titanium as implant material were performed, indicating that there are no adverse reactions to titanium (Leventhal, 1951, Beder et al., 1956). According to a publication of Albrektsson and coworkers in 1983, animal experiments in the 1960s and the beginning of the 1970s revealed that titanium implants integrate successfully in the bone with a direct bone-to-implant contact (Brånmark et al., 1969). This observation was termed “osseointegration” and an extensive clinical study in 1977 of Brånmark and coworkers with more than 200 patients with dental implants demonstrated that osseointegration also takes place in the human body (Brånmark et al., 1977). It was concluded that osseointegration using minimally traumatizing surgical techniques without load bearing for 3-5 months will provide a lasting anchorage of titanium implants in the bone (Albrektsson et al., 1983). As described in an article by Albrektsson in 1981, titanium was examined extensively end of the 1970s in many different clinical studies covering a variety of applications. Studies with hip or knee joint prostheses (Judet et al., 1978, Ring, 1978, Ritter et al., 1979) or in the upper extremities (Salzer et al., 1979) were carried out.

Until the 1980s, permanent bone implantation frequently involved the use of bone cement (Albreksson et al., 1981). As reviewed by Albrektsson and coworkers in 1987, there were several problems reported from cement usage (Albrektsson et al., 1987, Pedersen et al., 1983, DeHaven et al., 1986) as well as from cement free implants, and different surgical techniques were discussed to minimize surgical trauma in order to provide long-term stability of an implant in the bone.

Nowadays, titanium is state of the art as an implant material in medical disciplines such as the maxillofacial surgery or traumatology. Considering the function of the replaced part of the body, the choice of the operation technique is important to

enable long-term anchorage in the bone. In the case of hip or knee implants, for example, the artificial joints are placed in the bone using bone cement, whereas in the case of dental implants cement free implants are used to generate a direct contact of the implant to healthy bone tissue. In traumatology, bone fractures are fixed and stabilized using osteosynthesis plates and titanium screws.

1.1.1 Favorable Properties of Titanium for Medical Applications

As reported by Puleo and coworkers in 1999, each year, in the USA alone, there are 300000 hip and knee implants and up to 300000 dental implant surgeries. The reason why titanium is one of the most used implant materials in the world is due to its mechanical, physical and chemical properties (Lausmaa et al., 1990).The most important mechanical property in the context of medical application is that it has the highest strength-to-weight ratio of any metal (Donachie, 1988). The mechanical stability and stiffness of titanium is much higher than in bone, and as such, it can carry much larger stresses. This is the reason why difficulties of mechanical implant failure are to be expected in the bone or at the bond between bone and implant (Albrektsson et al., 1983).

The chemical property that arguably plays the most important role for the biological inertness and biocompatibility of titanium is its high corrosion resistance (Lausmaa et al., 1990). This is due to the stable oxide layer that is formed instantly during the implant manufacturing steps and is reported to grow up to 100 Å within one minute (Kaseamo, 1983). Several oxides such as TiO, TiO_2, Ti_2O_3 and Ti_3O_4 have been reported (Albrektsson et al., 1983), and it was found that the oxide layer consists out of an amorphous TiO_2 outer layer and an intermediate TiO_x layer, in contact with the titanium substrate and the outer layer (Pouilleau et al., 1997). Because of this oxide layer, the metal, metal compounds or ions of titanium are not exposed to or able to diffuse into surrounding biological tissues. Therefore, it can be regarded as a ceramic and not as metal (Albrektsson et al., 1981). Another favorable property of the oxide layer regarding to biological systems is the high dielectric constant which is near to that of water. Potentially, this may be the reason why it exhibits more “natural” interactions with biomolecules compared to other oxides e. g. aluminum oxides (Albrektsson et al., 1983).

Furthermore, because titanium is non-ferromagnetic, patients carrying long-term titanium implants can be safely examined with magnetic resonance imaging techniques (Devge et al., 1997).

1.1.2 Titanium and Its Alloys

Up until the middle of the last century (1900´s), materials commonly used for bone implantation were stainless steel and chromium cobalt. These materials were gradually replaced through titanium that gained widespread interest in the 70s and 80s (Van Noort, 1987).

Titanium and its alloys are currently used as implant material in its pure form so called commercially pure titanium (c. p. Ti.), and depending on the application as alloy with other metals in biomedical devices and components, especially as hard tissue replacement (Liu et al., 2004). The reason why titanium is used in an alloyed form is that the tensile and fatigue strength is increased compared to the pure form. This is indicated for example in high stress bearing situations such as artificial knee joints or hip prostheses (Van Noort, 1987).

Pure Titanium and Ti-6Al-4V i. e. titanium with 6% aluminum and 4% vanadium are still the most used ones for biomedical applications among the titanium alloys (Niinomi, 2003). However, it was found that aluminum and vanadium could dissolve from this alloy (Kodama, 1989). Since aluminum is a growth inhibitor for bone and might be a possible cause for alzheimer´s disease, and vanadium has strong cytotoxicity, this alloy has been partly replaced (Matsuno et al., 2001). According to Matsuno and coworkers in 2001, various other titanium alloys have been developed such as alloys with 6% aluminum and 7% niobium (Semlitsch et al., 1992, 1985). Due to their non-toxic properties niobium, tantalum and zirconium are currently used as suitable alloying elements for titanium in medical implants (Niinomi, 2003). Alloys with 5% zirconium and 5% tantalum were investigated due to their wear resistance (Faria et al., 2011). In applications involving dental implants, titanium is usually used in its pure form to prevent side effects of diffusing compounds, but current works could show that especially the titanium zirconium alloy provides improved mechanical properties for applications in more challenging clinical situations (Al-Nawas et al., 2011).

1.1.3 Osseointegration of Titanium Implants

The general understanding of molecular and cellular events that take place during osseointegration of an implant may be found in publications about bone and fracture healing. As reported in an article by Albrektsson in 2001, the reason for this understanding were observations that cellular processes during bone healing after bone fracture were similar to the events that take place after implantation. According to this, it is described that after bone fracture and/or after implantation, osteogenesis is induced and called osteoinduction. This means that immature, undifferentiated and pluripotent mesenchymal cells are recruited to develop into a bone forming cell lineage as reaction on growth factors e.g. the Bone Morphogenetic Protein (BMP) (Albrektson et al., 2001, Wilson-Hench, 1987, Urist, 1952, Levander, 1938, Huggins, 1931).

However, there are also differences between the bone-healing situation after a fracture compared to processes after implantation. For the healing situation around an implant, the physiological reaction on the foreign material itself has to be considered. To describe the molecular processes that take place after implantation at the implant - tissue interface, the new term osteoconduction was introduced and means the bone growth on a surface of a foreign material (Albrektsson et al., 2001). Factors that play an important role during osteoconduction include various growth factors such as the insulin-like growth factor (IGF), fibroblast growth factor (FGF), transforming growth factor-beta (TGF-ß) and platelet-derived growth factor (PDGF) (Albrektsson et al., 2001). These growth factors act as signaling agents for cells (Trippel, 1996) and are important for the cellular events that take place during bone formation on the implant surface.

Osteoinduction and osteoconduction lead to osseointegration, whereby the term osseointegration implies not only to the implant integration in the bone, but also the bone anchorage maintained over time (Albrektsson et al., 2001).

The events that take place at the interface between implant and tissue were described by Puleo and coworkers in 1999 (figure 1.1). Based on several publications, he gives a detailed describtion of the molecular events that occur after implantation. The first events proceed within seconds after implantation and are adsorption and desorption of proteins from blood and tissue fluids as shown

in figure 1.1 A and B (Andrade, 1985, Horbett et al., 1987). Surface changes such as oxide layer formation and material release (fig. 1.1 C) in the form of particles or ions occur (Sundgren et al., 1986, Lausmaa et al., 1988). A reaction on the foreign body occurs next and is a result of the healing process, whereby inflammatory and connective tissue cells approach the implant (fig. 1.1 D) and start to release matrix proteins such as bone sialoprotein (BSP) and osteopontin (OPN) as shown in figure 1.1 E. They then adsorb to the implant surface, leading to the formation of a non-collagenous protein layer called *lamina limitans* containing BSP, OPN, a2 HS glycoprotein and albumin. On this layer, osteogenic cells adhere (fig. 1.1 F) and start to release bone matrix proteins and the bone starts to deposit on both the exposed bone and implant surface (fig. 1.1 G). The final steps are remodeling processes of the newly formed bone.

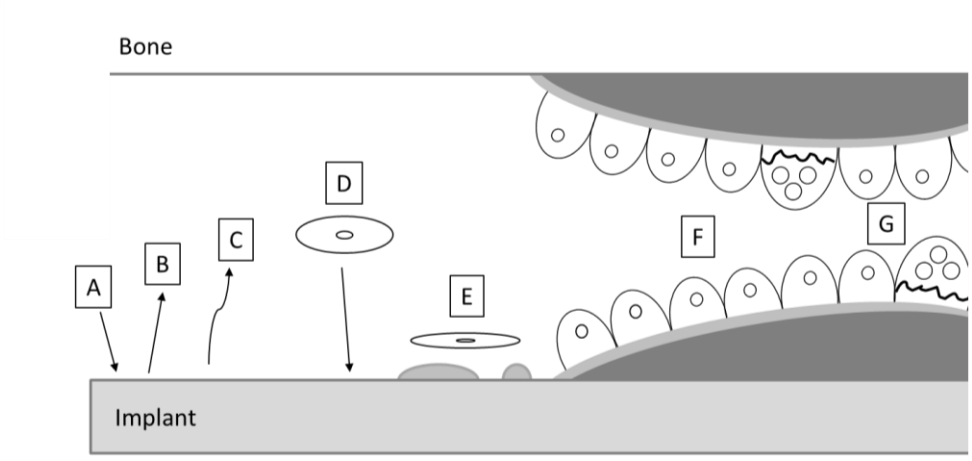

Figure 1.1 Schematic of the molecular and cellular interactions at the implant-tissue interface. A) protein adsorption, B) protein desorption, C) material release, D) inflammatory and tissue cells approach and adhere, E) release of matrix proteins, F) osteogenic cell adhesion and matrix production, G) bone formation on the surface (According to Puleo et al., 1999).

1.2 Medical Impact of Implant Modifications

Titanium is regarded as biocompatible and bioinert. But there are many problems that still occur after implantation. In so called foreign body reactions, a special form of the immune response of the human body on foreign materials, isolation of the material from the surrounding tissue occurs, in order to protect the body from harmful effects as result of material erosions (Ratner et al., 2004). These processes may lead to inflammatory reactions that can further result in fibrous

capsule formation and a loss of functionality of the implant. As a consequence the implant requires removal or replacement (Zdolsek et al., 2007). The successful integration of an implant depends on various factors and there is not only the material that has to be considered if one talks about osseointegration of implants. There are many difficult clinical situations that can negatively influence the success and survival of implants. In the case of dental implants, this negative prognosis is seen in patients with osteoporosis, a poor quality and quantity of bone, autoimmune diseases like Crohn´s disease, diabetes mellitus, alcohol and nicotine abuse or cancer can impair the implant success (Schiegnitz et al., 2012). Furthermore, treatments with bisphosphonates in cases of osteoporosis and bone influencing tumor diseases or anti-angiogenetic and immune-suppressive therapies are considered as possible risk factors for the survival and success rates for dental implants (Kämmerer et al., 2012).
Because of the fact that implant surface characteristics have a direct influence on the functional integration into the surrounding tissue (Kämmerer et al., 2011), promising approaches to counteract the described problems are modifications of the implant surfaces. There are different scientific approaches to modify a surface such as physicochemical, morphological and biochemical modifications (Puleo et al., 1999).

Physicochemical modification: According to Puleo and coworkers in 1999 many different studies have been conducted to alter the physicochemical surface features such as surface energy, surface charges, and surface composition with the aim to improve the bone implant interface. In regard of the surface composition, one of the most extensively investigated modifications are calcium phosphate coatings (Schirkhanzadeh, 1995). Because of their osteoconductive properties, calcium phosphate coatings on titanium implants are for example widely used in the orthopedic surgery (Habibovic et al., 2004).

Morphological modification: In order to influence bone and tissue response in a positive manner, the effect of alterations of surface morphology and roughness on the cellular response was extensively studied (Ziebart et al., 2012, Mustafa et al., 2008, Martin et al., 2004). There are different commercially produced titanium implants such as sand-blasted and acid etched implants on the market with a

defined structure and roughness (Li et al., 2002).The assumption that porous surfaces with higher roughness could increase the stability and fixation of implants in the bone could only be partly proven.

Biochemical modification: This type of modification is a promising alternative to the mentioned ones and uses the knowledge and understanding of biological processes and mechanisms involved in physiological reactions and cellular behavior. So called biomimetic modifications act via immobilized biomolecules in order to mimic a natural environment for cells. Examples of the types of molecules used for this kind of modifications are proteins of the extra cellular matrix (ECM) (Yoshida, 2012), adhesion motifs such as the RGD-peptide (Kämmerer et al., 2011, Ferris et al., 1999) or growth factors such as PDGF (Huh et al., 2011). A tremendous number of publications are available, showing that biochemical or biomimetic surfaces can influence cellular behavior such as cell adhesion, proliferation and differentiation in a positive manner.

1.3 Cellular Response on Biomimetic Surfaces

1.3.1 Integrin-Mediated Cell Adhesion

There are many clinical situations in which complications may occur after implantation. Particularly, foreign body reactions can influence the success of implant integration negatively as described in 1.2. In earlier works it was found that biomimetic surfaces can influence cellular behavior at the implant-tissue interface in a favorable way. In this context, the enhancement of cell adhesion is considered as promising approach to improve the biocompatibility of materials.
Cell adhesion influences cellular behavior e. g. cell shape, polarity, organization of the cyto skeleton, migration, proliferation and differentiation, survival and apoptosis (Takada et al., 2007). In the context of biomimetic surfaces, the transmembrane cell surface receptors, so called integrins, are responsible for cell interactions to immobilized peptide sequences or ECM proteins such as fibronectin, collagen, osteopontin etc. (Duewelhenke et al., 2007). Interestingly, the ligand specificity of these heterodimeric cell surface receptors correlates with the combination of α and β subunits contained in each integrin molecule (Hynes,

2002). In addition to the crucial role as adhesion mediators, the integrins are involved in various signal transduction reactions. With the outside-in signaling cells are able to recognize changes in their environment and can transfer this information over the integrins into the cell. At the same time cells are able to generate intracellular signals that are transferred to the environment (inside-out signaling) (Hynes, 2002). These complex interactions involve different proteins that act as adaptor molecules and connect the cytoplasmatic domains of the integrins with the intracellular actin filaments to form a so-called focal adhesion complex as shown in figure 1.2. The proteins that are involved in these interactions are Talin, Vinculin und ERM (Ezrin, Radixin, Moesin) (Takada et al., 2007). The biological mechanisms of integrin mediated cell adhesion show the potential of biomimetic surfaces to improve the biocompatibility.

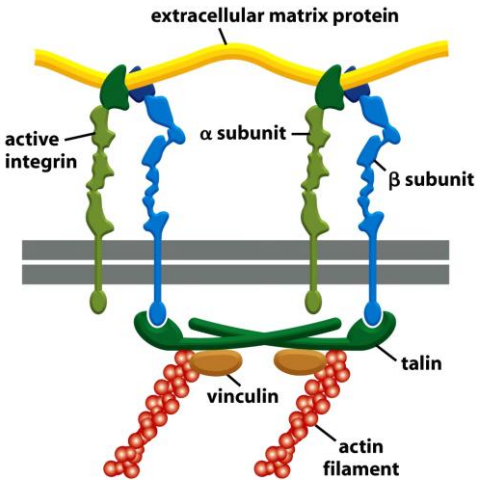

Figure 1.2 Schematic of heterodimer integrin receptors interacting with proteins of the ECM. Associated intracellular proteins such as vinculin, talin and actin filaments interact with the intracellular portions of the integrin molecules (Alberts, 2008).

1.3.2 Growth Factor Interactions: Overview

Growth factors are present in all tissues (Lind, 1996) in the body and influence critical functions such as cell division, matrix synthesis and tissue differentiation (Lieberman et al., 2002). There are three types of actions in which growth factors act: (1) autocrine - growth factors influence cells of its origin or with identical phenotype, (2) paracrine - growth factors influence e. g. neighboring cells with different phenotypes, (3) endocrine - growth factors influence cells with different

phenotype at a remote anatomical site (Liebermann et al., 2002). The high diversity found in growth factors is limited at the receptor level where they seem to share structural motifs and employ a restricted number of signal transduction systems (Waterfield, 1989). Especially the receptors for growth factors involved in the bone repair are based on an enzymatic kinase activity of receptor tyrosine kinase or receptor protein serine/threonine kinase (Liebermann et al., 2002). In the case of receptor tyrosine kinase the enzymatic activity initiates the autophosphorylation of intracellular receptor domains at the tyrosine residues, whereby the receptor protein serine/threonine kinase phosphorylates regulator proteins at the amino acids serine or threonine (Alberts, 2008). In both cases the phosphorylation and activation of acceptor domains or proteins initiates intracellular phosphorylation cascades of regulator proteins in order to stimulate cellular reactions (Campbell, 2003). Many proteins have been identified that interact with the receptor molecules and are involved in the intracellular signaling pathways such as MAP-Kinase (mitogen-activated-protein), signal transducers and activators of transcription (STATs) and protein tyrosine phosphatases (PTPs) (Hackel et al., 1999).

1.4 Immobilization of Biomolecules for the Design of Biomimetic Surfaces

Biomolecules can be immobilized on surfaces over non-covalent or covalent bonds (figure 1.3). Non-covalent or adsorptive immobilizations are based on intermolecular interactions such as electrostatic forces and hydrophobic interactions as the potentially strongest interactions, but also hydrogen bonds or Van der Waals forces between the solid phase and the biomolecules (Aslam et al., 1998). Despite the simplicity of this approach there are two major disadvantages of passive adsorptive immobilization. On the one hand, conformational changes and denaturation may lead to the loss of biological functionality (Butler et al., 1992, Berkowitz et al., 1981). On the other hand, depending on the strength of the physisorption, the adsorbed biomolecules might desorb again (Horbett, 1987). To counteract this disadvantages one promising approach is the covalent immobilization.

The covalent coupling methods that are mentioned in this section are partly based on “old” publications but they are still state of the art for certain applications in the context of biomolecule coupling to surfaces. Covalent chemical coupling techniques always require accessible functional groups on the surface or at the perimeter of the immobilized biomolecules. Functional groups that can be used for covalent immobilization are amines ($-NH_2$), carboxyl groups (-COOH), thiol groups (-SH) or hydroxyl groups (-OH) (Aslam et al., 1998). Biomolecules can be bound to a surface via linker molecules, so called cross-linkers. Well known methods for covalent protein coupling are e.g. amine reactive biotin reagents (Bayer et al., 1990), carboxyl reacting carbodiimides in combination with *N*-hydroxysuccinimide (EDC/NHS) (Philpott et al., 1980) or protein and tissue fixatives such as glutaraldehyde (Habeeb et al., 1968) or formaldehyde (Means et al., 1968). Other examples are polyethylene glycol linker molecules (PEG-linkers) with various functions such as epoxides (Bergström et al., 1992) or succinimides (Chiu et al., 1993). This functional groups react with primary amines in peptides, proteins or primary amines on surfaces. Furthermore, functions that can be introduced in polyethylene glycol chains are malemides (Goodson et al., 1990) that undergo reactions with thiol groups to name but a few.

Biomolecules such as peptides or proteins have, as a rule, accessible primary amines or carboxyl groups and sometimes also thiol groups, depending on the presence of the amino acid cysteine. These functions can be used as target sites for the covalent immobilization.

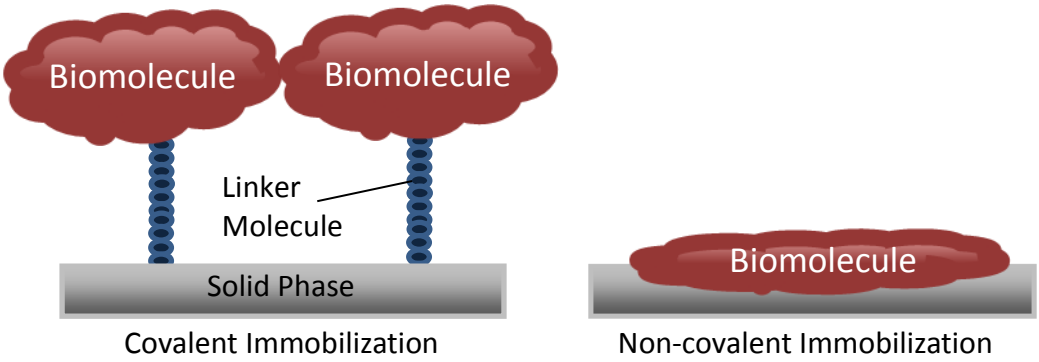

Figure 1.3 Covalent and non-covalent immobilization of biomolecules on a solid phase.

1.4.1 Immobilized Peptides and Proteins Enhance Cell Adhesion

As already mentioned, the immobilization of biomolecules is one strategy to create biomimetic surfaces in order to mimic a natural environment.

Pierschbacher and coworkers revealed in 1984 that the cell adhesion enhancing effect of the ECM protein fibronectin could be replaced by a small peptide sequence of the amino acids arginine-glycine-aspartate (RGD) (Pierschbacher et al., 1984). It was found that RGD is the recognition site for integrins (Ruoslahti et al., 1987). Different coupling techniques were used to immobilize RGD on different substrates. RGD was immobilized for example onto bovine serum albumin (BSA) coated surfaces by thiol linkers and onto poly (methyl methacrylate) via acrylamide linkers (Kantlehner et al., 2000). In 1999, Ferris and coworkers immobilized RGD on gold coated titanium surfaces using a non-covalent immersion technique (Ferris et al., 1999). In order to immobilize RGD covalently onto titanium, Kämmerer and coworkers (2011) functionalized titanium via (3-aminopropyl) trietoxysilane before binding RGD using a diepoxy-linker (Kämmerer et al., 2011). These and many other studies demonstrated a cell stimulating effect of RGD after immobilization *in vitro* and other works could show that RGD modified surfaces have also an positive influence on osseointegration *in vivo* (Schliephake et al., 2005).

In addition to RGD, many different active peptide motives within different proteins could be identified in the past decades to promote integrin mediated cell adhesion such as (-YIGSR-) und (-IKVAV-) in laminin (Vukicevich et al., 1990), (-REDRV-)

und (-LDV-) in fibronectin, (-DGEA-) in collagen (Aota et al., 1991) to name but a few.

Furthermore, in order to enhance cell adhesion, various ECM proteins containing the RGD sequence have been immobilized to design biomimetic surfaces. It was demonstrated that the immobilization of ECM proteins such as fibronectin (Yoshida et al., 2012, Harvey et al., 2012), collagen (Wang et al., 2008, Xu et al., 2010), and osteopontin (Martin et al., 2003) is a powerful method to enhance cell adhesion.

1.4.2 Immobilized Growth Factors for Specific Cell Stimulation

In order to regulate various higher functionalities of cells including growth, differentiation, apoptosis, transformation, the immobilization of growth factors might be a powerful approach for the development of biologically active materials (Ito, 2007). As mentioned in section 1.1.3, various growth factors are crucial during healing processes and bone regeneration after injury. Because of their manifold activities growth factors are believed to be attractive agents for stimulating bone and tissue repair (Lieberman et al., 2002, Greenhalgh, 1996). In the context of surface modification, different growth factors have been used to investigate their effects on the cellular response after immobilization on various materials. Investigated growth factors were EGF (Kuhl et al., 1996), TGF-ß (Bentz et al., 1998), FGF (Wissink et al., 2000) and PDGF (Huh et al., 2011). These works demonstrated different ways of covalent and non-covalent immobilization techniques and showed that cellular behavior can be stimulated regarding to cell growth, proliferation and migration. Due to the important role of blood vessel formation during new bone formation (Kämmerer et al., 2011, Ziebart et al., 2008, Albrektsson et al., 1981), especially angiogenic growth factors became the focus of research in the last years. Almost all growth factors are described to have an impact in angiogenesis (Ahrendt et al., 1998) but only some of them are described to be vascular specific. Although FGF is crucial for neovascularization (Lind, 1996), there is only VEGF that has been proven to be specific and critical for blood vessel formation (Yancopoulos et al., 2000).

As described in an article by Chiu and coworkers in 2011, VEGF has already been immobilized onto different substrates using various coupling methods. In

2006, Koch and coworkers immobilized VEGF in collagen matrices using homobifunctional polyethylene glycol spacer with *N*-hydroxysuccinimide functions (Koch et al., 2006). Furthermore, it could be demonstrated that VEGF can be immobilized using photoreactive gelatin (Ito et al., 2005). Another approach of covalent immobilization was demonstrated by Shen and coworkers in 2008. Here, VEGF was coupled to collagen scaffolds based on carbodiimide chemistry (Shen et al., 2008). In 2006, Backer and coworkers added a cysteine-tag in VEGF and created conjugates with fibronectin before well plates were coated (Backer et al., 2006). In this studies immobilized VEGF showed angiogenic effects on the cellular response such as promotion of cell growth, infiltration, survival, proliferation and surface coverage *in vitro* and blood vessel growth *in vivo* (Koch et al., 2006).

In order to add additional functionalities, several studies demonstrated the co-immobilization of VEGF together with various biological active molecules. As demostrated in a study of Taguchi and coworkers in 2000, VEGF was co-immobilized with fibronectin and collagen onto poly(acrylic acid) using carbodiimide chemistry (Taguchi et al., 2000). A similar approach concerning the coupling chemistry was presented by Chiu and coworkers in 2010. In this work, VEGF and angiopoietin-1 were immobilized in collagen scaffolds (Chiu et al., 2010). As already seen for the VEGF modified surfaces, also the surfaces with additional co-immobilized biomolecules stimulated cells regarding to cell growth and proliferation.

1.5 Functionalization of Implant Materials Using Plasma Polymerization

In general, plasma is regarded as the 4th state of matter (Grad, 1969) and is by far the most common state of matter throughout the known universe (d´Angelo, 1990). It takes place in stars and for us as best known example in the sun (Yasuda, 1985).

Commonly used wet chemical methods for covalent immobilization are limited to functional groups available on the substrate and the biomolecule as described in section 1.4. A promising approach to overcome these limitations on the material side is the method of plasma polymerization or plasma enhanced chemical vapor

deposition PE(CVD). This technique can be used to functionalize materials with creating a big variety of functional groups on surfaces that can further be used for biomolecule immobilization independent of the substrate.

In artificially induced plasma during the plasma polymerization electrons are separated from atoms and molecules by applying and external oscillating magnetic field. This separation leads to excited and highly reactive species such as radicals, ions, neutrals, electrons and photons (Beck et al., 2001). By collision of excited electrons of higher energy levels with neutrals, electrically excited neutrals are created. These excited species decay and emit light at characteristic wavelength (Donnelly et al., 2002).

The reactive species within the plasma undergo chemical reactions to form molecules with higher molecular weight (Yasuda, 1977) that are deposited on the surface. As reviewed by Förch (2007), the introduction of low-power processes coupled with the introduction of a duty cycle (DC) made a deposition of thin polymer-like films with high monomer retention and a high degree of functionality possible. In contrast to the continuous wave mode (CW) in which the power is applied continuously, the duty cycle means the modulation of the frequency in which the plasma is turned on or off in the range of micro- to milliseconds. The duty cycle was introduced in order to retain the chemical functionality and is defined such as: $DC = t_{on}/(t_{on} + t_{off})$. According to this, it was found that alcohols (Rinsch et al., 1996), carboxylic acids (Candan et al., 1998), acid chlorides (Calderon et al., 1998), anhydrides (Schiller et al., 2002), ethylene glycols (Wu et al., 2000) and amines (Choukourov et al., 2005) can be successfully deposited with a high retention of functionality and various degrees of cross-link density and stability (Förch et al., 2007). Plasma polymerization processes can take place in the gas phase or on the surface of a substrate after adsorption of monomer molecules (figure 1.4) (Friedrich et al., 2011). Due to the fact that substrate surfaces are exposed to plasma, they will also be excited to form reactive species that are able to react with molecules within the plasma.

Chemical reactions that can occur during the plasma polymerization process are (Friedrich et al., 2011):

- Radical chain growth starting from plasma produced radicals
- Ionic chain growth reactions (cationic or anionic)
- Ion molecule reactions
- Monomer fragmentation and poly-recombination
- Monomer conversation to polymer-forming intermediates
- Co-monomer fragmentation and recombination
- Radical chain growth co-polymerization
- Chemical grafting on radical sites or functional groups of plasma polymers or plasma exposed polymer surfaces

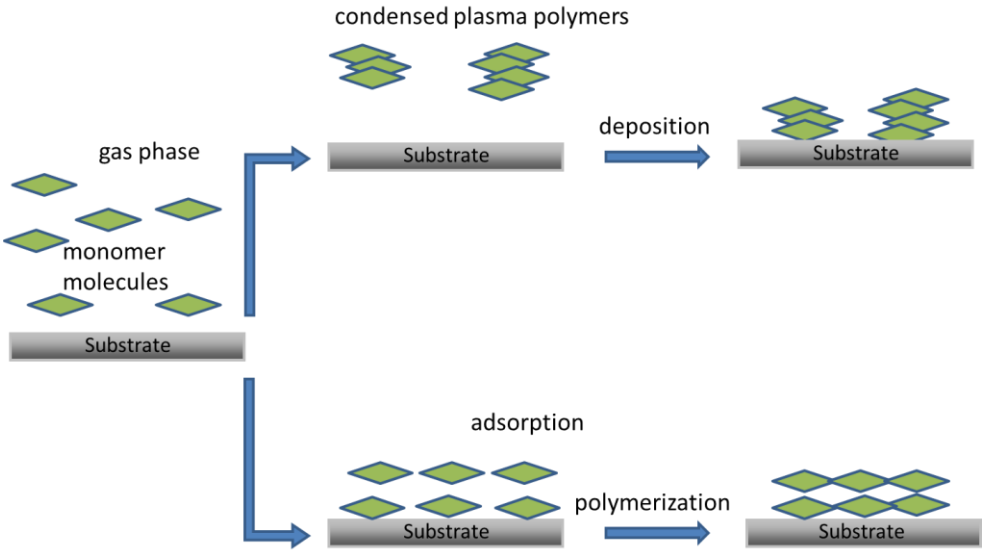

Figure 1.4 Location of the plasma polymerization process in the gas phase or within an adsorbed layer (According to Friedrich et al., 2011).

One promising approach to link biomolecules to a surface is the coupling to primary amines as described in 1.4. Therefore, the plasma polymerization of allylamine was demonstrated to be a powerful and suitable method to functionalize surfaces and to create primary amines on different substrates (Hsieh et al., 1997, Hamerli et al., 2003). The composition of plasma polymerized allylamine films (pp-AA) and the mechanisms of the plasma process have been extensively studied. Besides newly created compounds like nitriles, amides and imides within the polymer-like pp-AA network, an increased retention of primary

amine functions can be achieved by modulating the process power (Krishnamurthy et al., 1989). It has been discussed whether these pp-AA films might be affected by certain solvents or in aqueous solutions. Although a loss of material and changes in the chemical structure of pp-AA in aqueous solution could be observed, it was demonstrated that with increasing plasma process power the stability of pp-AA increased, due to a higher cross-link density of the polymer network (Zhang et al., 2003). In the context of biomolecule immobilization the attractive features of pp-AA films were shown in interesting works and various biomolecules such as DNA (Zhang et al., 2005, Chen et al., 2004), proteins and peptides (Lotz et al., 2012) have been successfully immobilized.

2 Aim of This Work

Although it was shown in earlier works that VEGF could be covalently co-immobilized with additional biomolecules, all developed co-immobilization procedures were conducted in a single non-separated step. In the context of co-immobilization, a single coupling procedure provides little or no control over the conjugation of two different biomolecules and may lead to unfavorable results such as inhomogenous distribution on the surface.

The aim of this work was the functional and independent co-immobilization of RGD and VEGF onto titanium, based on plasma polymerized allylamine. Furthermore, the biological effect of additional pro-adhesive factors such as fibronectin, collagen, laminin and osteopontin were to be investigated after immobilization onto titanium.

Due to the utilization of the material titanium, there were two main challenges to overcome. The first challenge was the stable amino-functionalization of titanium via plasma polymerized allylamine as described in section 1.5. The second challenge was a consequence of the assumption that various biomolecules underlie different reaction kinetics, due to different sizes and/or accessible functional groups. Because of this, the second aim was the development of a two-step co-immobilization procedure, in which the two molecules could be immobilized separately and in a controllable way. Finally, the developed biomimetic surfaces were to be investigated in biological systems *in vitro* and *in vivo*. The *in vitro* studies were conducted, investigating the behavior of endothelial cells and osteoblasts and the *in vivo* studies were performed using a rabbit animal model.

3 Materials and Methods

3.1 Materials

3.1.1 Laboratory Equipment and Consumables

Accu-jet® pro	Brand, Wertheim
Centrifuge Multifuge 1L-R	Thermo Fisher Scientific, Dreieich
Centrifuge 5417R	Eppendorf, Hamburg
15 ml Centrifuge Tubes	Greiner Bio-One, Frickenhausen
50 ml Centrifuge Tubes	Greiner Bio-One, Frickenhausen
Counting Chamber Neubauer	Roth, Karlsruhe
Cryo Tube	Nunc, Langenselbold
Culture Flask	Thermo Fisher Scientific, Dreieich
Edwards FL 400 Evaporator	Edwards, Crawley, England
Edwards Auto 500 System (Sputtering System)	Edwards, Crawley, England
Fluorescence Microscope Nikon Eclipse TE 2000-U	Nikon GmbH, Düsseldorf
Fluoroskan Ascent FL	Labsystems, Quickborn Nidderau
Glass Slides	Menzel, Braunschweig
Incubator BB16	Heraeus Instruments, Hamburg
Krüss DSA 10-MK2 Goniometer	A. Krüss Optronic GmbH, Hamburg
Laminar Flow Bench Hera Safe	Heraeus Instruments, Hamburg
LaSFN9 Glass	Hellma, Mühlheim

Micro Balance ABT 120-5DM	Kern, Ballingen-Frommern
Micro Balance R180D	Sartorius AG, Göttingen
Microscope Nikon TMS-F	Nikon GmbH, Düsseldorf
SU 8000 Scanning Electron Microscope	Hitachi High-Technologies Europe GmbH, Krefeld
Mr. Frosty Vassel	Thermo Fisher Scientific, Dreieich
MS1 Minishaker	IKA® Labortechnik, Staufen Nidderau
Multiskan Ascent	Labsystems, Quickborn
Nicolet 850 IR (IRRAS)	Thermo Fisher Scientific, Nidderau
Nicolet FT-IR 730 (ATR)	Thermo Fisher Scientific, Nidderau
Osteosynthesis plates	Stryker GmbH & Co. KG, Duisburg
Overhead Shaker REAX2	Heidolph, Schwabach
P-16+ Profilometer	KLA Tencor, Milpitas, USA
PH Meter CG 840	Schott, Mainz
Plasma Reactor	custom-made (Lotz et al., 2012)
Pipettes (5 ml, 10 ml, 25 ml)	Eppendorf, Hamburg
0,5 ml Reaction Tubes	Eppendorf, Hamburg
1,5 ml Reaction Tubes	Eppendorf, Hamburg
Shaker Polymax 1040	Heidolph, Schwabach
Silicon Wafer	Silicon Materials, Kaufering
Spectralphotometer Ultrospec® 3100 Pro	Amersham Pharmacia Biotech, Wien, Austria
Surface Plasmon Resonance Setup	custom-made (Knoll, 1998)
Titanium Screws	Medicon eG, Tuttlingen
99,7 % Pure Titanium	Alfa Aesar, Karlruhe
24 Well-Plate	Greiner Bio-One, Frickenhausen
96 Well-Plate	Nunc GmbH, Langenselbold

Specs Sage X-Ray Photoelectron Spectrometer	Specs GmbH, Berlin

3.1.2 Chemicals

Acetone	Roth, Karlsruhe
Allylamine ≥95%	Sigma-Aldrich Chemie GmbH, Taufkirchen
Allyl mercaptane	Ward Hill, USA
α, ω-bis-*N*-hydroxysuccinimide polyethylene glycol (2000 Dalton)	Rapp Polymere GmbH, Tübingen
Collagenase	Roche Diagnostics Deutschland GmbH, Mannheim
Collagen (human placenta)	Sigma-Aldrich Chemie GmbH, Taufkirchen
CRGD	Panatecs, Tübingen
Dimethyl sulfoxide	Roth, Karlsruhe
Ethanol	Applichem, Darmstadt
Fluorescein isothiocyanate (FITC)	Sigma-Aldrich Chemie GmbH, Taufkirchen
Fibronectin (human plasma)	Sigma-Aldrich Chemie GmbH, Taufkirchen
Formalin 4%	Sigma-Aldrich Chemie GmbH, Taufkirchen
Hellmanex	Hellma GmbH u. Co, KG Müllheim
Hydrogen peroxide	Merck, Darmstadt
Laminin	Santa Cruz Biotechnology, Heidelberg
Osteopontin	AbD Serotec, Düsseldorf
α-maleinimidohexanoic-ω-*N*-hydroxysuccinimide polyethylene glycol (5000 Dalton)	Rapp Polymere GmbH, Tübingen

Sodium hydrogencarbonate	Roth, Karlsruhe
Sodium orthovanadate	Sigma-Aldrich Chemie GmbH, Taufkirchen
Sulfosuccinimidyl-4-*O*-(4, 4´-dimethoxytrityl)-butyrate (sulfo-SDTB)	Thermo Fisher Scientific, Dreiech
99,8 % Sulfuric acid	Roth, Karlsruhe
Trypan blue 0,4 %	Sigma-Aldrich Chemie GmbH, Taufkirchen
Toluidine blue	Sigma-Aldrich Chemie GmbH, Taufkirchen
Vascular Endothelial Growth Factor 165	ImmunoTools, Friesoythe

3.1.3 Buffer and Solutions

Accutase	Ready to use mixture of PAA Laboratories GmbH, (Pasching, Austria), no information about the mixture
Calcein Stock Solution	1 mg/ml calcein in DMSO
Carbonate Buffer	50 mM sodium hydrogencarbonate, pH 8
Chromium Etching Solution No. 1	MicroChemicals GmbH, Ulm
Cryo-Solution	90% (v/v) FCS, 10 % (v/v) DMSO
Etching Solution	9% (w/v) amoniumhydrogendifluoride, 8,5% (v/v) conc. sufuric acid, 0,5% (w/v) hexamethylentetramine

FITC-Solution	0,5 mg fluoresceine isothiocyanate, 100µl DMSO, 1 ml carbonate buffer, pH 8
PBS (Dulbecco)	8 g/l NaCl, 0,2mg/l KCl, 1,15 g/l Na_2HPO_4, 0,2 g/l KH_2PO_4, pH 7,4
Piranha-Solution	50 % (v/v) conc. sulfuric acid 50 % (v/v) hydrogen peroxide
Sulfo-SDTB Solution	3,03 mg sulfo-SDTB, 1 ml DMSO, 50 ml 50mM carbonate buffer, pH 8
Trypsine/EDTA	Ready to use mixture of PAA Laboratories GmbH, (Pasching, Austria). 0,5 g/l trypsine (from pork) 0,2 g/l sodium-EDTA 0,85 g/l NaCl

3.1.4 Reagents and Kits

Duo Set® Human VEGF	R&D Systems, Wiesbaden
Duo Set® IC Human Phospho-VEGF R2/KDR	R&D Systems, Wiesbaden
Substrate Reagent Pack	R&D Systems, Wiesbaden
Reagent Diluent Concentrate 2	R&D Systems, Wiesbaden

3.1.5 Cell Culture

3.1.5.1 Used Cell Types

Endothelial cells: Primary culture from human umbilical vein endothelia cells (HUVECs)

Osteoblasts: Human osteoblasts (HOBs) were purchased by Promocell, Heidelberg.

3.1.5.2 Cell Media

Endothelial cell medium: For the HUVECs Endopan 3 from Pan Biotech was used with the delivered supplements: ascorbic acid, gentamicin sulfate, amphotericin B, EGF, hydrocortisone, heparin, FGF 2, R3-IGF-1, VEGF, BSA.

Osteoblast medium: osteoblasts were cultivated in DMEM (*Dulbecco´s modified Eagle Medium*) from Gibco supplemented with 10% (v/v) fetal calf serum, 1% (v/v) L-Glutamine, 1% (v/v) penicillin/streptomycin, 150 mg ascorbic acid and 20 µg dexamethasone.

3.2 Methods

3.2.1 Titanium Preparation

The titanium disks used in the experiments had a thickness of 2 mm and a purity of 99,7%. Prior cell experiments in 24 well plates, they were cut in appropriate 1 cm² plates. Because of irregularities and contaminations of the titanium surface from manufacturing steps, titanium disks were serial sanded with sand paper of 1200 and 2000 graining. For a reproducible model system and in order to eliminate scratches of the sanding procedure, titanium plates were etched for 3 minutes in etching solution at room temperature. Afterwards the plates were oxidized for 1 hour in acidic piranha solution.

3.2.2 Plasma Polymerization of Allylamine

The plasma polymerization of allylamine was conducted in a custom-made plasma reactor (Lotz et al., 2012). The basic setup is shown in figure 3.1 and consists of a 30 cm long, cylindrical Pyrex glass tube with a diameter of about 10 cm. The alternating current with radio frequency (13,56 MHz) was applied over an electrode coiled around the glass tube. The vacuum inside the chamber was generated with a Leybold D16 BCS vacuum pump and controlled using a manometer. In order to protect the vacuum pump from effluent monomer contamination, a cold trap, cooled with liquid nitrogen, was used. Before plasma polymerization the reactor was cleaned for 30 minutes using cleaning plasma, consisting of argon and oxygen with flow rates of 3 sccm and 10 sccm, respectively. The flows of argon and nitrogen were controlled over a mass flow controller. For the cleaning plasma a process power of 150 W was used. The manometer and the flow controller were from MKS Instruments Deutschland GmbH, München.

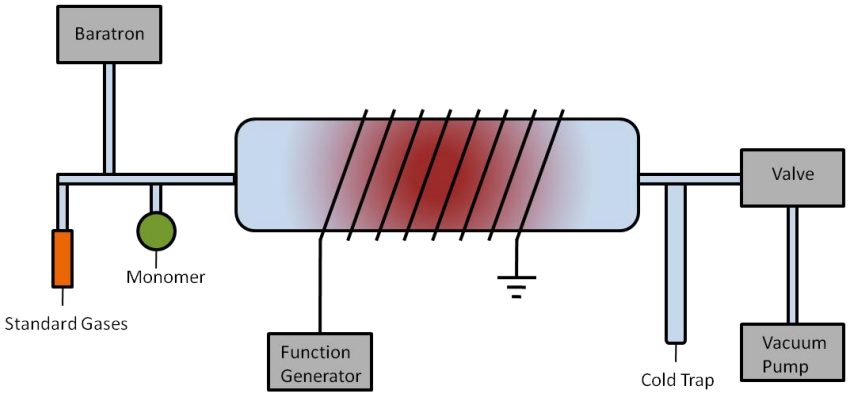

Figure 3.1 Schematic of a plasma reactor setup used in this work.

Before allylamine was used for plasma polymerization, it was degassed at least 3 times using liquid nitrogen in order to remove dissolved gas contaminations. For the plasma polymerization of allylamine (figure 3.2), the base pressure inside the reactor was 0,001 mbar. Afterwards the flow of allylamine was adjusted via a needle valve at 0,1 mbar. Plasma was ignited and controlled with a function generator. The impedance was controlled using a custom-made matching box. For the development of the immobilization procedures it was necessary to investigate the influence of different plasma polymerization parameters such as process power on the stability and functionality of pp-AA films. Furthermore, due to different requirements of the used surface characterization methods, different layer thicknesses were deposited. The layer thicknesses of the pp-AA films was controlled over the deposition time, and analyzed with a step profiler as described in 3.2.5. Due to various used substrates and changing requirements for the different characterization methods, the plasma polymerization parameters of the pp-AA films used in the different experiments will be described in the referring sections of this chapter.

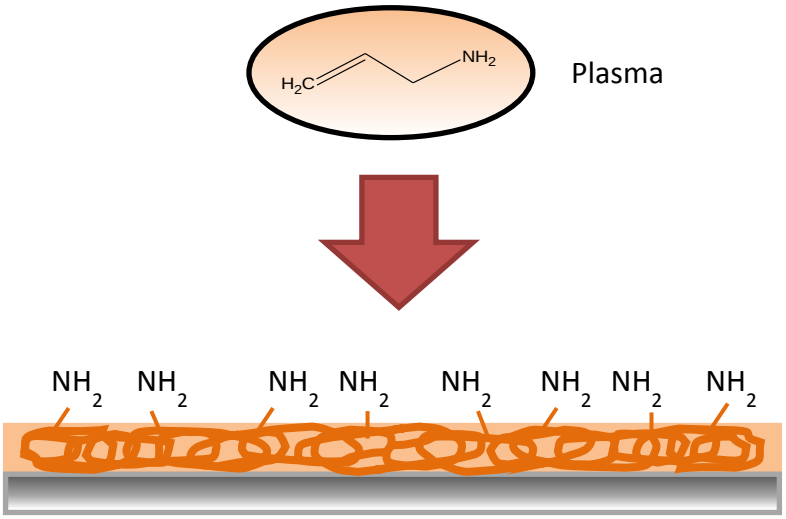

Figure 3.2 Schematic of the plasma polymerization of allylamine to create primary amines on a surface. Radicals, ions, neutrals, electrons and photons undergo complex reactions and form polymer-like network structures that are deposited on the surface.

3.2.3 Immobilization/Co-immobilization of RGD and VEGF

For all developed immobilization and co-immobilization procedures onto titanium samples, a 100 W pp-AA film deposited with 0,1 mbar monomer pressure and a deposition time of 5 minutes was used. As discussed in 5.2, especially these pp-AA films have been proven to be the most stable and suitable ones for the wet chemical modification steps. Furthermore, RGD and VEGF were first immobilized separately onto titanium, before they were co-immobilized. To investigate the immobilization/co-immobilization in real time, SPR kinetic measurements were conducted as described in 3.2.12.

3.2.3.1 Immobilization of the RGD-peptide

For the development of the co-immobilization procedure, an extra amino acid cysteine was added to the RGD peptide, in order to obtain a thiol group. This addition was necessary for the establishment of a coupling chemistry for the RGD immobilization different from that of the VEGF immobilization. The cross-linker used for the RGD immobilization was the heterobifunctional α-maleinimido-hexanoic-ω-*N*-hydroxysuccinimide polyethylene glycol (Mal-NHS-linker) with 5000 Dalton as shown in figure 3.3. Before immobilization procedures, titanium samples with 100 W pp-AA films were incubated in PBS in 24 well plates for 1

hour. This step was found to be necessary in order to obtain stable plasma polymer films. Afterwards, titanium was incubated with 400 µl of a 5 % (w/v) Mal-NHS-linker in PBS for 15 minutes. Samples were then carefully washed with PBS and incubated with 500 µg/ml cysteine-RGD in PBS for 1 hour. A 30 µl droplet of cysteine-RGD-Solution was pipetted onto the bottom of 24 well plates and the samples were carefully placed with the upside on top of the droplet and thus the entire surface was wetted with the solution. After a final washing step the modified titanium samples were carefully dried with an air stream and stored in a closed vessel until use. All steps were performed at room temperature. The RGD immobilization schematic is shown in figure 3.5 A.

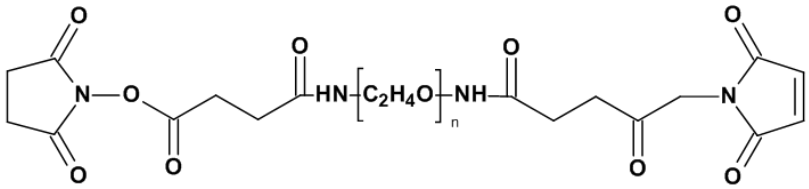

Figure 3.3 α-maleinimidohexanoic-ω-*N*-hydroxysuccinimide polyethylene glycol cross-linker for the immobilization of RGD.

3.2.3.2 Immobilization of VEGF

100 W pp-AA films were first incubated in PBS for 1 hour. VEGF was immobilized using the homobifunctional cross-linker α, ω-bis-*N*-hydroxysuccinimide polyethylene glycol (Di-NHS-linker) with 2000 Dalton as shown in figure 3.4. In brief, pp-AA modified titanium samples were incubated in 24 well plates with 400 µl of 5% (w/v) α, ω-bis-*N*-hydroxysuccinimide polyethylene glycol in PBS for 15 minutes. After a washing step, a 30 µl droplet of VEGF solution in PBS was dropped onto the bottom of a well and the titanium samples were placed on top of the droplet. For the VEGF immobilization different concentrations of 1 µg/ml, 10 µg/ml and 20 µg/ml VEGF in PBS were used. After a final washing step, samples were carefully dried using an air stream. The immobilization of VEGF is shown in figure 3.5 B.

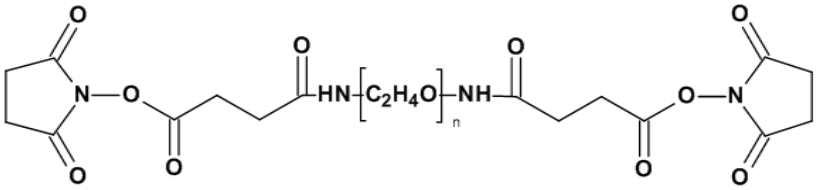

Figure 3.4 α, ω-bis-*N*-hydroxysuccinimide polyethylene glycol cross-linker for the immobilization of VEGF.

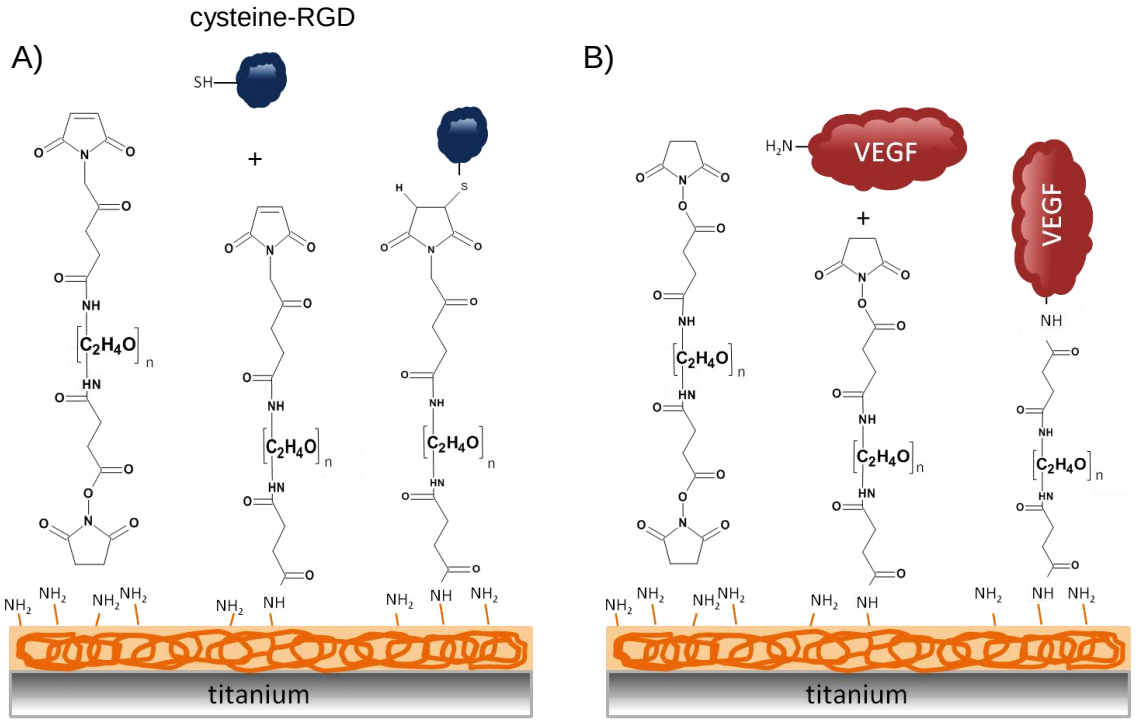

Figure 3.5 Schematic of the developed immobilization procedures of A) RGD using α, ω-bis-*N*-hydroxysuccinimide polyethylene glycol and B) VEGF using α-maleinimidohexanoic-ω-*N*-hydroxysuccinimide polyethylene glycol.

3.2.3.3 Co-immobilization of RGD and VEGF

For the development of a two-step co-immobilization procedure, cross-linker molecules with different functionalities were used as described in section 3.2.3.1 and 3.2.3.2. Furthermore, to counteract steric hindrances during the immobilization steps, due to different sizes of RGD and VEGF, different linker lengths were employed. Details concerning the choice of the linker-molecule lengths are discussed in section 5.3.4.

For the co-immobilization of RGD and VEGF, 100 W pp-AA films were incubated in PBS for 1 hour. Then pp-AA coated titanium samples were incubated with both

cross-linkers in 24 well plates for 15 minutes. In brief, a mixture of 400 µl of α-maleinimidohexanoic-ω-*N*-hydroxysuccinimide polyethylene glycol (5000 Dalton) and α, ω-bis-*N*-hydroxysuccinimide polyethylene glycol (2000 Dalton) with a ratio of 1:1,5 and a total concentration of 5% (w/v) in PBS was added to the samples. After washing with PBS, the samples were first placed with the upside on a 30 µl droplet of VEGF in a 24 well plate and incubated for 1 hour. As already described in 3.2.3.2, also for the co-immobilization procedure different concentration of 1 µg/ml, 10 µg/ml and 20 µg/ml VEGF in PBS were used for the immobilization. As next step, the samples were rinsed again with PBS and placed on a 30 µl droplet of 500 µg/ml RGD in PBS for another hour. After final rinsing, the samples were carefully dried using an air stream. Figure 3.6 shows schematically the co-immobilization procedure of VEGF and RGD.

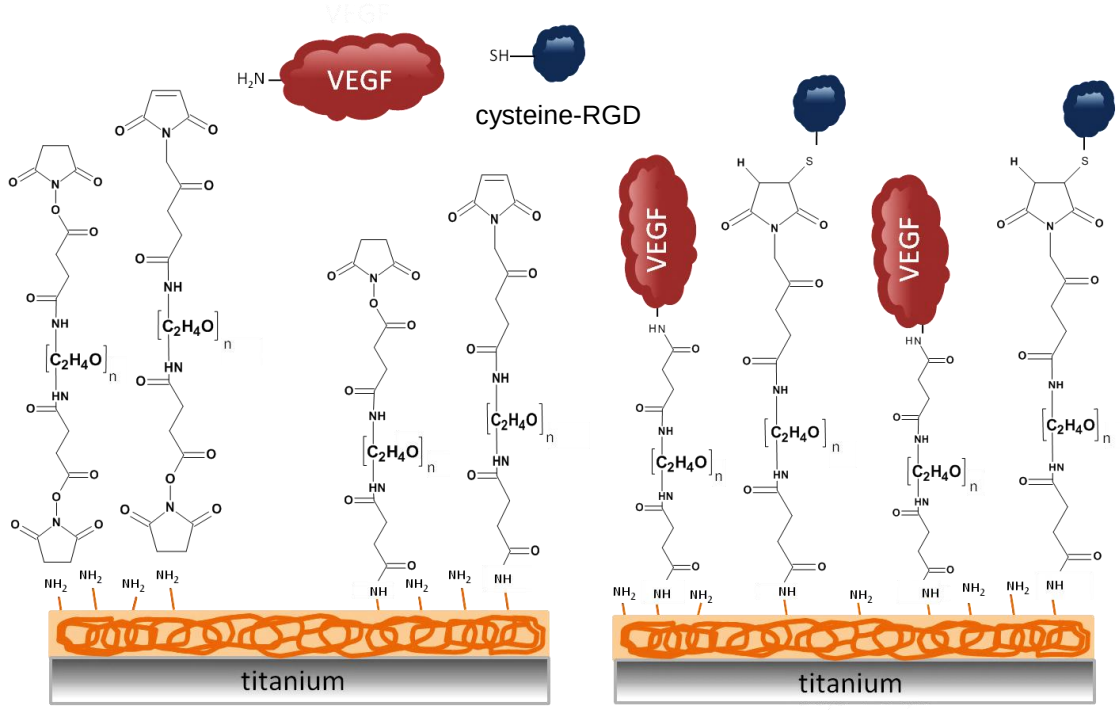

Figure 3.6 Schematic of the developed RGD/VEGF co-immobilization procedure using α, ω-bis-*N*-hydroxysuccinimide polyethylene glycol and α-maleinimidohexanoic-ω-*N*-hydroxysuccinimide polyethylene glycol.

3.2.3.4 ECM Protein Immobilization as Alternative to RGD

As alternative to RGD, different proteins of the ECM were immobilized on titanium such as fibronectin, collagen, laminin and osteopontin in order to enhance cell

adhesion. For the immobilization of the ECM proteins the same procedure was used as described in 3.2.3.2 for the VEGF immobilization. Before immobilization, the pp-AA modified titanium samples were incubated for 1 hour. For the cross-linker immobilization the titanium samples were transferred in clean 24 well plates and incubated for 15 min with 5% (w/v) α, ω-bis-*N*-hydroxysuccinimide polyethylene glycol in PBS. After rinsing the titanium samples in PBS they were incubated with the protein solutions of the ECM proteins. Fibronectin was dissolved in PBS using a concentration of 1 mg/ml, collagen 500 µg/ml, laminin 500 µg/ml and osteopontin 10 µg/ml. Due to the hydrophobic behavior of collagen, it was first dissolved in 50 µl DMSO and incubated for 5 minutes in an ultrasonic bath before it was dissolved in PBS. As described for VEGF, a 30 µl droplet of each concentrate was given onto the bottom of a 24 well. For the immobilization of the different proteins the samples were placed with the upside on the droplet for 1 hour as already described above. After rinsing with PBS, samples were carefully dried under an air stream.

3.2.4 Contact Angle Goniometry

The contact angle goniometry can be used to investigate the wettability of a surface. A droplet of water is placed on a surface and the contrast of water and surface is estimated. At a sessile, non-moving droplet with a constant volume, the contact angle can be determined. Figure 3.7 shows different ranges of static contact angle measurements.

In this work this method was used to investigate changes of the wettability during surface preparation and between the wet chemical surface modification steps. Contact angle measurements were performed after every titanium preparation step and during wet chemical modification. Thus, it was estimated whether the change in contact angle indicates the oxidation of titanium or the immobilization of a biomolecule. The contact angle of water was investigated using ultrapure water from a water purification system Millipore Milli-Q+ 185 (Molsheim, France) with a resistivity of 18.2 MΩcm. For the measurement a 3 µl droplet was placed on the surface and the contact angle was determined via software. In all experiments 3-fold measurements were conducted for each sample and reproduced 3 times.

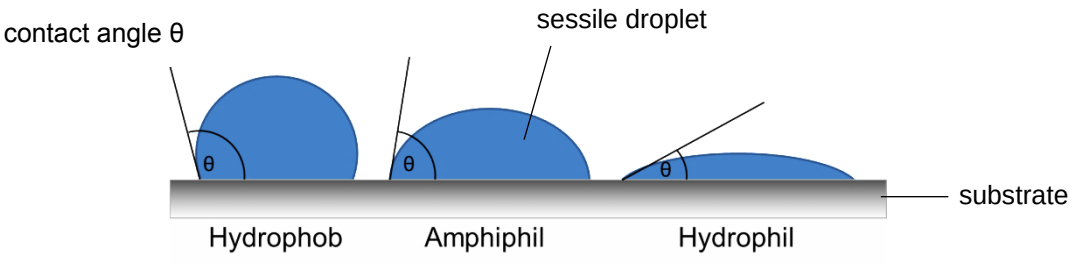

Figure 3.7 Schematic of various ranges of sessile drop contact angle measurements.

3.2.5 Step Profiling

This method can be used to determine the layer thickness of pp-AA films or to conduct roughness measurements on a surface. For the roughness measurements of the titanium surfaces during and after preparation as well as for the thickness measurements of various pp-AA films, the scan rate was 50 µm/s at 100 Hz with a needle weight of 1 mg. The roughness value Ra in µm was determined for acid etched and acid etched/oxidized titanium. The thickness measurements of various pp-AA films were conducted on ethanol cleaned silicon wafers. Measurements were conducted 3-fold for each point of interest. The basic principle of the measurement is shown in figure 3.8.

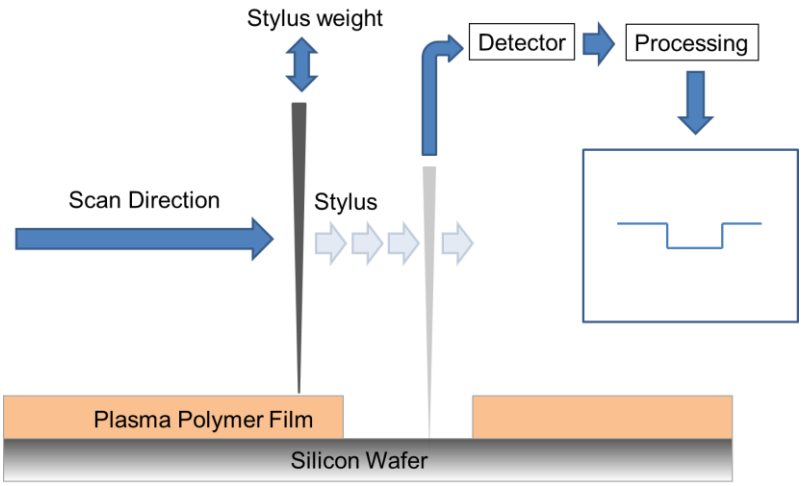

Figure 3.8 Basic principle of step profiling. By scanning over a surface or a scratch with a fine stylus, information of the surface roughness or the scratch depth can be obtained.

3.2.6 Distribution of Primary Amines via Fluoresceine Isothiocyanate (FITC)

To determine the distribution of primary amines on the pp-AA modified titanium surfaces fluoresceine isothiocyanate (FITC) was used. The distribution of primary amines of different pp-AA films was investigated. In this experiment pp-AA was deposited using 40, 60, 80 and 100 W and a monomer pressure of 0.1 mbar for 5 minutes onto titanium samples.

To prepare the FITC staining solution, 0,5 mg of FITC was first dissolved in 100 µl of DMSO and 1 ml of carbonate buffer was added. The titanium samples were in total incubated for 30 min in the fresh prepared FITC solution. After 15 minutes, titanium samples were turned and incubated for another 15 minutes to ensure that the FITC could reach all areas of the samples. After staining, the samples were rinsed with 70% of ethanol in order to remove all non-bound FITC molecules. Afterwards, samples were analyzed via fluorescence microscope using a standard FITC filter. Figure 3.9 shows the reaction scheme of the FITC reaction. The distribution of primary amines of different pp-AA films was investigated in triplicate. For evaluation, representative spots of each surface were photographed with 100-fold magnification and analyzed.

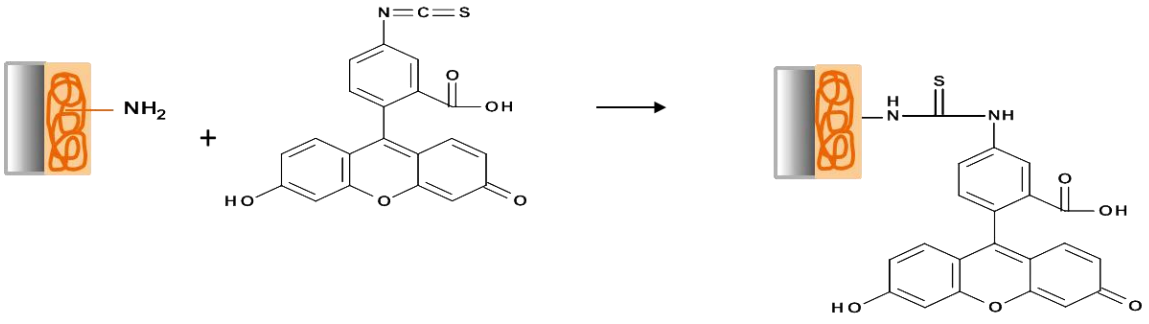

Figure 3.9 Reaction scheme of the FITC staining. The excitation wavelength of fluoresceine isothiocyanate is 494 nm.

3.2.7 Quantification of Primary Amines via Sulfo-SDTB

For the quantification of the primary amines on pp-AA modified titanium surfaces Sulfo-succinimidyl-4-*O*-(4, 4´-dimethoxytrityl)-butyrate (sulfo-STDB) was used (Gaur and Gupta, 1989). Additionally, the influence of PBS on the stability of primary amines within the pp-AA films was tested. In these experiments, the same plasma polymerization parameters for pp-AA films were used as described in 3.2.6 and the density of primary amines of pp-AA coated titanium samples was evaluated before and after 1 hour of PBS incubation. For each pp-AA surface, measurements in triplicate were performed and reproduced 3 times. In order to compare the different measurements and to keep experiment influencing parameters constant, pp-AA films of 20-30 nm were used. The layer thicknesses were controlled over the deposition times and checked via step-profiler.

For the preparation of the sulfo-SDTB solution, 3 mg of sulfo-SDTB were dissolved in 1 ml DMSO and 50 ml of a 50 mM carbonate buffer were added. For the binding reaction of sulfo-SDTB to the primary amines, 1 ml of the fresh prepared solution was pipetted on the samples and incubated for 30 minutes. Reference was an unmodified titanium sample. After incubation, samples were washed thoroughly with milliQ water, dried and transferred into a new 24 well plate. For the release of the dimetoxytrityl kations as shown in figure 3.10, 1 ml of 35% perchloric acid was added to the samples and incubated for 10 min. The photometrical measurements were performed using a wavelength of 498 nm and standard cuvettes. To determine the primary amine density, Lambert-Beer calculations were conducted using the mean values and standard deviations.

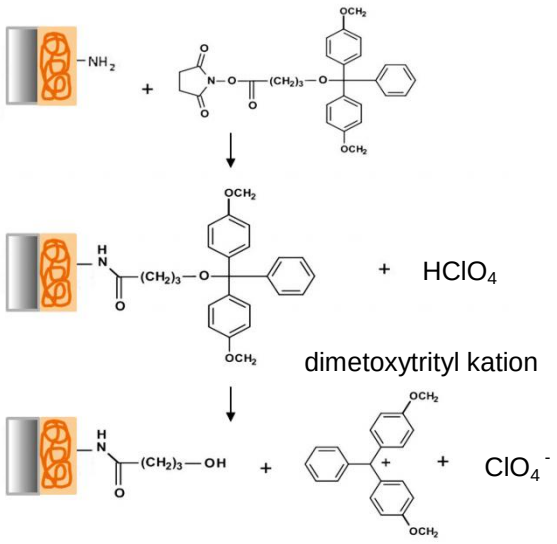

Figure 3.10 Reaction scheme of sulfo-SDTB with primary amines. After binding to primary amines perchloric acid leads to the release of dimetoxytrityl kations that are proportional to the amount of primary amines. The density of primary amines is determined using Lamber-Beer.

3.2.8 Physical Vapor Deposition

For different surface characterization methods used in this work such as infrared spectroscopy and surface plasmon resonance spectroscopy, it was necessary to produce samples with a gold layer, due to the optimal optical properties of gold that are necessary for the mentioned methods. Physical Vapor Deposition (PVD) can be used to deposit metallic thin films such as chromium, silver or gold onto surfaces. Small amounts of these metals are heated up within a vacuum of 10^{-6} bar in order to obtain metal vapor that is deposited on surfaces of various substrates.

The gold layers were deposited on glass slides that were cleaned with 99 % ethanol and helmanex. Each cleaning step was conducted in an ultrasonic bath for 15 minutes.

For infrared spectroscopy glass slides were deposited with a 1,5 nm thick chromium layer for better attachment of gold and afterwards gold was deposited with a thickness of 80 nm. For surface plasmon resonance spectroscopy, Hellma LaSFN9 glass was coated with a chromium layer as described above and afterwards the gold layer was deposited with a thickness of 47 nm. In order to enhance adhesion of plasma polymerized allylamine on gold, gold slides were always incubated in 50 mM allyl mercaptane in ethanol before usage to obtain a

self-assembled monolayer, susceptible for plasma treatment. A schematic of the obtained samples is shown in figure 3.11.

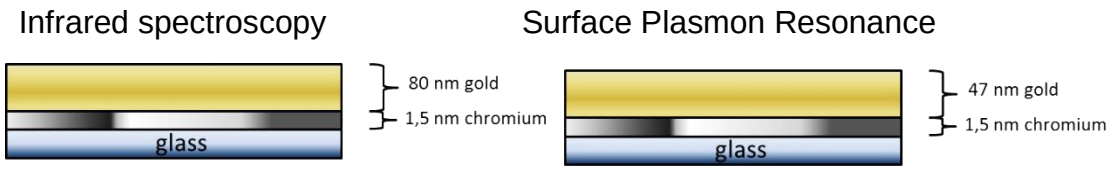

Figure 3.11 Sample preparation for infrared spectroscopy and surface plasmon resonance spectroscopy. Due to the different requirements of the used methods, different thicknesses of gold layers were deposited.

3.2.9 Sputtering

In order to investigate the stability of various pp-AA films in PBS on titanium oxide via infrared spectroscopy it was necessary to deposit a thin layer of titanium oxide on top of the gold samples. The basic principle of the sputtering used in this work is the bombardment of excited species such as argon and oxygen ions on a titanium target. This leads to the ejection of atoms and erosion of material from the target that is deposited on surfaces. For the cleaning of the oxidized titanium target argon plasma was used for approximately 5 minutes. After the oxide layer was removed from the target, samples were placed in the sputtering chamber. After generating a vacuum, oxygen plasma was used to sputter and deposit a 10 nm thick titanium oxide layer on the surface (figure 3.12).

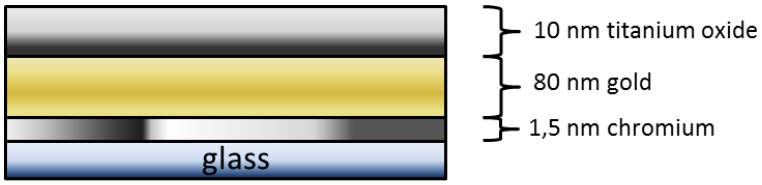

Figure 3.12 Titanium oxide sample for infrared spectroscopy.

3.2.10 Infrared Spectroscopy

To obtain information about the chemical structure and composition of plasma polymerized thin films infrared spectroscopy can be used. The principle of this method is based on the absorption of electromagnetic energy of infrared light by molecules. The electromagnetic energy is transformed into vibrational changes of

chemical bonds and occurs at chemical bond or functional group specific wavelengths of infrared light.

3.2.10.1 Infrared Reflection Absorption Spectroscopy

The infrared reflection absorption spectroscopy (IRRAS) is a powerful method to obtain information about the chemical structure of thin films on metallic surfaces such as silver, gold or titanium oxide. For this purpose, infrared light is directed at a metallic surface, coated with the surface coating of interest with an angle of incidence of 5°. After passing the thin film, the infrared light is reflected on the metallic surface and passes the film again, before it is detected by a nitrogen cooled detector. During the passing steps, chemical bond specific wavelengths of the infrared light are absorbed. In comparison to a gold reference, this absorption leads to compound specific signals in the infrared spectrum, giving information about chemical structures.

Samples for the measurements were gold samples as described in section 3.2.8 or titanium oxide coated gold samples as described in section 3.2.9.

Various measurements were performed via IRRAS such as analysis of the chemical structure of pp-AA, analysis of the stability of different pp-AA films in PBS and analysis of the immobilization of the used cross-linkers. All different treated samples used in the IRRAS measurements were measured against a gold reference.

For the analysis of the chemical structure, pp-AA was deposited for 5 minutes on gold using 100 W and 0,1 mbar monomer pressure. To examine the stability of various pp-AA films in PBS on gold, as well as on titanium oxide, pp-AA films were deposited for 5 minutes using 40, 60, 80 and 100 W at a monomer pressure of 0,1 mbar. The IRRAS measurements were conducted before and after 1 hour of PBS incubation. In order to investigate the binding process of the used cross-linkers and to detect the linker molecules on the gold surface, very thin pp-AA films were required. Because of this, pp-AA was deposited for 20 seconds using 100 W and a monomer pressure of 0,1 mbar, obtaining films of approximately 10 nm. Samples were analyzed before and after cross-linker incubation as described in 3.2.3.1 - 3.2.3.3.

3.2.10.2 Attenuated Total Reflection Infrared Spectroscopy

The attenuated total reflection infrared spectroscopy (ATR) is a method in which infrared light is led through a crystal with high refractive index. To obtain information about chemical structures of various substances, samples are pressed upon the crystal. Due to the total reflection at the crystal and the interaction of the evanescent waves with chemical substances, information about chemical structure can be obtained. The reflected infrared light is detected by a nitrogen cooled detector. This method was used in this work, in order to obtain information of the chemical structures of the used cross-linkers in order to create reference spectra for a comparison with IRRAS spectra.

3.2.11 X-Ray Photoelectron Spectroscopy

X-ray photoelectron spectroscopy (XPS) is a method to obtain information about the elemental composition of a surface. The basic principle of the XPS is the irradiation of a surface with X-rays that causes the release of electrons. Over the kinetic energies and quantity of the released electrons within the upper 10 nm, surface information concerning the respective chemical composition can be obtained. Since XPS is a very sensitive characterization method, it requires high vacuum conditions to avoid impurities and contaminations.

The XPS measurement was used to gather information about changes in elemental composition during the wet chemical surface modification steps to give evidence for a successful immobilization process. The setup used was a SPECS SAGE spectrometer with a Mg Kα radiation source (hv 1253,6 eV) operating at 10 kV and 20 mA. The hemi-spherical analyzer was a Phoibos 150, with an MCD-9 detector. The elements present were identified from a survey spectrum recorded over the energy range 0-1200 eV at pass energy of 30 eV and a resolution of 0,5 eV. The areas under the photoelectron peaks in the spectrum were used to calculate the percentage atomic concentrations. All binding energies were referenced to the aliphatic C1s carbon peak at 285 eV, to compensate for the effect of surface charging. The analysis area was circular and 5 mm in diameter. All spectra were recorded as soon as practicable after deposition in order to avoid air-ageing effects such as radical-induced oxidation which are known to be significant in amine plasma polymers.

3.2.12 Surface Plasmon Resonance Spectroscopy

Surface plasmon resonance spectroscopy (SPR) is a powerful tool to obtain information about dynamic processes on metallic surfaces on a molecular level. The basic principle (figure 3.13) of this method is based on the excitation of electrons at a metallic/dielectric interface such as gold/air or gold/liquid interface at a certain angle of incidence of a light beam. At this angle of incidence the energy of the light beam is totally absorbed and transferred into an evanescent wave, in which electrons are excited and start to oscillate. This oscillation is called plasmon resonance. Depending on the refractive index (*n*) and the layer thickness (*d*) of e.g. plasma polymer films or protein layers that are deposited or adsorbed on the gold surface, the angle of incidence changes at which resonance occurs. By following this angle shift of the plasmon over time, qualitative adsorption kinetic information can be obtained that correlate to the optical thickness (*nd*).

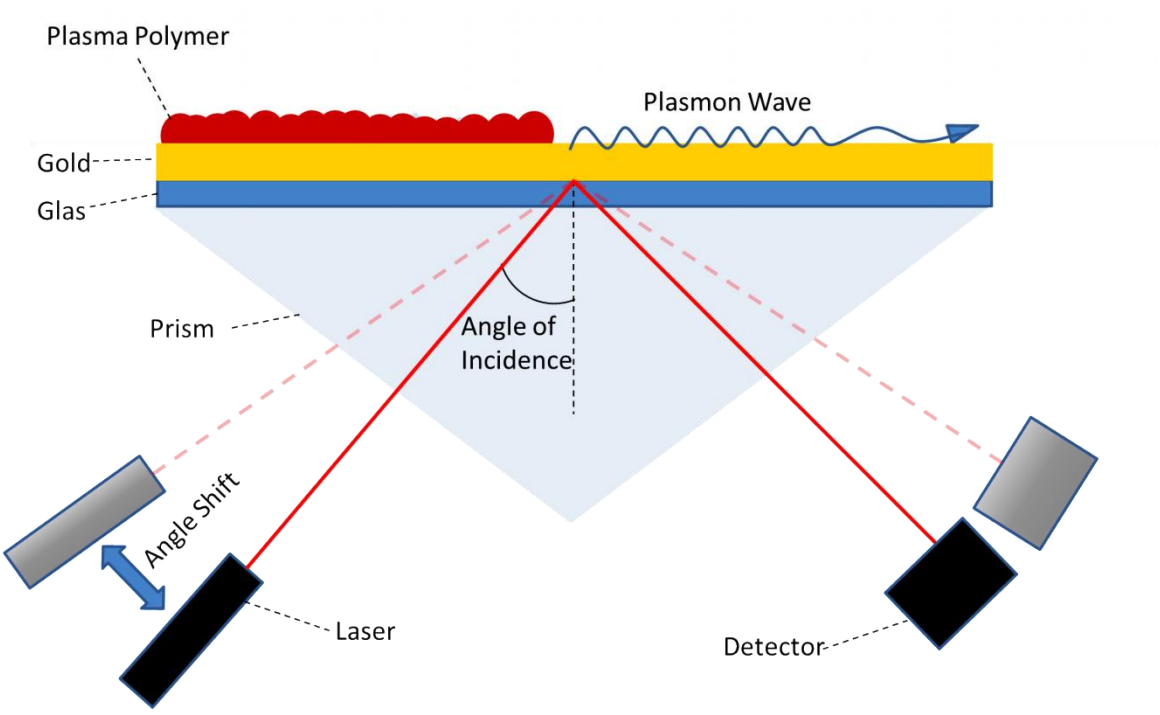

Figure 3.13 Basic principle of the surface plasmon resonance spectroscopy. The angle of incidence at which a plasmon wave occurs depends on the refractive index and layer thickness of adsorbed layers such as plasma polymer films or protein layers.

Kinetic measurements in this work were performed using a custom-made SPR setup (Knoll, 1998). For all SPR kinetic measurements, 100 W pp-AA films were used. Since SPR is a very sensitive method, very thin pp-AA films were required. In brief, pp-AA films were deposited for 20 seconds using 100 W and 0,1 mbar monomer pressure on SPR gold samples. With these plasma polymerization parameters pp-AA layers with a thickness of approximately 10 nm were obtained.
In order to investigate the wet chemical immobilization procedure as described in 3.2.3.1 - 3.2.3.3 via SPR kinetic measurements, a flow chamber attached on top of the pp-AA coated gold slides was used. As reference, the plasmon of an uncoated gold sample was analyzed. Afterwards the plasmon of an approximately 10 nm thick 100 W pp-AA film was determined in air and PBS in order to define the starting point of the kinetic measurements. For the kinetic measurements, the angle of the plasmon minimum of the 100 W pp-AA film in PBS was determined and followed using the software Wasplas 2.60 (© Andreas Scheller, 2003). The solutions and buffers used for the wet chemical immobilization as described above were carefully syringed into the flow chamber and the immobilization process was investigated following the angle at the minimum of the shifting plasmon. For a simplified experiment, VEGF was replaced by Bovine Serum Albumin (BSA) to prove the principle of the immobilization and co-immobilization procedure. For the development of the immobilization/co-immobilization procedure, the kinetic measurements were reproduced for the RGD, BSA and RGD/BSA immobilization, varying in plasma polymerization parameters for pp-AA, protein concentrations of BSA and cross-linker ratios. For the kinetic measurements of various BSA concentrations of 1, 2, 5, 10 mg/ml in PBS as well as for the different used ECM proteins, gold slides and pp-AA films of one batch were used for evaluation and comparison of the immobilization processes.

3.2.13 Scanning Electron Microscopy

Scanning electron microscopy (SEM) resolves surface structures in a range of micro- and nanometers. The basic principle is the scanning of a sample with a focused beam of electrons lead to the ejection of electrons of the sample, so

called secondary electrons. These electrons can be detected and give information about the topography and composition of a surface.
SEM was used in this work to determine the surface topography of the prepared titanium samples as described in 3.2.1 and to investigate the mechanical stability of pp-AA films on commercially titanium screws used in various medical applications.

3.2.13.1 Mechanical Stability of pp-AA Films

To investigate the mechanical stability of the pp-AA films regarding to shearing forces during the screwing into bone, medical titanium screws were inserted into a femur bone of a pig *ex vivo* as shown in figure 3.14. Since this measurement was performed in an early stage of this work, the titanium screws were modified with pp-AA films that were deposited with different parameters compared to the parameters as described in section 3.2.2. For this experiment titanium screws were coated with pp-AA films for 5 minutes, using a monomer pressure of 0,15 mbar and 40 W process power. Reasons for this are discussed in 5.4.7. To stay as close as possible to medical praxis, first a hole was drilled in the bone using a medical driller suitable for the used screws. Then the screws were screwed into the bone and removed again. To visualize the effect of the shearing forces on the pp-AA films, screws were analyzed with SEM. The experiment was performed in triplicate.

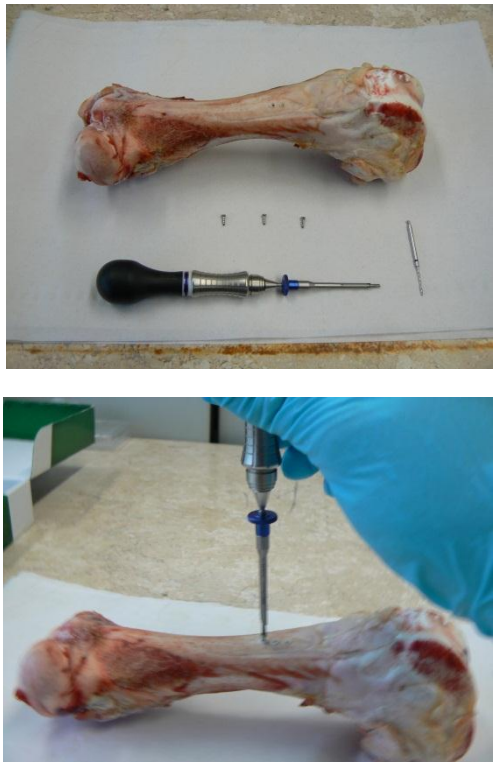

Figure 3.14 Mechanical stability of pp-AA films was tested after screwing pp-AA modified titanium screws into a femur of a pig.

3.2.14 Solid Phase ELISA

Usually the Enzyme Linked Immuno Sorbent Assay (ELISA) is a method to quantify proteins such as antibodies, growth factors and cytokines in physiological liquids such as blood, serum and other body fluids. The basic principle of this method is based on the specific interaction of antibodies - so called capture antibodies - with the proteins of interest and a following visualization step via detection antibodies. The detection antibodies are usually labeled with an enzyme such as horseradish peroxidase that is used for staining. The intensity of staining correlates with the amount of proteins that are bound to the capture antibody. The solid phase ELISA uses only the detection antibody to quantify the immobilized protein of interest on a surface. For the development of the solid phase ELISA the Duo Set® Human VEGF from R&D Systems was used. Since this ELISA-Kit was developed to perform standard ELISA analysis, the solid phase ELISA required to be established to quantify the immobilized VEGF on the titanium surfaces. The titanium samples were modified with VEGF as described in section 3.2.3.1. For the establishment of the solid phase ELISA only a VEGF concentration of 1 µg/ml in PBS was used.

In the adapted solid phase ELISA procedure, the modified titanium samples were placed in 24 well plates. Then the samples were blocked, adding 400 µl of reagent diluent for 1 hour. After 3 washing steps with the wash buffer, 400 µl of the detection antibody diluted in reagent diluent was added to each well and incubated for 2 hours at room temperature. After another washing step as described above, 400 µl of the working dilution of streptavidin-horseradish peroxidase was added to the wells and incubated for 20 minutes at room temperature in a dark box. Afterwards the samples were washed again and 400 µl of the substrate solution was added to each well and incubated for another 20 minutes to develop the staining. As last step 200 µl of stop solution was pipetted to the substrate solution and the samples were measured in the Multiskan Ascent. The samples were analyzed with 450 nm and a wavelength correction of 540 nm. A crucial step for the quantification of the VEGF was the creation of a suitable standard. For the standard, capture antibody pre-coated titanium samples were incubated with various concentrations of $VEGF_{165}$. The lowest used VEGF concentration of 50 ng/ml was gradually increased up to a concentration of 20 µg/ml. The incubation of the different concentrations of VEGF and the further ELISA procedure was conducted as described above. ELISA measurements were performed in triplicate and reproduced 3 times.

3.2.15 Cell Experiments

3.2.15.1 Cell Culture

Endothelial cells were isolated from umbilical cords that were first washed with sterile PBS to clean them from blood. After localizing the central vein, PBS was inserted in it using a syringe and rinsed until no blood was inside the vein anymore. Afterwards, the cord was closed with two clamps on each side at the ends. Then, a collagenase solution was inserted in the closed cord and incubated in 37° pre-warmed PBS for 5 min. During the collagenase incubation, the cord was massaged to allow the cell to detach from the vein walls. As final step the collagenase solution with the cells was collected in a 50 ml tube and the vein was rinsed once with cell type specific medium and the obtained fluid was collected in a 50 ml tube as well. After centrifuging for 5 min at 1200 rpm the cells were suspended in endothelial cell medium and seeded in culture flasks.

Human primary osteoblasts were stored in cryo-tubes containing 1 ml cryo-solution in liquid nitrogen. For defrosting, the cryo-tubes were warmed in a water bath. Defrosted and suspended cells were directly transferred in a midi cell culture flask and 12 ml of osteoblast specific medium was added.

The cell media were changed in the case of the HUVECs every 2 days and for the HOBs every 4 days. After the flasks were completely covered, cells were split in new flasks. For passaging HUVECs, Accutase Solution from PAA was used. After rinsing the fully seeded culture flasks with PBS the ready to use mixture of Accutase was added and incubated until the cells were detached. The adhesion status was checked via microscope. After detaching from the flasks HUVECs were transferred to a 50 ml centrifuge tube and 10 ml cell culture medium was added. Cells were centrifuged at 1500 rpm for 5 min. Finally the supernatant was discarded and the cell pellet was suspended in 15 ml in the specific cell medium. To passage HOBs, Trypsin/EDTA was used to detach cells from the culture flasks and cell specific osteoblast medium was used. The further procedure was as described for HUVECs. HUVECs and HOBs were cultivated at 37°C and 5% CO_2 content in the incubator.

For freezing cells, all necessary reagents were pre-cooled on ice before use. After detaching cells, as described above, they were taken up with a pipette in cell specific medium and afterwards centrifuged twice. The supernatant was discarded and the cells were suspended in cryo-solution and transferred in cryo-tubes. To slow down the freezing process, cells were first stored at -80°C overnight before they were transferred to liquid nitrogen.

In order to determine the cell number, a Neubauer chamber was used. Cells were detached and resuspended as described above. After mixing the suspension carefully, 50 µl of cell suspension was added to 50 µl trypan blue and pipetted in the Neubauer chamber.

Counting was conducted in the microscope and cell number was calculated using the following formula:

$$\frac{\text{Cell number in 8 big squares x Dilution factor (2500) x Total volume in ml of cell suspension}}{\text{Total volume in ml of cell suspension}} = \text{Cell number/ml}$$

3.2.15.2 Biological Effect of Dissolved VEGF on HUVECs

In order to investigate the biological effect of dissolved VEGF on the cellular response on HUVECs and to analyze, whether only VEGF is sufficient for cell stimulation, different concentrations of $VEGF_{165}$ (1, 10, 20, 50, 100 ng/ml) were dissolved in supplement free basic endothelial cell medium. An amount of 50000 cells were seeded in 24 well plates and cultivated with the described medium. After 24 hours and 3 days cell adhesion was analyzed using calcein staining.

3.2.15.3 Cell Adhesion Analysis

For the cell adhesion experiments, HUVECs and HOBs were seeded on the modified titanium samples as described above. HUVECs from passage 1-4 and HOBs from passage 1-8 were used. In order to seed the samples with cells, titanium samples were placed in 24 well plates. Afterwards 50000 cells were seeded on each sample and incubated in 2 ml of the cell specific culture medium in the incubator. The adhesion of HUVECs was analyzed after 24h, and 3 days on the samples that were modified with VEGF and RGD/VEGF and 24 hours, 3 days and 7 days for RGD modified samples. Samples modified with ECM proteins were investigated after 24 hours, 3 days and 7 days regarding to cell adhesion of HUVECs and HOBs. For evaluation, cells were stained using calcein staining and visualized in the fluorescence microscope with a standard FITC filter and 100-fold magnification.

The experiments of RGD modified surfaces were performed in triplicate and reproduced 3 times. For the investigation of VEGF and RGD/VEGF surfaces, different concentrations were used for the modification as described in 3.2.3.2. Each concentration was analyzed in pilot studies once in triplicate. To evaluate the effect of immobilized ECM proteins, one triplicate measurement was performed for each surface and each investigation time. In all cell experiments, several representative spots of each surface were visualized and photographed with 100-fold magnification. To determine the percentage of cell coverage, the software imageJ (NIH, Bethesda, USA) was used. For this purpose, three representative pictures of each surface were analyzed and the determined values were statistically calculated. Detailed information about the statistical analyses is given in 3.2.16.3.

3.2.15.4 Biological Activity of Immobilized VEGF

The biological activity of immobilized VEGF was analyzed using the phosphorylation status of the respective transmembrane receptor tyrosine kinase. The ELISA Kit Duo Set® IC Human Phospho-VEGF R2/KDR was used to determine the activated i.e. the phosphorylated amount of $VEGF_2$ receptors. The basic principle of ELISA was already described in section 3.2.14.
Since this measurement was performed straight on modified and cell seeded titanium samples, the standard protocol was adjusted. In order to get enough amounts of cell lysates, each sample was seeded with 100000 cells. Cells were incubated on the titanium plates for one hour to enable cell interactions with the surface bound VEGF. For cell lysis the standard protocol was followed using the lysis buffer contained in the kit. The lysis was conducted straight on the titanium samples. Then 100 µl of the standards and the cell lysates were pipetted on the pre-coated 96 well ELISA plates and incubated for 2 hours. After a washing step, samples were incubated with the detection antibody as described in the protocol, and afterwards washed again. In order to develop the staining, samples were incubated with the substrate solution for 20 min in a dark box. Afterwards 50 µl of the stop solution was added and the samples were measured with 450 nm. As wavelength correction 540 nm was used.

3.2.16 Animal Experiments

3.2.16.1 Implantation of Modified Osteosynthesis Plates in the *Tibia* of Rabbits

Due to the close clinical collaboration, the respective animal experiments and sample preparations were performed by Dr. P. Kämmerer from the Department of Maxillofacial Surgery. For these experiments osteosynthesis plates were modified with RGD, VEGF, and RGD/VEGF as described in section 3.2.3. For the modification procedure of the osteosynthesis plates 100 W pp-AA films were used as described in 3.2.2. The immobilization/co-immobilization was conducted using a RGD concentration of 500 µg/ml and a VEGF concentration of 1 µg/ml in PBS. The modified osteosynthesis plates were implanted in the proximal tibia of rabbits as shown in figure 3.15. In brief, a bone crate, measuring approximately 2x1 mm was created and the plates were inserted into the spongious part of the

bone. In total, 6 animals were used. They received a non-coated plate (control) on the right side and a modified plate (RGD (n=2), VEGF (n=2), RGD/VEGF (n=2) on the left side. The animals were sacrificed after 30 days and the induction of spongious bone formation was analyzed descriptively.

Figure 3.15 Implantation of RGD, VEGF and RGD/VEGF modified osteosynthesis plates in the tibia of rabbits. Pictures supplied by the kind courtesy of Dr. P. Kämmerer from the Department of Maxillofacial Surgery.

3.2.16.2 Histological Preparation and Analysis

After fixation in 4 % formalin, samples were prepared after the method of Donath and Breuner (Donath and Breuner, 1982). The bone samples with the integrated osteosynthesis plates were cut and ground to a thickness < 5 mm. After embedding in Technovit and grinding to a thickness of 30-50 µm, samples were stained with toluidine blue. Finally the samples were analyzed in the microscope.

3.2.16.3 Statistics

Mean values as well as standard deviations for all experiments were calculated. For the statistical analysis of the cell experiments a one-way analysis of variance (ANOVA) with Bonferroni´s multiple comparison test was carried out to compare the groups of: (1) RGD modified samples with pp-AA coated surfaces and titanium controls after 24 hours, 3 days and 7 days, (2) various VEGF concentrations (1, 10, 20, 50, 100 ng/ml) in supplement free medium and their effect on HUVECs after 24 hours and 3 days, (3) VEGF modified surfaces using VEGF concentrations of 1, 10 and 20 µg/ml for the immobilization with pp-AA

coated surfaces and titanium controls after 24 hours and 3 days, (4) RGD/VEGF modified surfaces using VEGF concentrations of 1, 10 and 20 µg/ml for the immobilization with pp-AA coated surfaces and titanium controls after 24 hours and 3 days, (5) all surfaces, modified with ECM proteins, with titanium controls in the case of HUVECs and HOBs after 24 hours, 3 days and 7 days.

The p-values provided are only descriptive: p-values ≤ 0,05 were termed significant, p-values ≤ 0,001 were termed highly significant and p-values ≤ 0,0001 extremely significant. The analysis was performed using GraphPad Prism 4.00 for Windows, GraphPad Software, San Diego, California, USA.

4 Results

4.1 Titanium Preparation

The titanium used in this work was prepared to fabricate surfaces with reproducible topography and oxide layer composition. In order to establish a model system in cell culture the utilization of defined and well-characterized titanium surfaces was fundamental.

4.1.1 Titanium Etching and Oxidation

Usually, the oxide layer of titanium is created spontaneously through the reaction with atmospheric oxygen during industrial manufacturing steps as described in section 1.1.1. In order to control the oxide layer formation for reproducible and comparable results, oxidation was artificially induced. Figure 4.1 shows titanium samples after acid etching and after additional oxidation. Apparently, the acid etched titanium sample is lighter grey, whereas the oxidized titanium is colored dark grey as result of the oxide layer. For the contact angle measurements at least 3 different titanium samples from different batches were analyzed. Regarding to the wettability it can be observed that the oxidation leads to a distinctly decreased contact angle (figure 4.2 B) in comparison to the acid etched surface (figure 4.2 A).

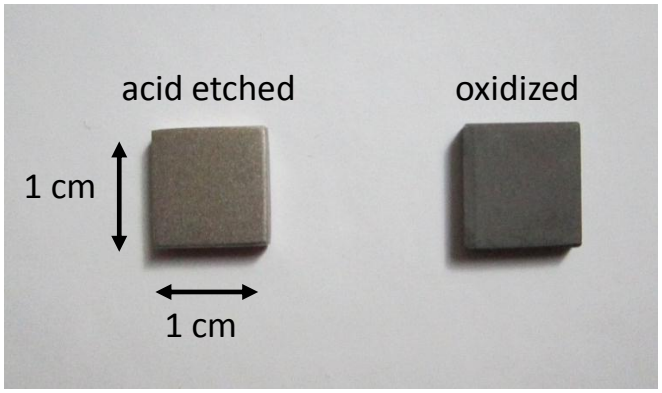

Figure 4.1 Acid etched and additionally oxidized titanium.

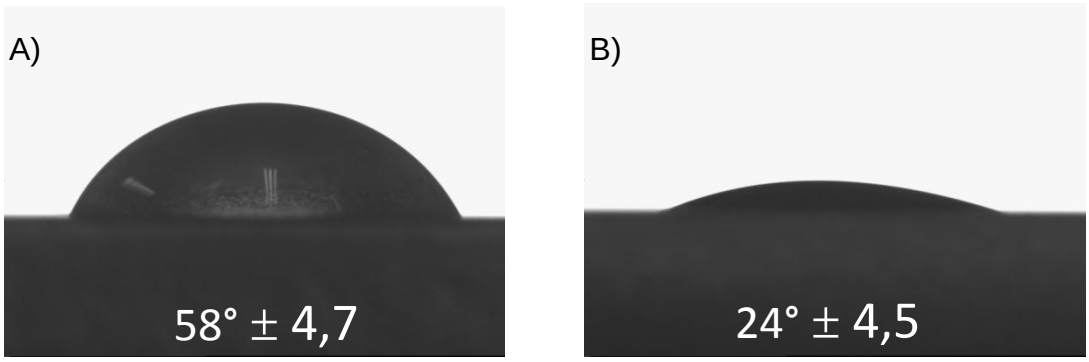

Figure 4.2 Water contact angle measurements onto A) acid etched and B) acid etched/oxidized titanium. The shown values are based on 3 independent measurements of 3 different batches.

For analyzing the different treated titanium surfaces regarding topography, the samples were investigated via Scanning Electron Microscope. Figure 4.3 shows SEM pictures of the differently treated titanium surfaces as described in 3.2.1. It can be observed that the differently treated surfaces have a homogenous and crystallite structure. There seems to be no distinct difference between the different surfaces.

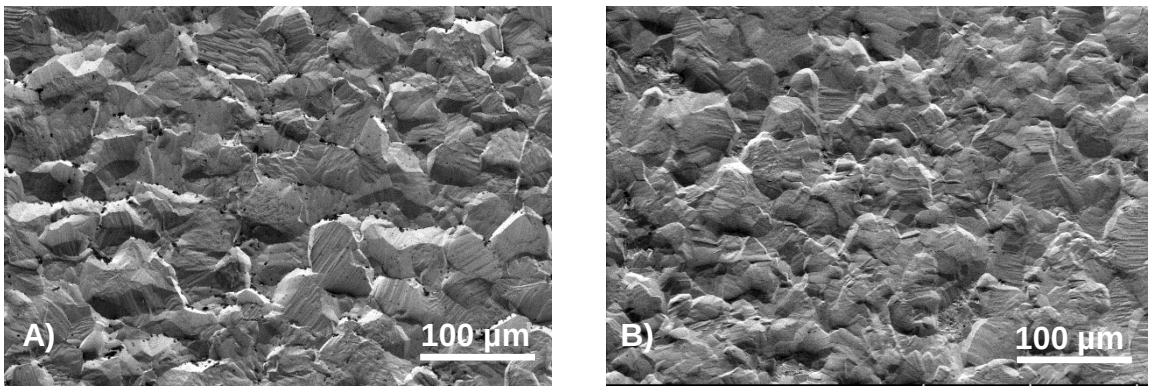

Figure 4.3 SEM pictures of A) acid etched titanium and B) acid etched/oxidized titanium.

4.1.2 Comparison of the Roughness

In order to analyze the roughness of the used titanium surfaces, the prepared samples were investigated with the step profiler as described in section 3.2.5. Here, at least 3 random titanium samples from different batches were analyzed independently. According to the SEM pictures (figure 4.3) the roughness

measurements (Table 4.1) reveal that the oxidation process leads to no distinct changes of surface roughness.

Table 4.1 Roughness [Ra] in µm of acid-etched and acid-etched/oxidized titanium. The calculated values are based on 3 independent measurements.

Surface Treatment	Mean [µm]	SD
Acid etched	3,63	0,29
Acid etched+oxidized	3,62	0,27

4.2 Plasma Polymerization of Allylamine

4.2.1 Chemical Structure of Plasma Polymerized Allylamine

Allylamine is a well-investigated monomer for plasma polymerization and many details were found concerning the chemical structure (Yang et al., 2010, 2009, Krishnamurthy et al., 1989). Figure 4.4 shows an IRRAS spectrum of a 100 W pp-AA film that was deposited with 0,1 mbar monomer pressure. According to literature, in table 4.2 a selection of IR signals of pp-AA are shown (Yang et al., 2010, 2009, Krishnamurthy et at., 1989).

The spectrum in figure 4.4 is characterized by N-H stretching absorption peaks between 3500 and 3300 cm^{-1}. At 1630 cm^{-1} there is a distinct peak showing N-H bending. These signals show the presence of primary amines, secondary amines and imines. Because of overlapping signals it is not possible to distinguish between primary amines and imines. The signals around 3000-2800 cm^{-1} and at 1450 cm^{-1} and 1380 cm^{-1} show the aliphatic structures of carbon and hydrogen. The signal at 2200 cm^{-1} shows nitrile stretching vibrations. The newly created nitriles during the plasma process indicate the conversion of primary amines of allylamine (Krishnamurthy et al., 1989).

Table 4.2 Infrared signals of plasma polymerized allylamine.

Chemical structure	wavenumber/cm $^{-1}$
CH, CH_2 and CH_3 in plane deformation	1450-1280
C=C, C=N stretch and NH_2 bend	1650
C≡N and C≡C stretch	2240
R_3C-H stretch	3000-2800
NH_2 stretch	3280
=N-H stretch, N-H, and O-H stretch	3340

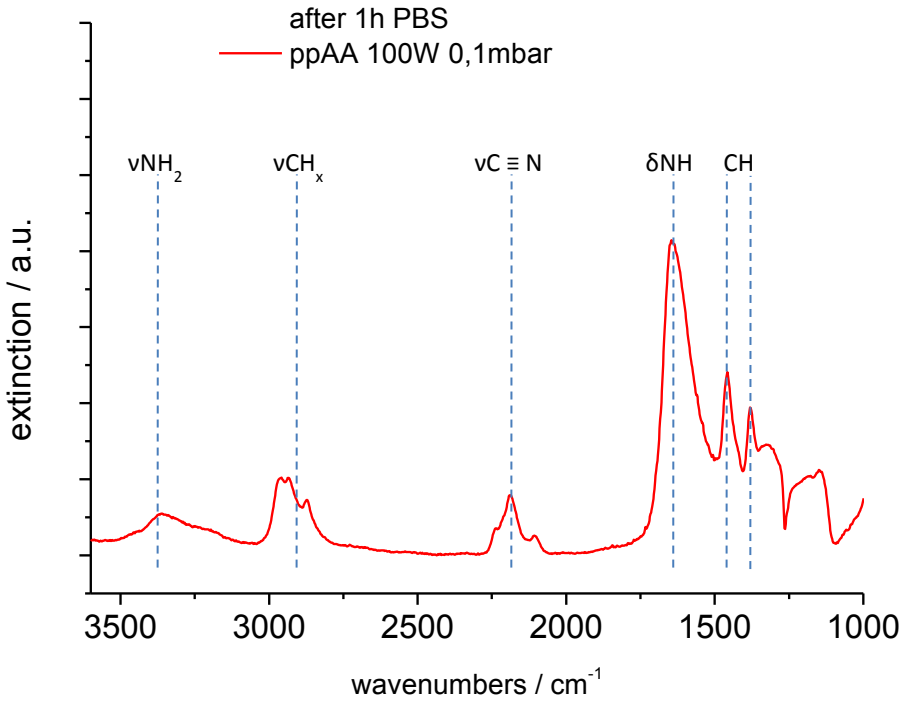

Figure 4.4 IRRAS spectrum of pp-AA deposited with 100W and 0,1 mbar process power. The distinct signals are highlighted.

4.2.2 Stability of Plasma Polymerized Allylamine in PBS

One of the problems that occur with pp-AA films is the stability in aqueous solutions or in certain solvents as described in section 1.5. In order to increase the stability of pp-AA films, the approach in this work was the adjustment of plasma polymerization parameters such as monomer pressure and process

power. Since all surface modification steps for the biomolecule immobilization were performed in PBS, the influence of PBS on the stability of differently deposited pp-AA films was investigated. One indicator to investigate the stability is the loss of thickness after incubation in aqueous solution as a result of leaching processes of non-bound material and oligomers within the plasma polymer network. Shown in figure 4.5 are the results of 3 independent measurements of different pp-AA batches. It can be seen that pp-AA films deposited with 40 W exhibit the lowest stability, indicated by the loss of thickness of 67 % in average after 1 hour of PBS incubation. In the case of the 60 W pp-AA films, the stability seems to be slightly increased, indicated by the average loss of thickness of 49 %. The highest stability can be observed for 80 W and 100 W pp-AA films. Here, the average loss of thickness is 32 %.

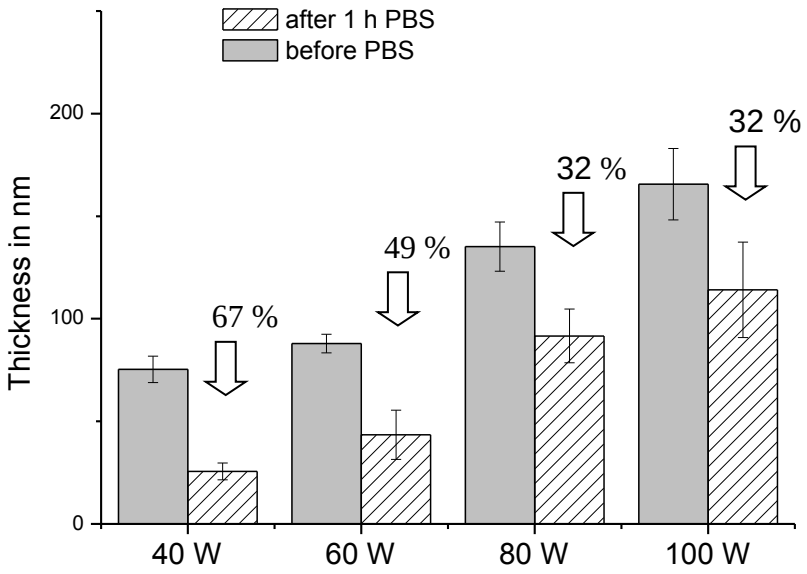

Figure 4.5 Loss of thickness and stability of pp-AA-films deposited with 40, 60, 80 and 100 W after PBS incubation. Shown values are based on 3 independent measurements using different batches.

In order to investigate the influence of PBS on the chemical structure, pp-AA films deposited with different process powers were investigated via IRRAS, before and after PBS incubation. IRRAS measurements were conducted on gold and on titanium oxide samples.

Shown in figure 4.6 are the IR spectra of pp-AA films deposited with different process powers before and after 1 hour of PBS incubation on gold. The pp-AA

specific IR signals were already described above. Since IR spectroscopy is not a quantitative method, changes in signal intensity can be used as indicator for changes in the chemical structure and composition, thus can be taken to draw conclusions about the stability.

In figure 4.6 A, it can be seen that the IR spectra of 40 W pp-AA films change distinctly after 1 hour of PBS incubation. The signals at 3000-2800 cm^{-1} from aliphatic hydrocarbons, at 3300 cm^{-1} and 1630 cm^{-1} from amines and amides and at 2200 cm^{-1} from nitriles decrease in comparison to the spectrum before PBS incubation. At 1450 cm^{-1} and 1380 cm^{-1} the specific signals for aliphatic carbon and hydrogen get lost, indicating that the pp-AA film dissolves in PBS.

For the pp-AA films deposited with 60 W (figure 4.6 B), 80 W (figure 4.6 C) and 100 W (figure 4.6 D) before as well as after PBS incubation the specific IR signals for pp-AA can be seen as described in 4.2.1. Corresponding to these spectra, it stands out that the ratio changes between the signal intensities at 1630 cm^{-1} and 1450 cm^{-1} (black arrows) for 60 W and 80 W films, indicating the decrease of the content of nitrogen compounds compared to the content of carbon and hydrogen within the films. For 100 W films, signal changes before and after PBS incubation are minimal, demonstrating that the influence of PBS on 100 W films concerning the chemical structure is lower than on the other investigated films.

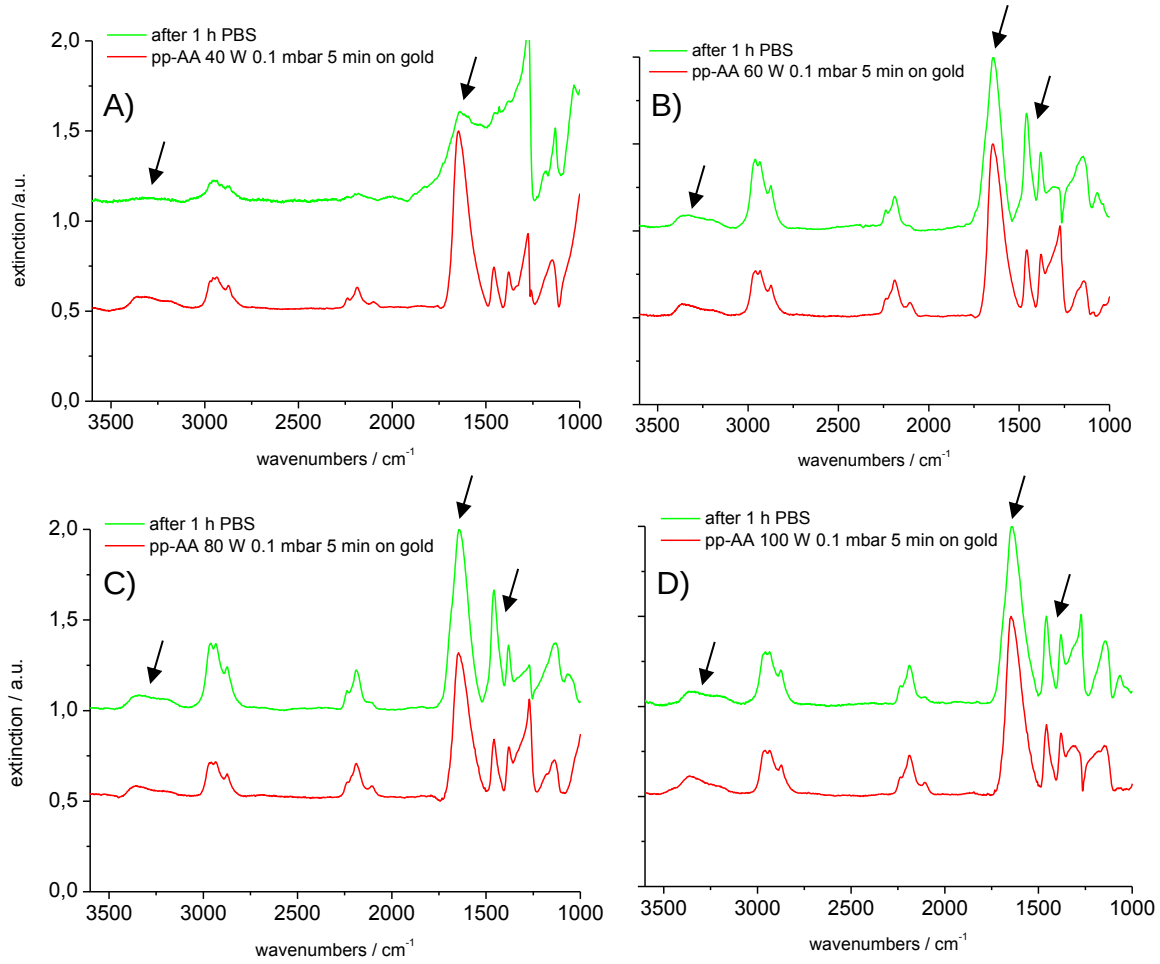

Figure 4.6 IRRAS spectra of pp-AA films on gold deposited with A) 40 W, B) 60 W, C) 80 W, D) 100 W process power and 0,1 mbar monomer pressure before and after PBS incubation. IR signals for amines and amides at 3300 cm^{-1} and 1630 cm^{-1} and for hydrocarbons at 1450 cm^{-1} and 1380 cm^{-1} are highlighted with black arrows.

A similar result than in 4.6, can also be observed on titanium oxide as shown in figure 4.7. The influence of PBS on the pp-AA films seems to be even more distinct for titanium oxide than for gold. In the case of the 40 W pp-AA films all pp-AA specific signals in the IR spectrum got lost after PBS incubation (figure 4.7 A). According to the results of 4.5 it is obvious that big parts of the 40 W pp-AA films dissolve in PBS. The spectra of the 60 W (figure 4.7 B) and 80 W (figure 4.7 C) pp-AA films show on titanium oxide a more distinct decrease in the specific IR signals after 1 hour of PBS incubation compared to gold. The decrease at 3300 cm^{-1} and 1630 cm^{-1} indicates the loss of amines and amides, while the ratio of the signal intensities changes at 1630 cm^{-1} and 1450 cm^{-1}, suggesting a relative increase in the content of hydrocarbons as already mentioned above. For

the 100 W pp-AA films (figure 4.7 D), it can be observed that also on titanium oxide there is a slight change in IR signal intensities after PBS incubation. However, compared to pp-AA films deposited with lower process power, the decrease is marginal. The shown results demonstrate the highest stability for 100 W pp-AA films in PBS concerning the chemical structure.

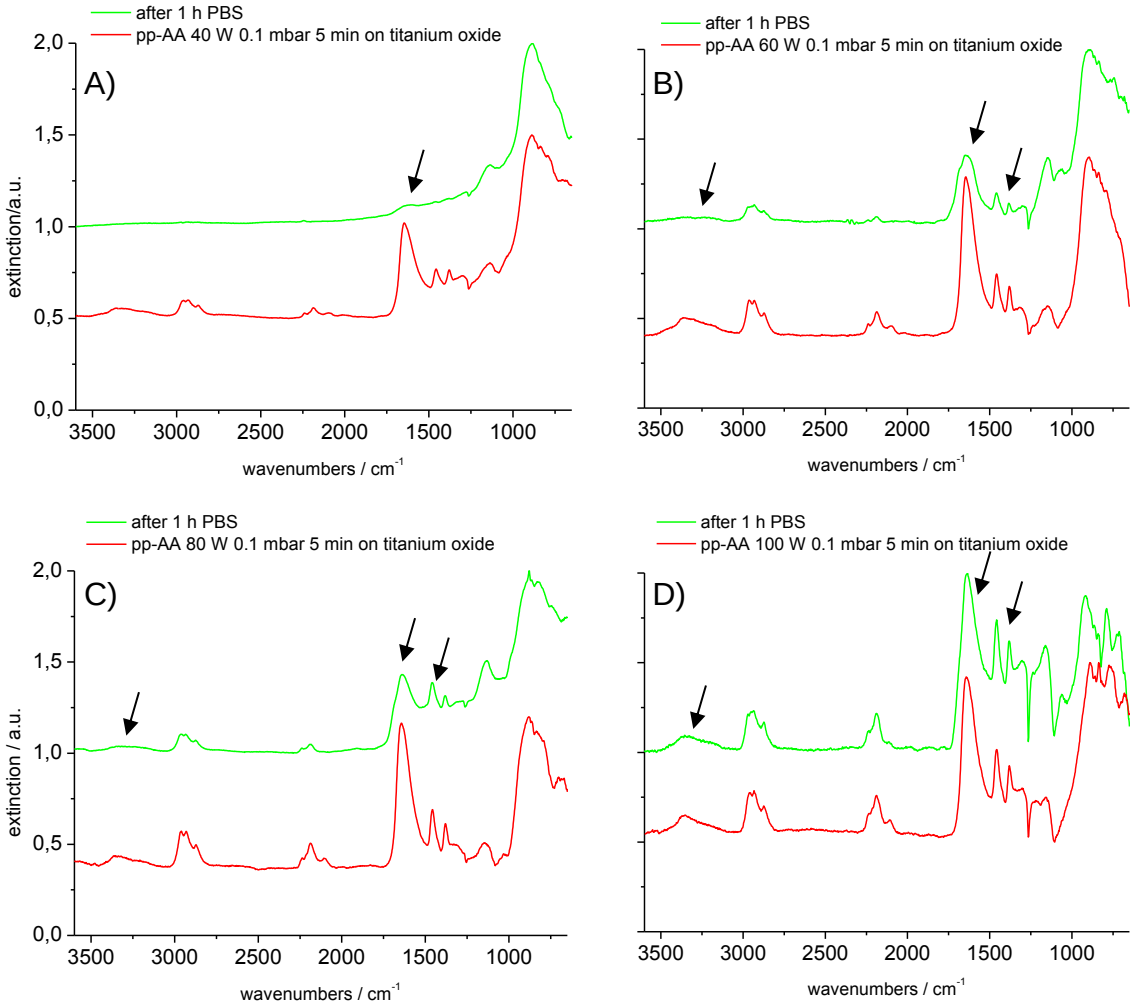

Figure 4.7 IRRAS spectra of pp-AA films on titanium oxide deposited with A) 40 W, B) 60 W, C) 80 W, D) 100 W process power and 0,1 mbar monomer pressure before and after PBS incubation. IR signals for amines and amides at 3300 cm^{-1} and 1630 cm^{-1} and for hydrocarbons at 1450 cm^{-1} and 1380 cm^{-1} are highlighted with black arrows.

In 4.5 – 4.7 it could be demonstrated that an increased stability of pp-AA films in PBS can be achieved by increasing the process power for the deposition. In order to obtain more information about the processes that occur during PBS incubation 100 W pp-AA films were investigated via SPR kinetic measurements. As

described in 3.2.2.12, changes of layer thickness and refractive index result in shifts of the surface plasmon. By following the SPR signal, the angle shifts provide qualitative information about dynamic processes within the plasma polymer film. Shown in figure 4.8 is one exemplary SPR kinetic measurement of a 100 W pp-AA film, incubated in PBS. This experiment has been repeated at least 3 times with a comparable outcome. It can be observed that the angle of incidence θ decreases within the first 60 minutes distinctly. According to literature, there are several events that take place during the incubation of plasma polymer films in aqueous solution such as swelling and leaching processes, resulting in changes of layer thickness and refractive index (Zhang et al., 2003). It can be suggested that for the 100 W pp-AA films, the events such as loss of unbound material and uptake of water, take place within the first 60 minutes. Afterwards, the angle of incidence stagnates, suggesting that the pp-AA films are stabilized and the mentioned processes are finished. A detailed discussion concerning the behavior of pp-AA films in aqueous solution is given in 5.2.1.

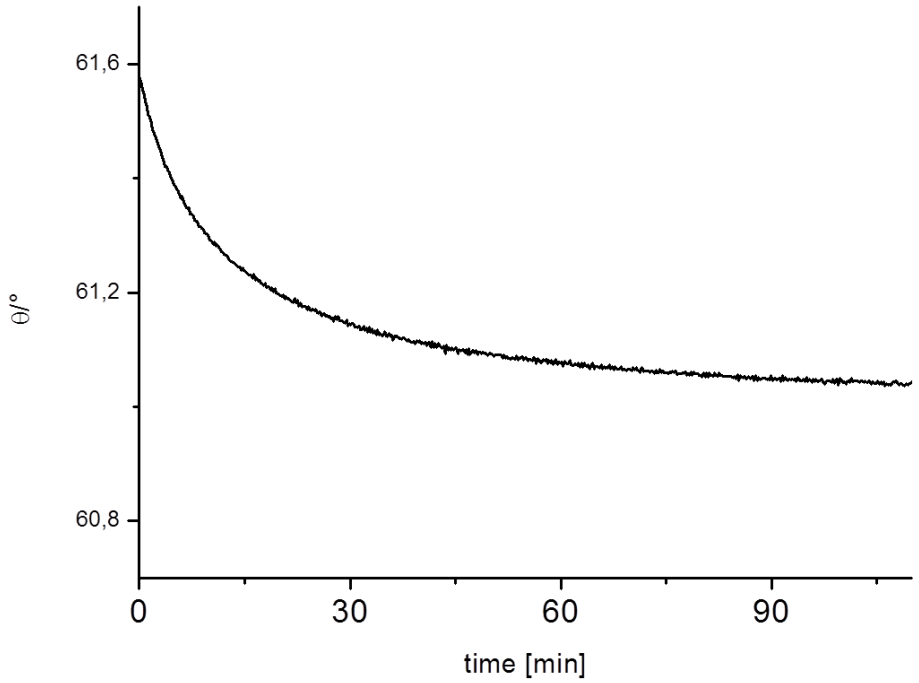

Figure 4.8 SPR kinetic measurement of a pp-AA film deposited with 100 W and 0,1 mbar monomer pressure in PBS. The decrease of the angle of incidence θ indicates swelling and leaching processes of pp-AA in PBS.

4.2.3 Functionality of Plasma Polymerized Allylamine

The functionality of pp-AA films correlates to the distribution and amount of primary amines on the surface, available for coupling chemistry. In figure 4.9 the distribution of primary amines of different pp-AA films is shown that were deposited with different process powers onto titanium. For the staining of the primary amines the FITC assay was used. Since the used assay is a qualitative method, the pp-AA films deposited with 40, 60, 80 and 100 W were investigated before PBS incubation. In comparison to the titanium control on which no staining can be seen, the green staining on pp-AA surfaces indicates a homogenous distribution of primary amines on all investigated samples.

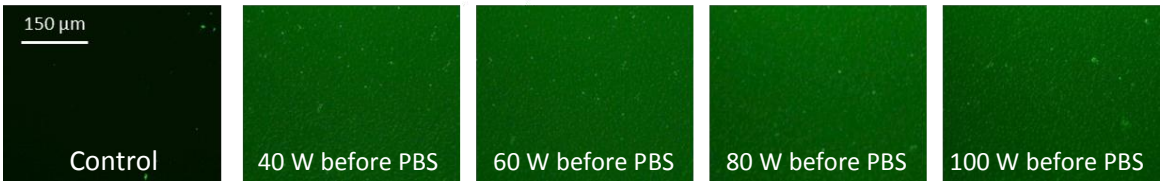

Figure 4.9 Distribution of primary amines of different pp-AA films before PBS incubation.

4.2.4 Quantification of Primary Amines in pp-AA Films

Since it could be shown that pp-AA films deposited with different plasma conditions partly lose material in aqueous solution, it was necessary to investigate the effect of material loss on the amount of primary amines. The amount of primary amines is thought to be the key parameter to evaluate the functionality of pp-AA films. For this reason, the sulfo-SDTB assay was used to determine the amount of primary amines on the pp-AA coated titanium samples as described in section 3.2.7. Due to the stability of pp-AA films in aqueous solution the primary amines were quantified before and after PBS incubation. Figure 4.10 shows the amount of primary amines, calculated as density per nm² of 3 independent experiments with pp-AA films of 20-30 nm thickness. In general, it can be observed that the amount of primary amines decreases in all investigated pp-AA films. In the case of the 40 W pp-AA films it can be observed that the amount of approximately 17 primary amines per nm² decreases after 1 hour of PBS incubation to 8 primary amines. An average loss of primary amines in the case of 60 W pp-AA films from approximately 14 to 6, for 80 W pp-AA films

from approximately 9 to 8 and in the case of 100 W pp-AA films from 8 to 6 can be seen.

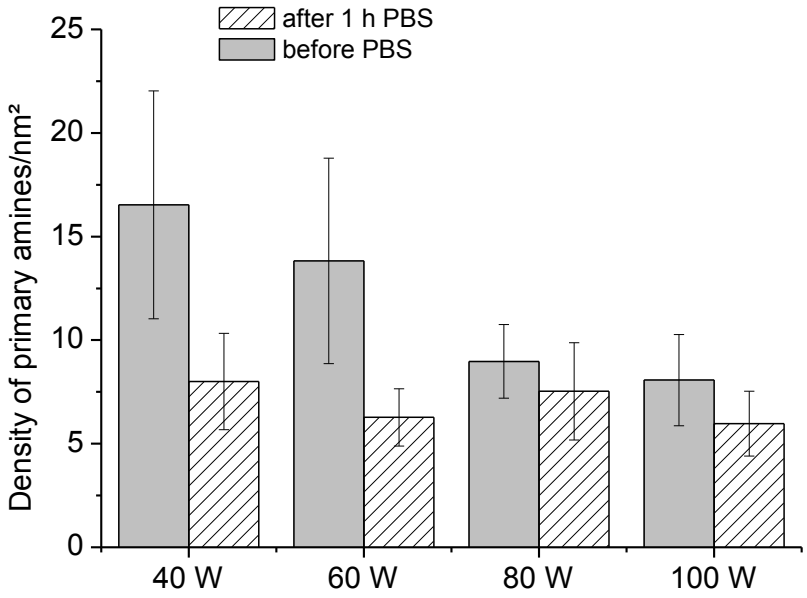

Figure 4.10 Quantification of primary amines in pp-AA films deposited with 40, 60, 80 and 100 W before and after 1 hour PBS incubation. Values are based on 3 independent experiments with pp-AA films of 20-30 nm thickness.

4.2.5 Mechanical Stability of pp-AA Films

When titanium implants are used as bone implants e.g. dental implants, the surfaces underlie strong shearing forces during the implantation procedure. Since pp-AA is the base of the surface modification it was important to investigate the mechanical stability of pp-AA as close as possible to the surgical bearing situation. For this purpose, commercial medical titanium screws were used and the mechanical stability was tested as described in 3.2.13.1. In total, three titanium screws were analyzed and representative pictures with various magnifications are shown in figure 4.11 and 4.12. It can be observed that the pp-AA film suffers from the screwing procedure. In the lower part of the screw the screwing procedure seems to attack the film stronger compared to the upper part. In 4.12 the higher magnification reveals that the screwing procedure has a strong scratching effect on the pp-AA film. Nevertheless, the pp-AA film remains partly on the surface.

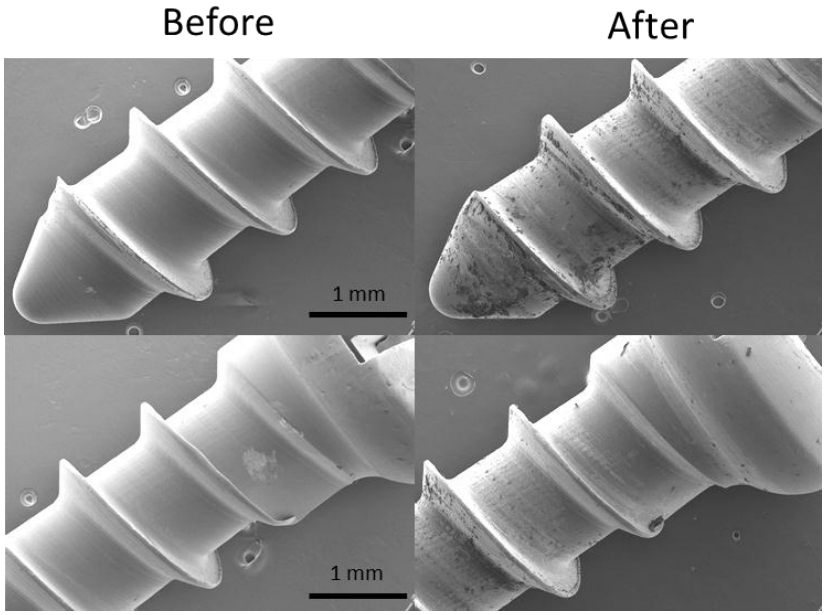

Figure 4.11 SEM pictures of pp-AA coated titanium screws before and after screwing in a femur bone of a pig.

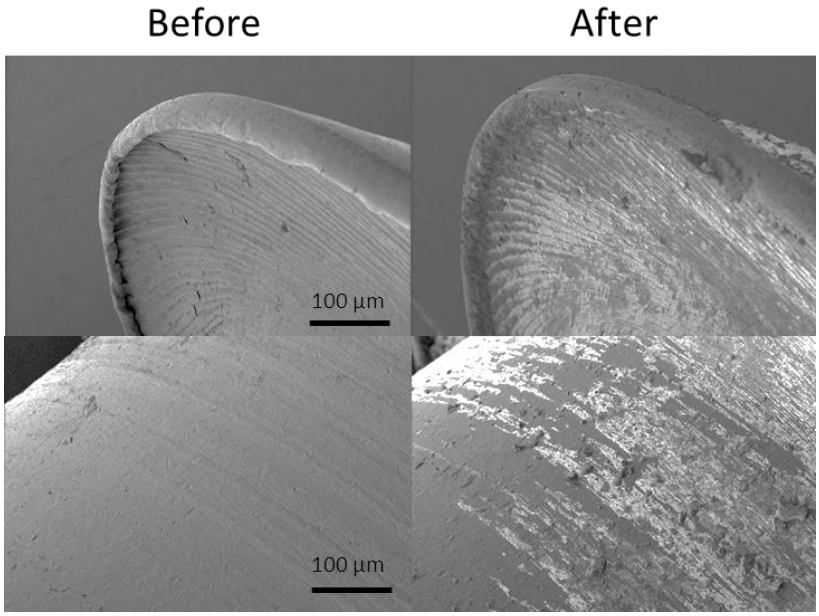

Figure 4.12 SEM pictures with a higher magnification of pp-AA coated titanium screws before and after screwing in a femur bone of a pig.

4.3 Immobilization/Co-Immobilization of Biomolecules

The main aim of this work was the development of biomimetic surfaces with co-immobilized RGD and VEGF in order to stimulate cells regarding to cell adhesion and cellular stimulation. For a controllable wet chemical co-immobilization, as mentioned in section 3.2.3, it was necessary to use various cross-linkers with two different functionalities.

4.3.1 Cross-linker Immobilization

4.3.1.1 Immobilization of α-Maleinimidohexanoic-ω-*N*-Hydroxysuccinimide-Polyethylene Glycol

In the SPR kinetic measurement of figure 4.13 A, the immobilization of the cross-linker α-maleinimidohexanoic-ω-*N*-hydroxysuccinimide polyethylene glycol can be observed. After the 100 W pp-AA film is stabilized in PBS, indicated by the stagnating SPR signal, the cross-linker is added to the sample for approximately 15 minutes. A drastic rise of the signal occurs after addition of the Mal-NHS-linker due to the change of refractive index of the linker solution compared to PBS. The adsorption kinetics that can be observed during SPR measurements can be understood as superposition effects of adsorption and diffusion (Laschitsch et al., 2000). After rinsing with PBS, the signal drops to a plateau. The increase of the angle of incidence after cross-linker incubation and rinsing with PBS of 0,29° indicates the successful immobilization due to the change in refractive index and/or layer thickness. Analyzing the IR spectra before and after cross-linker incubation as shown in figure 4.13 B, it can be observed that in comparison to the IR spectrum of the pp-AA film (black spectrum), after incubation of the Mal-NHS-linker, there are new signals created (green) at approximately 1740 cm^{-1} and 1705 cm^{-1} (right arrow) and at approximately 2900 cm^{-1} (left arrow). The comparison with the ATR spectrum of the cross-linker gives evidence that the new created signals stem from the Mal-NHS-linker. According to literature, the signals around 1700 cm^{-1} indicate the symmetric and asymmetric maleimide C=O stretches, whereby the signals around 3000 are due to maleimide and aromatic C-H stretching (Shen et at., 2004).

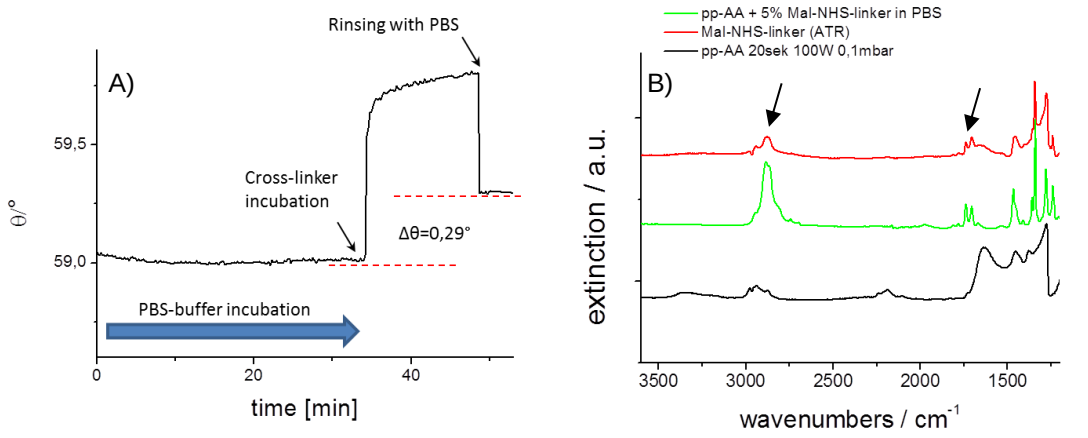

Figure 4.13 A) SPR kinetic measurement of the binding process of α-maleinimidohexanoic-ω-*N*-hydroxysuccinimide polyethylene glycol (Mal-NHS-linker). The change of the angle of incidence (Δθ) indicates the successful cross-linker immobilization. B) Infrared spectra of pp-AA before and after cross-linker incubation. New peaks are created after cross-linker immobilization, indicating the presence of the Mal-NHS linker on pp-AA (black arrows).

4.3.1.2 Immobilization of α, ω-Bis-*N*-Hydroxysuccinimide Polyethylene Glycol

Figure 4.14 A shows the SPR kinetic measurement of α, ω-bis-*N*-hydroxysuccinimide polyethylene glycol on a 100 W pp-AA film. Corresponding to the result as shown in figure 4.8, the decrease of the SPR signal within the first 60 minutes, indicates leaching and swelling processes of the pp-AA film. Reasons for the distinct increase of the signal after cross-linker incubation were already described above. After approximately 75 minutes, it can be observed that after PBS rinsing the SPR signal drops to a plateau. The increased angle of incidence of 0,17° after cross-linker incubation and rinsing with PBS gives evidence of the successful cross-linker immobilization, due to changes in the refractive index and/or layer thickness of the immobilized linker molecules. The presence of the cross-linker after immobilization can be seen in the IR spectrum of 4.14 B), indicated by newly created IR signals after Di-NHS-linker immobilization (arrows). At 1740 cm^{-1} there is one distinct peak, showing the C=O stretching of the *N*-hydroxysuccinimide group on the pp-AA film. At 2890 cm^{-1} the C-H signal is increased after immobilization indicating the presence of the cross-linker after immobilization. The comparison of the ATR spectrum of the Di-NHS linker with the new created signals after cross-linker immobilization, gives evidence of the presence of the cross-linker.

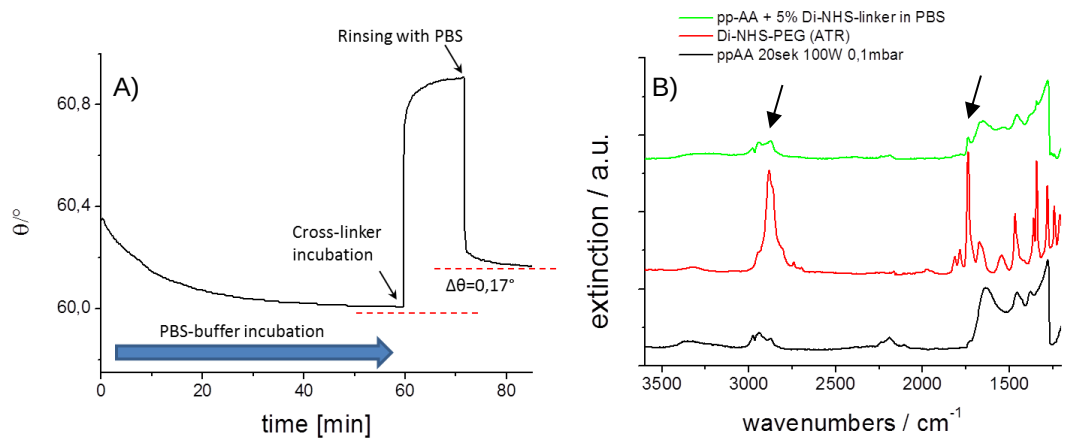

Figure 4.14 A) SPR kinetic measurement of the binding process of α, ω-bis-*N*-hydroxysuccinimide polyethylene glycol Di-NHS-linker. The change of the angle of incidence (Δθ) indicates the successful cross-linker immobilization. B) Infrared spectra of pp-AA before and after cross-linker incubation. New peaks are created after cross-linker incubation, indicating the presence of the Di-NHS-linker on pp-AA (black arrows).

4.3.1.3 Co-immobilization of α-Maleinimidohexanoic-ω-*N*-Hydroxysuccinimide Polyethylene Glycol and α, ω-Bis-*N*-Hydroxysuccinimide Polyethylene Glycol

Figure 4.15 shows the SPR kinetic measurement of the binding process of the two used cross-linker as described in 3.2.3.3. Corresponding to the results of the single immobilization of the used linker molecules, the co-immobilization can be observed after incubation on a 100 W pp-AA film. The increased angle of incidence of 0,31° after cross-linker incubation and rinsing with PBS shows the successful cross-linker immobilization. The Infrared spectra are not shown here. Because of superposition of both spectra it was not possible to distinguish between specific IR signals of the used linker molecules.

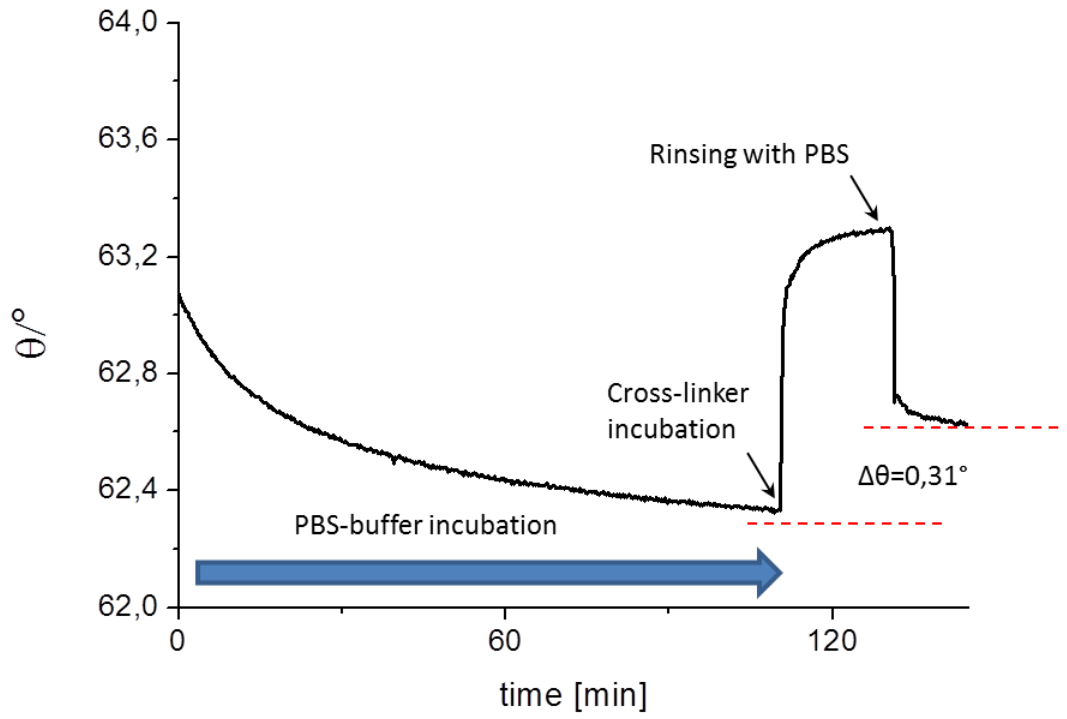

Figure 4.15 SPR kinetic measurement of the binding process of α-maleinimidohexanoic-ω-*N*-hydroxysuccinimide polyethylene glycol and α, ω-bis-*N*-hydroxysuccinimide polyethylene glycol. The change of the angle of incidence (Δθ) indicates the successful cross-linker immobilization.

4.3.2 RGD Immobilization

The covalent immobilization of the RGD peptide was conducted using α-maleinimidohexanoic-ω-*N*-hydroxysuccinimide polyethylene glycol. The SPR kinetic measurement of 4.16 shows in the first 80 minutes the PBS incubation of the pp-AA film. The decrease of the SPR signal during the PBS incubation time was described above. After cross-linker incubation a drastic increase of the angle of incidence occurs and the adsorption can be observed. Rinsing with PBS leads to a distinct decrease of the SPR signal. The change of 0,05° before and after Mal-NHS-linker incubation indicates the successful cross-linker immobilization. After 120 minutes RGD is added to the pp-AA sample. An adsorption curve can be seen and after rinsing with PBS the increased angle of incidence of 0,03° indicates the successful RGD immobilization. The water contact angle measurements reveal that the immobilization of the cross-linker leads to a distinct decrease of the water contact angle to 23°, indicating the presence of the hydrophilic polyethylene glycol cross-linker. After the immobilization of RGD the

contact angle rises again to 51°, giving a hint of the presence of the immobilized RGD.

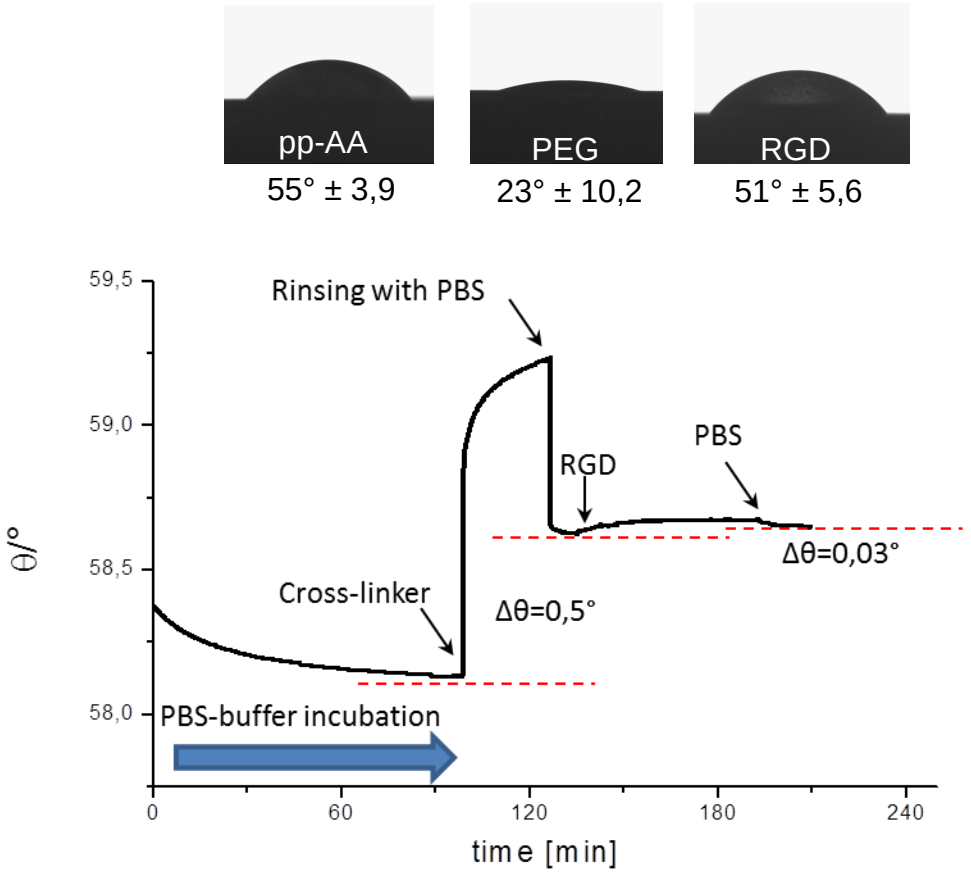

Figure 4.16 SPR kinetic measurement of the RGD immobilization using α-maleinimidohexanoic-ω-*N*-hydroxysuccinimide polyethylene glycol. The step-wise increase of the angle of incidence (Δθ) indicates the immobilization of RGD. Additionally, results of water contact angle experiments of 3 independent measurements during the RGD modification steps on titanium are shown.

4.3.3 VEGF Immobilization

For the VEGF immobilization α, ω-bis-*N*-hydroxysuccinimide polyethylene glycol was used as described in section 3.2.3.2. BSA was used as VEGF replacement for the SPR kinetic measurement, to prove the principle of the immobilization procedure as described in 3.2.12.

Figure 4.17 shows SPR kinetic measurements of the BSA immobilization using different protein concentration in PBS. In order to compare the influence of different BSA concentrations on the immobilization, SPR sensors as well as pp-AA films from the same batch were utilized to keep parameters of possible influence of the measurements constant.

The stepwise increase of the SPR signal in all measurements after cross-linker incubation and after BSA incubation indicates the covalent immobilization, first of the cross-linker molecules and finally of BSA. It can be seen that a higher concentration of 2 mg/ml BSA also results in a higher signal increase of 0,08° (4.17 B) after BSA immobilization, compared to a concentration of 1 mg/ml BSA with 0,027°. It was found in earlier works that the plasmon shift is approximately proportional to the adsorbed amount of adsorbates (Laschitsch et al., 2000). Due to this, it can be assumed that a concentration of 2 mg/ml BSA results in higher amounts of immobilized BSA compared to 1 mg/ml BSA.

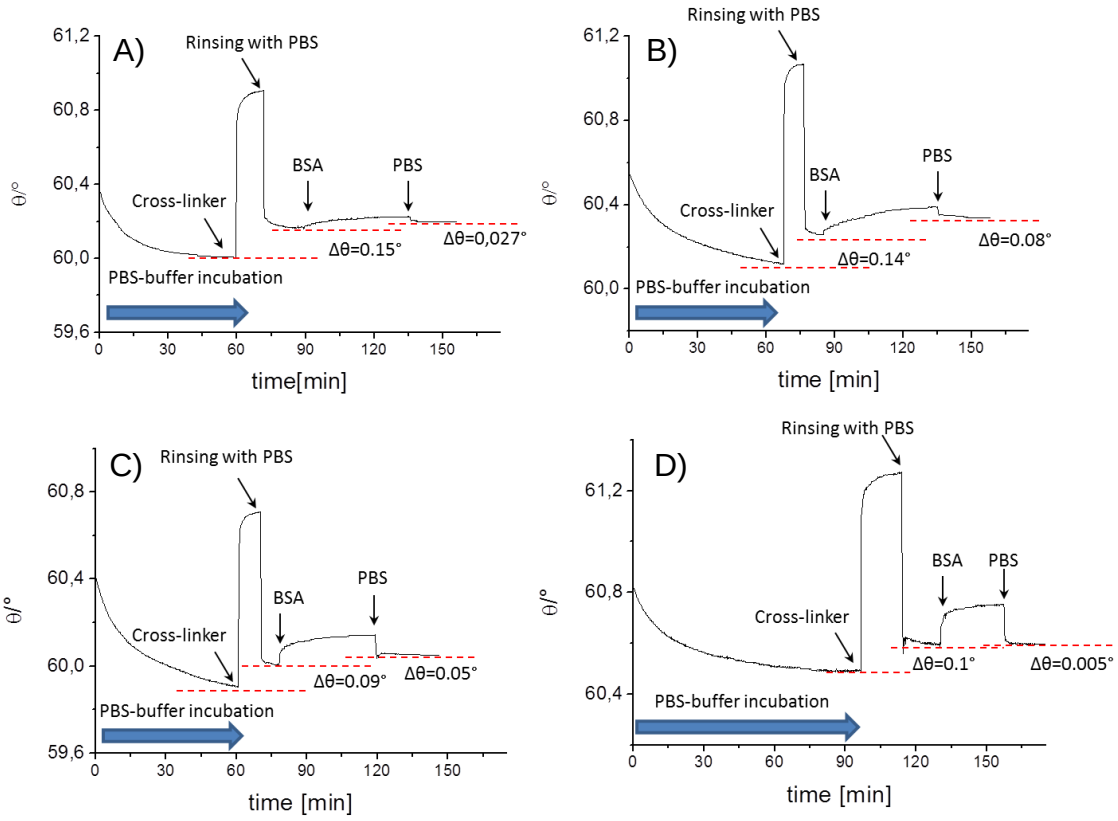

Figure 4.17 SPR kinetic measurement of Bovine Serum Albumin (BSA) immobilization using α, ω-bis-*N*-hydroxysuccinimide polyethylene glycol and different concentrations of BSA in PBS. A) 1 mg/ml, B) 2 mg/ml, C) 5 mg/ml, D) 10 mg/ml. The step-wise increase of the angle of incidence (Δθ) indicates the immobilization of BSA.

After increasing the BSA concentration, more distinct changes of the SPR signal were expected, due to higher amounts of immobilized BSA, associated with changes in layer thickness and/or refractive index. In contrast to this, higher concentrations than 2 mg/ml of BSA result in decreased changes of the angle of

incidence of 0,05° in the case of 5 mg/ml BSA and 0,005° using 10 mg/ml BSA. It can be suggested that the amount of immobilized protein depends on the used protein concentration. The excess of a certain concentration threshold seems to result in a decreased amount of immobilized protein.

Figure 4.18 shows the SPR kinetic measurements of the passive BSA adsorption on pp-AA (A) and the covalent immobilization of BSA (B) with a concentration of 2 mg/ml as already shown in figure 4.17 B. Furthermore, results of the water contact angle measurements of the covalent VEGF immobilization can be seen.

The decrease of the SPR signal during the PBS incubation of the pp-AA coated surfaces in 4.18 A and B was already described above. In 4.18 A, it can be observed that the BSA incubation results in a distinct increase of the SPR signal. After BSA adsorption and rinsing with PBS the increased angle of incidence of 0,65° indicates the passive BSA adsorption. In the case of the covalent BSA immobilization as shown in figure 4.18 B, the Di-NHS-linker incubation leads to a distinct rise of the SPR signal and an adsorption curve can be seen. After approximately 75 minutes, PBS rinsing leads to a drastic decrease of the signal that drops to a plateau. The overall increase of the angle of incidence before and after cross-linker incubation of 0,14° indicates the immobilization of the linker molecules. After incubation with BSA an adsorption curve can be observed and after rinsing with PBS the signal increase of 0,08° gives evidence of the successful BSA immobilization. The higher increase of the SPR signal in the case of the passive BSA adsorption compared to the covalent BSA immobilization can be understood as consequence of higher amounts of passive adsorbed BSA molecules as already described above.

For water contact angle measurements, VEGF was used for the immobilization. Corresponding to the results of the RGD immobilization as shown in section 4.3.2, a change of the water contact during wet chemical modification steps can be seen. After cross-linker immobilization the contact angle decreases due to the hydrophilic properties of the polyethylene glycol chain of the cross-linker as already seen in the case of the RGD immobilization in figure 4.16. After VEGF immobilization an increase of water contact angle can be observed, giving a hint of the presence of VEGF.

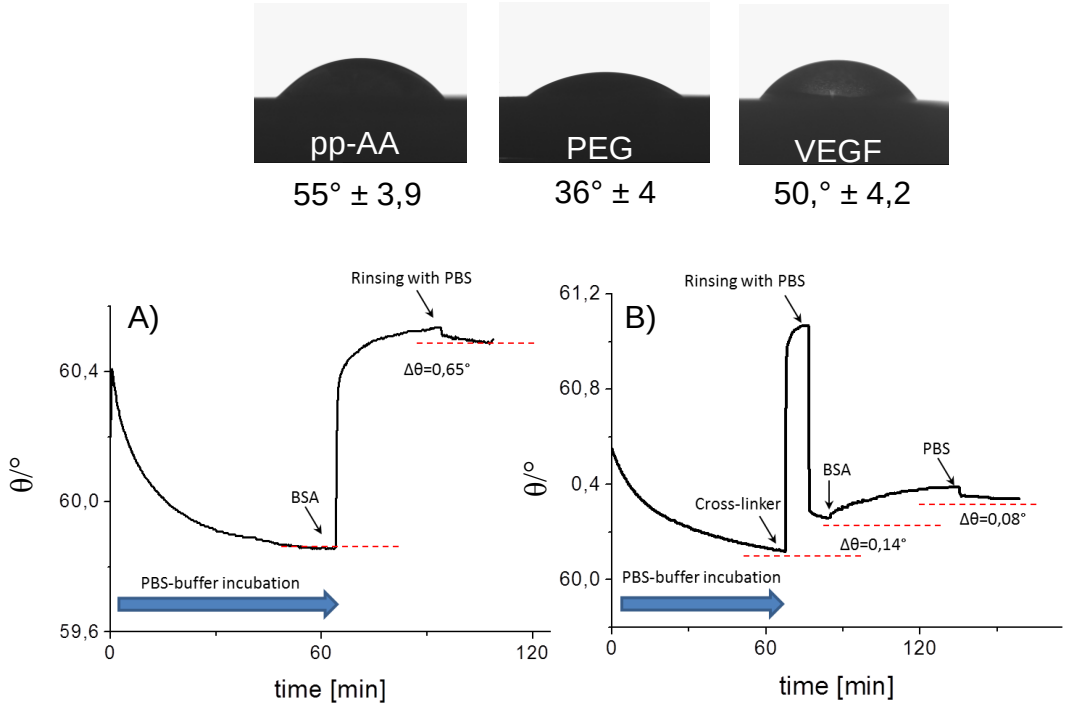

Figure 4.18 SPR Kinetic measurement of A) passive absorbed Bovine Serum Albumin (BSA) and B) covalent immobilization of BSA on pp-AA using α, ω-bis-*N*-hydroxysuccinimide polyethylene glycol. Additionally, results of water contact angle experiments of 3 independent measurements during the covalent VEGF immobilization steps on titanium are shown.

4.3.4 RGD/VEGF Co-Immobilization

The SPR kinetic measurement of figure 4.19 demonstrates the developed two-step co-immobilization procedure of BSA and RGD.

Corresponding to the results of the co-immobilization of the used linker molecules as described in 4.3.1.3, the SPR signal increase of 0,22° after cross-linker incubation and rinsing with PBS demonstrates the immobilization of the used linker molecules.

The two-step co-immobilization of BSA and RGD can be demonstrated by the stepwise increase of the angle of incidence, first after BSA incubation of 0,04°, and finally after the RGD incubation of 0,05°. The results of the water contact angle measurement in 4.19 support the presented data of the SPR kinetic measurement. Corresponding to the results of the RGD and VEGF immobilization as described in 4.3.2 and 4.3.3, the water contact angle first decreases after the immobilization of the used cross-linkers due to their hydrophilic properties. After

the co-immobilization of RGD and VEGF, the increased contact angle gives a hint of the presence of the biomolecules.

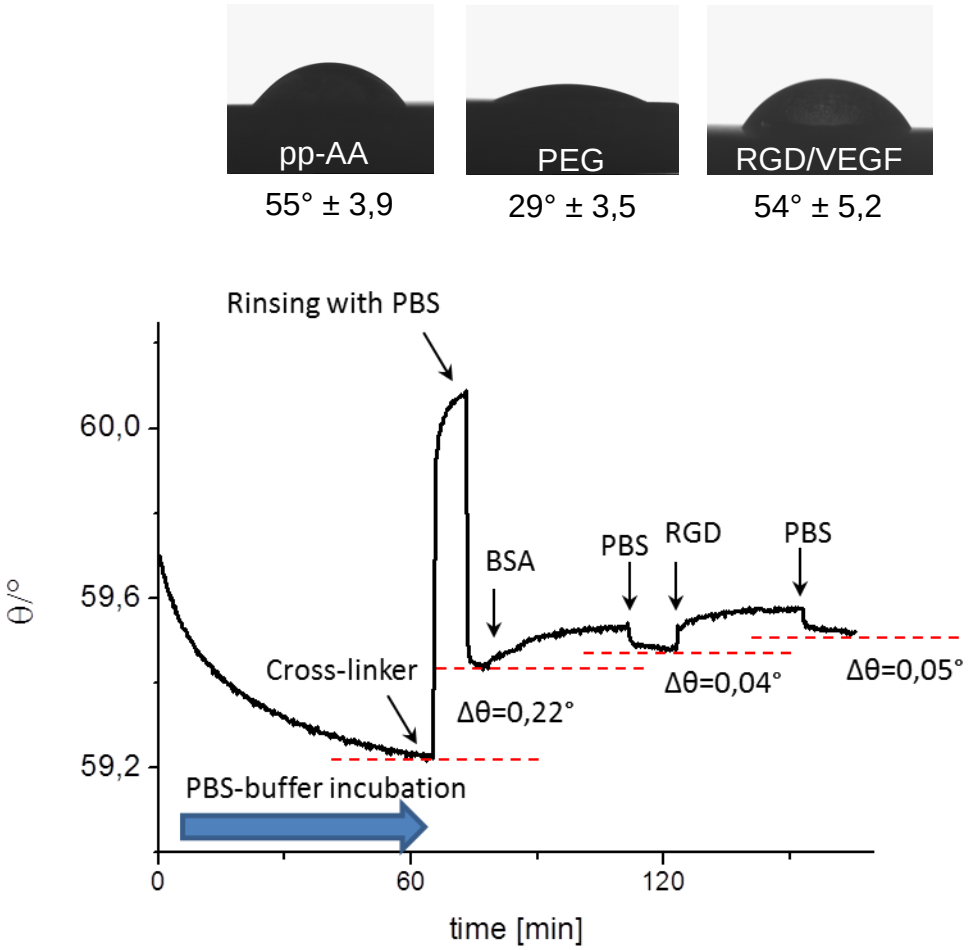

Figure 4.19 BSA and RGD co-immobilization via two-step procedure. Used cross-linkers are α-maleinimidohexanoic-ω-*N*-hydroxysuccinimide polyethylene glycol and α, ω-bis-*N*-hydroxysuccinimide polyethylene glycol. The stepwise increase of the angle of incidence (Δθ) indicates the separated two-step co-immobilization of BSA and RGD. Additionally, results of water contact angle experiments of 3 independent measurements during the RGD and VEGF co-immobilization steps on titanium are shown.

4.3.5 X-Ray Photoelectron Spectroscopy

XPS measurements were used to determine the elemental composition of the different modified surfaces as described in section 3.2.11. Table 4.3 shows the original data set of the elemental survey measurements of the different modified surfaces during the wet chemical modification steps. Looking at the spectra of the 100 W pp-AA film, a carbon to nitrogen ratio of 6:1 can be seen. After immobilization of the cross-linker molecules the amount of nitrogen decreases,

whereby the oxygen content increases. The amount of nitrogen after RGD and VEGF immobilization does not increase compared to the samples that were modified only with the cross-linkers. In the case of the modified surfaces with co-immobilized RGD and VEGF the amount of oxygen decreases, whereby the amount of nitrogen increases.

The carbon/nitrogen ratio of the 100 W pp-AA films differs from the ratio found in the monomer of carbon to nitrogen of 3:1, suggesting a high degree of monomer fragmentation during the plasma process at 100 W, associated with an increase of hydrocarbon component and a loss of primary amines (Zhang et al., 2003). The increase of the oxygen content after cross-linker incubation was expected due to the higher content of oxygen in the polyethylene glycol chain compared to that found in allylamine. After RGD/VEGF co-immobilization the decreased oxygen content in combination with a higher content of nitrogen gives a hint for the presence of the biomolecules due to an increased relative amount of primary amines within the biomolecules compared to the cross-linker molecules. Against expectations, the relative amount of nitrogen did not increase after RGD and VEGF single immobilization.

Table 4.3 Elemental composition of the surfaces during the RGD, VEGF and RGD/VEGF modification steps.

Surface	C/%	O%	N/%
pp-AA	80,82	4,96	13,44
pp-AA/Linker 1*	76,96	10,61	10,43
pp-AA/Linker 1/RGD	77,37	13,64	7,73
pp-AA/Linker 2*	73,2	13,95	11,53
pp-AA/Linker 2/VEGF	75,99	15,83	6,81
pp-AA/Linker 1+2	75,35	13,05	9,33
pp-AA/Linker 1+2 / RGD/VEGF	77,45	9,51	11,21

* Linker 1 = α-maleinimidohexanoic-ω-*N*-hydroxysuccinimide polyethylene glycol

* Linker 2 = α, ω-bis-*N*-hydroxysuccinimide polyethylene glycol.

4.3.6 VEGF Quantification

The challenge of the VEGF quantification on the titanium surfaces was the development of the solid phase ELISA. Because of the fact that the standard human VEGF ELISA Kit purchased by R&D systems was not designed for the utilization as solid phase ELISA, the whole ELISA procedure had to be adapted to the system of 1 cm^2 titanium samples in 24 well plates. The first crucial step for a reliable quantification was the establishment of an appropriate standard. In figure 4.20 A a standard curve of different VEGF concentrations on capture antibody coated titanium samples is shown. It can be seen that the amount of adsorbed VEGF increases in correlation to the used concentrations. Above the concentration of 5 µg/ml the standard curve shows only a slight increase, suggesting that at this concentration the capture antibody coated surfaces are saturated and no further amounts of VEGF can be bound. In figure 4.20 B the results of one representative VEGF Solid Phase ELISA is shown. It can be observed, that on the surface that was co-immobilized with RGD and VEGF the measured optical density is distinctly increased compared to the titanium control, indicating immobilized VEGF. On the surface that was immobilized with VEGF only, a more distinct increase of optical density can be seen, suggesting a higher amount of immobilized VEGF. In order to determine the amount of immobilized VEGF, it is essential to generate a standard with values of optical density in the range of the investigated samples via solid phase ELISA. Comparing the scales of the optical density of the shown diagrams of figure 4.20, the range of the solid phase ELISA for the VEGF quantification is way below the scale of the standard, making a determination of immobilized VEGF impossible. Nevertheless, the results can be understood as qualitative proof of the VEGF immobilization and/or co-immobilization. The measurements of all experiments are shown in annex 8.1.3. More details of the analysis will be discussed in section 5.3.6.

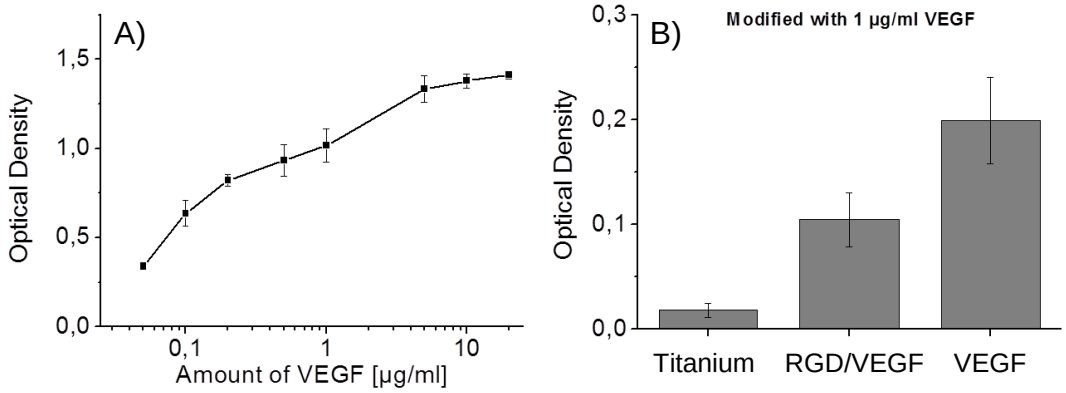

Figure 4.20 Shown representative result has been performed in triplicate. A) Standard curve of different VEGF concentrations on capture antibody coated titanium samples. B) Results of the solid phase ELISA of VEGF and RGD/VEGF modified samples.

4.4 Cell Experiments

4.4.1 Cell Adhesion on RGD Modified Titanium

In Figure 4.21, the results of the cellular response regarding to cell adhesion of HUVECs on RGD modified titanium surfaces are shown. After 24 hours and 3 days, there seems to be no enhancing effect on RGD modified surfaces compared to titanium and pp-AA modified samples. After 7 days, there is a slightly enhanced effect on cell adhesion observable. In accordance to this, similar values of the calculated cell coverage after 24 hours on titanium with 4,7 % and on RGD modified samples with 5,7 % can be seen in 4.22. On pp-AA coated surfaces there is after 24 hours the highest cell coverage observable with 15,7 %. After 3 days the highest calculated value for cell coverage can be observed on titanium with 7,9 %, 6 % on pp-AA coated surfaces and the lowest cell coverage on RGD modified surfaces with 3,5 %. In contrast to this after 7 days the cell coverage on RGD modified samples with 28,5 % is significantly increased ($p<0,05$) compared to titanium with 13 %. On pp-AA coated samples, a cell coverage of 23,4 % can be observed.

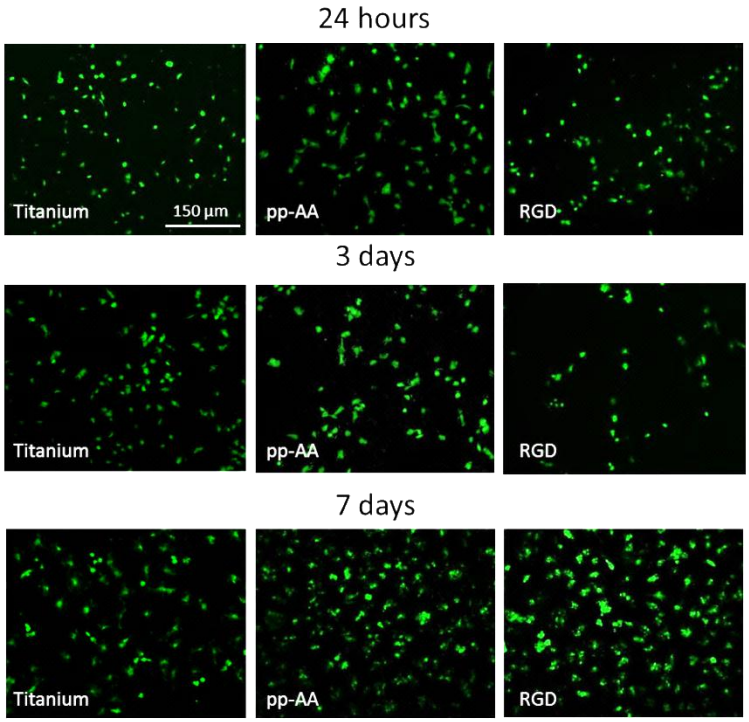

Figure 4.21 Cell adhesion of HUVECs on titanium, pp-AA coated titanium and RGD modified titanium surfaces. Only after 7 days an enhanced cell adhesion can be observed on RGD modified samples.

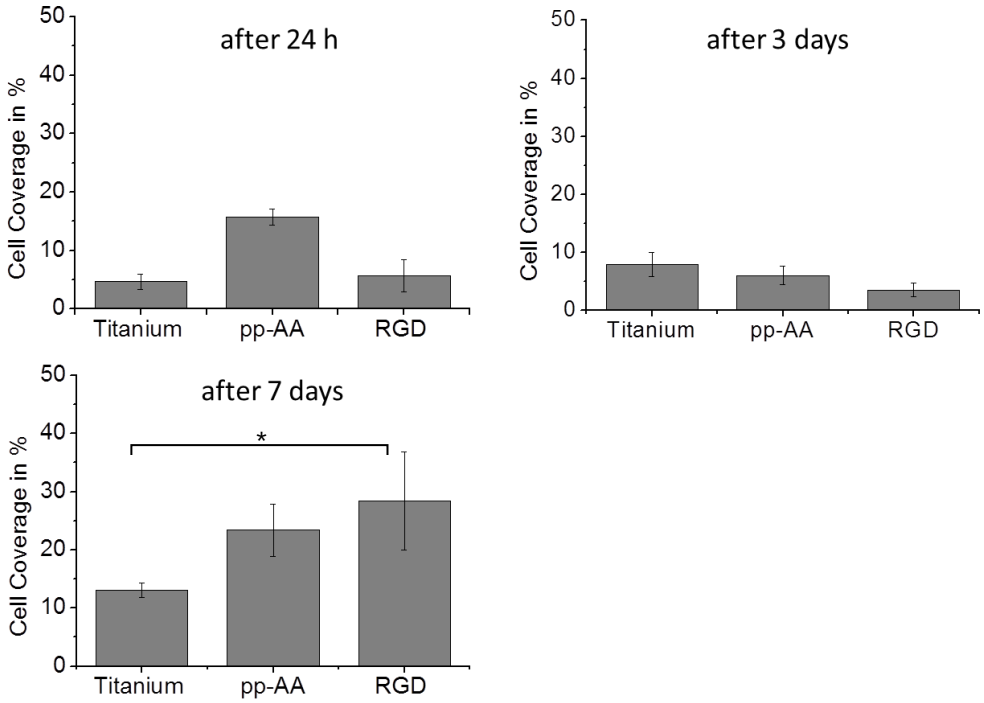

Figure 4.22 Cell coverage of HUVECs on titanium, pp-AA coated titanium and RGD modified titanium surfaces (* for p<0,05 is significant).

4.4.2 Effect of dissolved VEGF on HUVECs

In figure 4.23 it can be seen that gradual increase of VEGF concentration leads to a gradual increase of cell adhesion. After 24 hours, HUVECs adhesion is equally increased in 10 ng/ml, 20 ng/ml and 50 ng/ml VEGF compared to the lowest concentration of 1 ng/ml. The highest concentration of 100 ng/ml leads to the most distinct enhancement of cell adhesion compared to all other samples. Accordingly, the results of the determined cell coverage in 4.24 reveal significantly increased cell coverage of 31,3 % in medium with 100 ng/ml VEGF compared to 1 ng/ml with 9,7 % ($p<0,001$), 10 ng/ml with 17,8 % ($p<0,05$), 20 ng/ml with 19,9 % ($p<0,05$) and 50 ng/ml with 20,2 % ($p<0,05$). After 3 days it can be observed that the number of adhered HUVECs is distinctly decreased compared to 24 hours. Nevertheless, also after 3 days the stimulating effect on cellular adhesion of HUVECs shows a concentration dependent effect. In samples with 1 ng/ml and 10 ng/ml VEGF there is the lowest number of adhered cells observable. In 20 ng/ml, 50 ng/ml and 100 ng/ml VEGF, cell adhesion seems to be equally enhanced. Corresponding to this, a cell coverage of samples with 1 ng/ml VEGF with 2,3 % and 10 ng/ml with 2 % can be observed. The Cell coverage of samples with 20 ng/ml (5,7 %), 50 ng/ml (4,2 %) and 100 ng/ml (6,7 %) shows equal values. Concerning the statistical analysis, the cell coverage of samples with 100 ng/ml is significantly increased compared to concentrations of 1 ng/ml ($p< 0,01$) and 10 ng/ml ($p< 0,01$) VEGF. Additionally, significant increased cell coverage was calculated in samples with 20 ng/ml VEGF compared to 1 ng/ml ($p<0,05$) and 10 ng/ml ($p<0,05$) VEGF.

The results of figure 4.23 and 4.24 reveal that the cell adhesion and cell coverage on all samples decreases distinctly after 3 days compared to 24 hours. Although an effect of higher VEGF concentrations can also be seen after 3 days, it seems that only VEGF is not sufficient to stimulate cells over a longer period than 3 days. Due to the fact that this experiment has been performed in triplicate once, the shown observations can be regarded as preliminary results. Nevertheless, they demonstrate that the cellular response seems to depend strongly on the VEGF concentration.

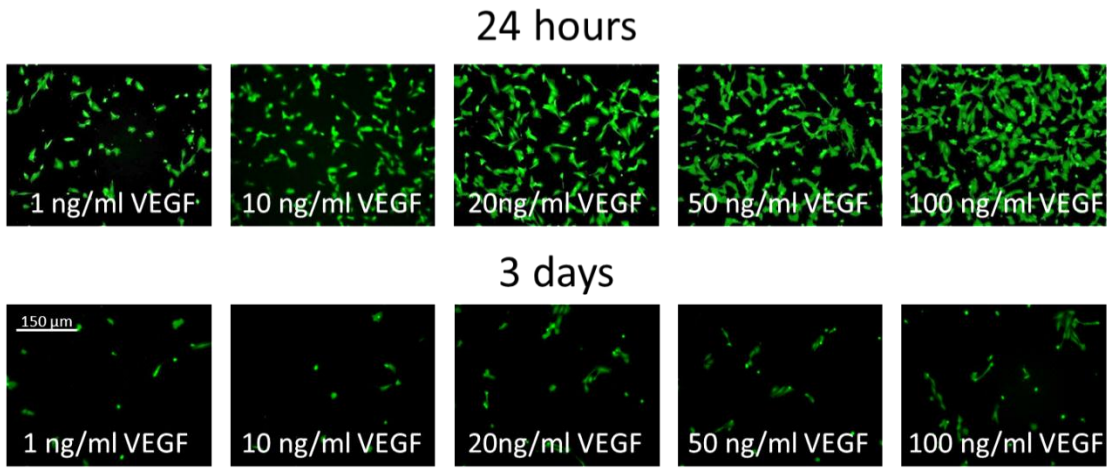

Figure 4.23 Effect of various dissolved VEGF concentrations on cell adhesion of HUVECs. Cell stimulation of HUVECs correlates to the VEGF concentration.

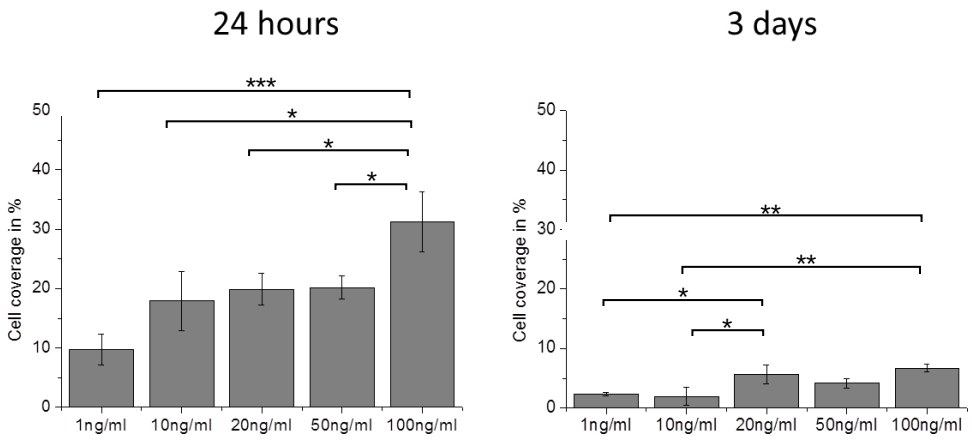

Figure 4.24 Percentage of cell coverage of HUVECs in various VEGF concentrations (* for p<0,05 is significant, ** for p<0,01 is highly significant, *** for p<0,001 is extremely significant).

4.4.3 Effect of VEGF Modified Titanium on the Cellular Response

The Vascular Endothelial Growth Factor plays an important role in angiogenesis as described in section 1.2.3. In order to investigate the cellular response of HUVECs on VEGF modified titanium, cells were visualized with calcein staining after 24 hours and 3 days of cultivation on the modified surfaces. Furthermore, the percentage of cell coverage was determined and statistical calculations were conducted as described above. Different concentrations of VEGF were used for the immobilization in order to investigate, whether differences in cellular response can be observed, due to different amounts of immobilized VEGF. The results of

4.24 show three different pilot studies that were performed for each concentration once in triplicate. The cell adhesion experiments reveal that on modified titanium using 1 µg/ml and 10 µg/ml VEGF for the immobilization, no distinct enhancement of cell adhesion can be observed compared to titanium and pp-AA coated samples after 24 hours. On titanium modified with a concentration of 20 µg/ml VEGF, cell adhesion is distinctly enhanced. After 3 days of cultivation similar results can be found. Only the surfaces modified with 20 µg/ml VEGF show a strong enhancement of cell adhesion. Corresponding to this, it can be seen in figure 4.26 that the cell coverage only on samples modified with 20µg/ml VEGF is after 24 hours with 32,3 % significantly increased compared to titanium with 7,4 % ($p<0,001$) and pp-AA coated samples with16 % ($p<0,01$) cell coverage. The same observation can be made after 3 days. With 28,8 % only on samples modified with 20 µg/ml VEGF the cell coverage is significant higher than on titanium with 8,2 % ($p<0,001$) and on pp-AA coated titanium with 5,3 % ($p<0,001$) cell coverage. It can be suggested that only with a concentration of 20 µg/ml VEGF, sufficient amounts of protein are immobilized that are necessary for cellular stimulation of HUVECs.

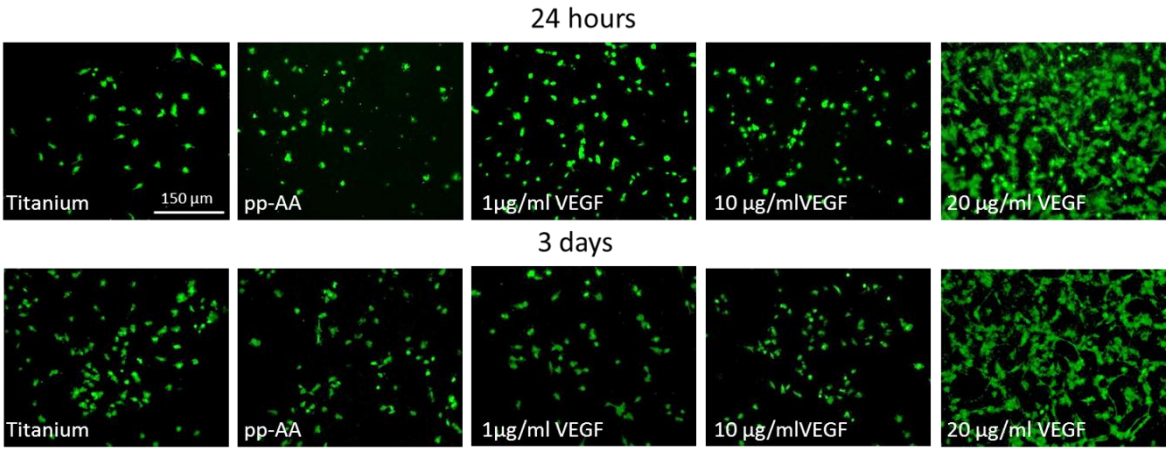

Figure 4.25 Cell adhesion of HUVECs on titanium, pp-AA coated titanium and VEGF modified titanium surfaces. For the VEGF immobilization used VEGF concentrations: 1 µg/ml, 10 µg/ml, 20µg/ml.

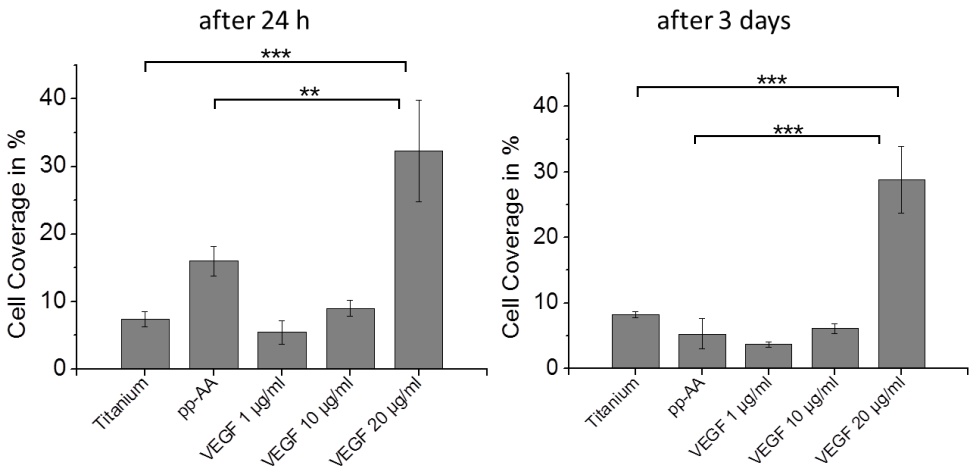

Figure 4.26 Cell coverage of HUVECs on titanium, pp-AA coated titanium and VEGF modified titanium surfaces using different VEGF concentrations (* for p<0,05 is significant, ** for p<0,01 is highly significant, *** for p<0,001 is extremely significant).

4.4.4 Effect of RGD/VEGF Modified Titanium on the Cellular Response

In figure 4.27 the results of the cell adhesion experiments of HUVECs are shown that were cultivated on titanium, co-immobilized with RGD and VEGF. According to the different concentrations that were used for the single immobilization of VEGF, also for the co-immobilization the described concentrations of VEGF were used. In the case of the RGD-peptide, only one concentration was used as described in 3.2.3.1. As described above, also in the case of the RGD/VEGF surfaces, the cell experiments were performed in pilot studies once in triplicate for each VEGF concentration. After 24 hours it can be observed, that there is a slightly higher cell adhesion of HUVECs recognizable on modified samples using 1 µg/ml and 20 µg/ml VEGF compared to the titanium control. Concerning the fact that on the pp-AA modified samples the cell adhesion is equally enhanced, a distinct effect of neither RGD nor VEGF can be suggested. After 3 days only on the modified sample that was modified with RGD and VEGF using a concentration of 20 µg/ml VEGF an enhancement of cell adhesion can be seen compared to all investigated surfaces. Analyzing the cell coverage in figure 4.28, after 24 hours a slight increase on all samples can be observed compared to titanium. With reference to the samples co-immobilized with RGD and VEGF only on samples co-immobilized with RGD and a concentration of 20 µg/ml VEGF a significant higher cell coverage of 13,2 % compared to titanium with 7,3 % (p<0,01) can be seen. Since on pp-AA coated surfaces also a significantly

increased cell coverage of 17,8 % (p<0,001) can be seen, it cannot be distinguished whether the biological effect on the RGD/VEGF modified surfaces is based on one of the immobilized biomolecules. After 3 days the cell coverage is significantly increased (p<0,05) only on modified samples that were co-immobilized with RGD and VEGF using 20 µg/ml (15,8%) compared to titanium (6,4 %) with.

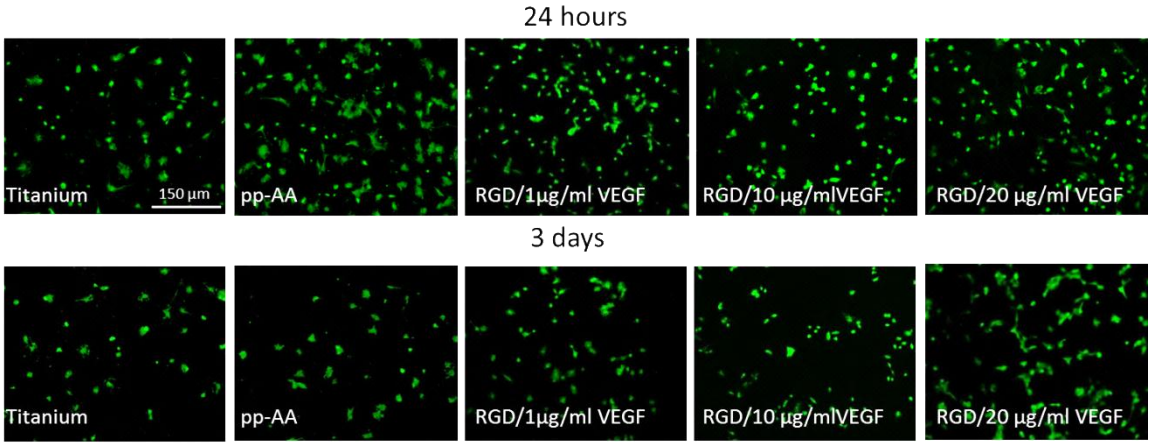

Figure 4.27 Cell adhesion of HUVECs on titanium, pp-AA coated titanium and modified titanium surfaces with co-immobilized RGD and VEGF. For the VEGF immobilization used VEGF concentrations: 1 µg/ml, 10 µg/ml, 20µg/ml.

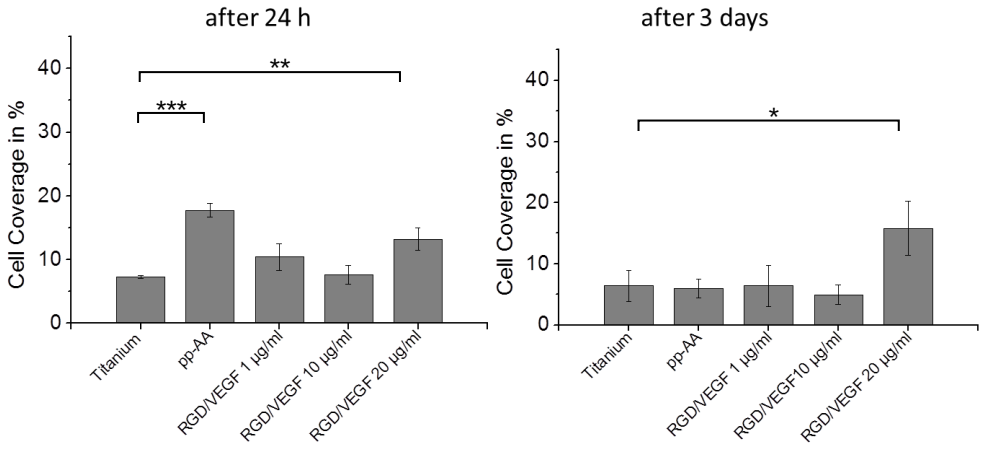

Figure 4.28 Cell coverage of HUVECs on titanium, pp-AA coated titanium and RGD and VEGF modified titanium surfaces using different VEGF concentrations (* for p<0,05 is significant, ** for p<0,01 is highly significant, *** for p<0,001 is extremely significant).

4.4.5 VEGF Receptor Stimulation

To investigate the biological activity of immobilized VEGF, the VEGF receptor stimulation of HUVECs was investigated determining the amount of phosphorylated VEGF receptors via ELISA as described in 3.2.15.9. It was expected that the cultivation of HUVECs on VEGF and RGD/VEGF modified samples leads to an activation of VEGF receptors and thus an increased amount of phosphorylated VEGF receptors. In figure 4.29 A the standard of different concentrations of phosphorylated VEGF receptor is shown. It can be seen that gradual increase of concentrations leads to gradual increase in optical density. The representative results of the quantification of phosphorylated VEGF receptors of HUVEC cell lysates can be seen in 4.29 B. It was found, considering the error bars of all investigated samples, that there is no distinct difference in optical density observable on any modified sample. This experiment was in total repeated twice and the outcome did not reveal distinct differences between the different treated surfaces. It seems that the amount of cells that could be used in the cell experiments was not sufficient for ELISA analysis.

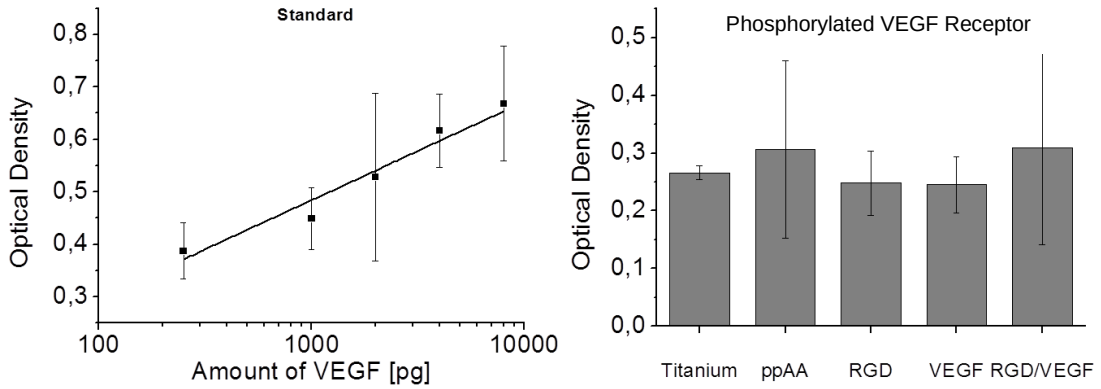

Figure 4.29 Results of the ELISA measurement for the quantification of phosphorylated VEGF receptor. A) Standard of different concentrations of phosphorylated VEGF receptor, B) Result of one representative ELISA measurement for the determination of phosphorylated VEGF receptors using cell lysates of HUVECs that were cultivated on different modified samples for 1 hour.

4.4.6 Immobilization of Alternative Adhesion Molecules

In 4.4.2 the results of the cell experiments on RGD modified surfaces revealed that cell adhesion is not distinctly enhanced by the developed RGD surfaces. This

result will be discussed in section 5.3.2 in detail. Due to the fact, that the designed RGD surfaces did not enhance cell adhesion as expected, alternative adhesion molecules were investigated. As replacement for RGD various proteins of the ECM were immobilized such as fibronectin, collagen, laminin and osteopontin as described in 3.2.3.4 and the cell adhesion was investigated on HUVECs and human osteoblasts (HOBs). In figure 4.30, SPR kinetic measurements of the immobilization procedures of the mentioned proteins are shown. As described in 3.2.3.4, for the immobilization of the ECM proteins the same cross-linker was used than for the VEGF immobilization. Corresponding to SPR kinetic measurements that were shown above, the gradual increase of the SPR signal after Di-NHS-linker incubation and addition of the ECM proteins indicates the biomolecule conjugation. The immobilization of the linker molecules in all kinetic measurements (figure 4.30 A, B, C, D) can be seen by the increased angle of incidence after incubation and rinsing with PBS of 0,07° (4.30 A), 0,14° (4.30 B), 0,1° (4.30 C) and 0,1° (4.30 D). The immobilization of the different used ECM proteins is demonstrated for fibronectin in 4.30 A, with an increase of 0,11°, for collagen in 4.30 B of 0,24°, for laminin in 4.30 C of 0,7° and for osteopontin in 4.30 D of 0,015°.

Although the immobilization for all used proteins could be demonstrated, the curve progressions of all kinetic measurements show distinct differences in direct comparison. Reasons for these differences are discussed in section 5.4.6.

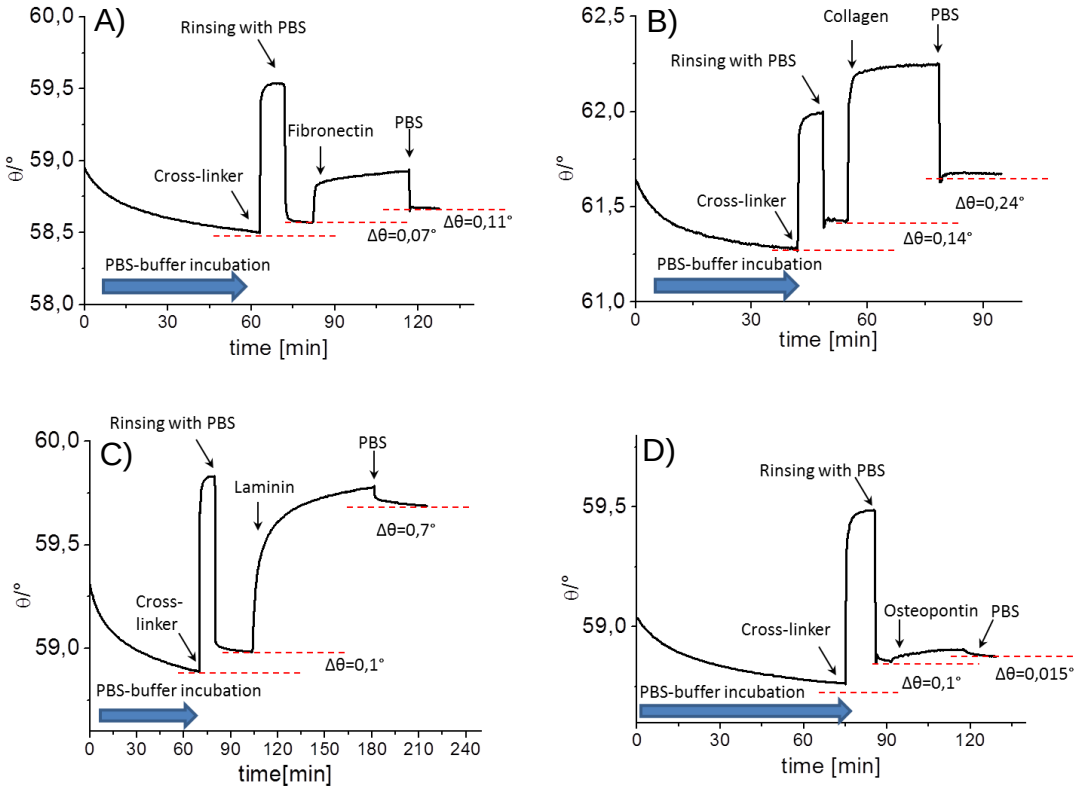

Figure 4.30 SPR Kinetic measurements of the covalent immobilization of A) fibronectin, B) collagen, C) laminin and D) osteopontin. The step-wise increase of the angle of incidence (Δθ) indicates the immobilization of the used proteins.

4.4.7 Cell Adhesion on Titanium Modified with ECM Proteins

4.4.7.1 Cell Adhesion of HUVECs

As described in section 1.2.3, blood vessel formation plays an important role for successful osseointegration of titanium implants. Because of this reason the adhesion of endothelial cells (HUVECs) and osteoblasts (HOBs) on titanium surfaces that were modified with various proteins of the ECM was investigated as described above.

In figure 4.31, the cell adhesion of HUVECs on the different modified titanium surfaces is shown after 24 hours, 3 days and 7 days. Cell adhesion of HUVECs is strongly enhanced on titanium samples modified with fibronectin and collagen at all investigation times compared to the titanium control. It can be observed that the cell shape of the HUVECs on fibronectin and collagen modified surfaces is more expanded compared to the titanium samples, on which the cells have a

more rounded shape. In contrast to this, on the surfaces that were modified with laminin almost no adherent cells at any investigation time are observable. The cells on these surfaces look rounded and seem to detach from the surface. On the osteopontin modified surfaces, a slightly increased cell adhesion can be seen after 24 hours, but after 3 days and 7 days no distinct difference between osteopontin modified surfaces and titanium can be observed.

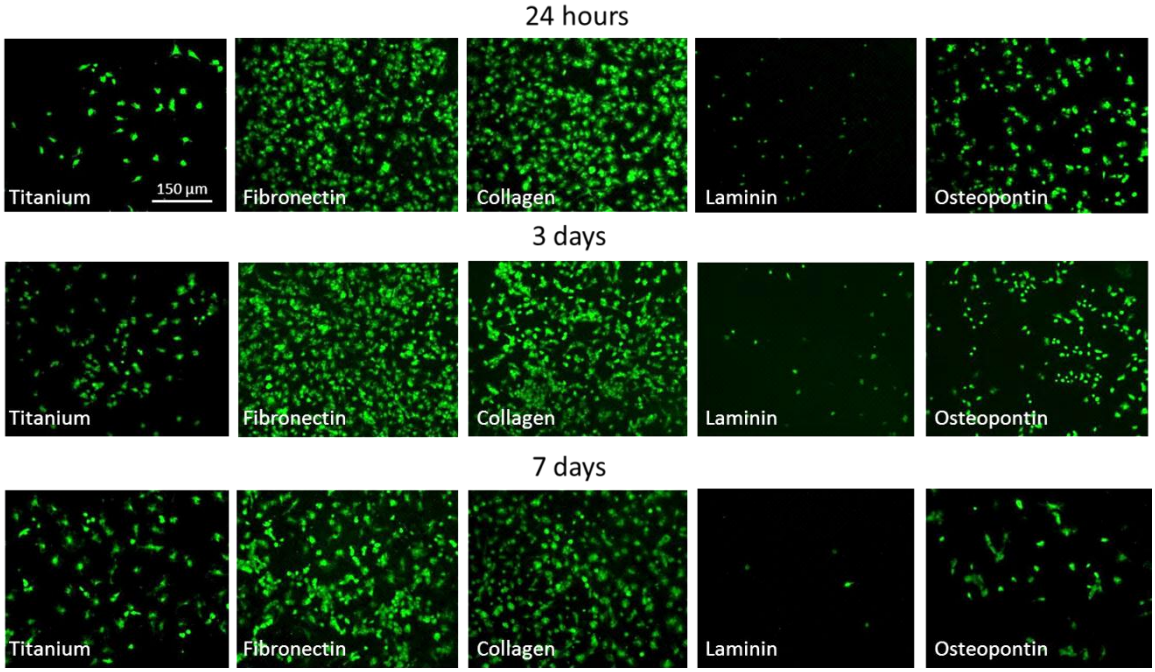

Figure 4.31 Cell adhesion of HUVECs on titanium surfaces with immobilized fibronectin, collagen, laminin and osteopontin after 24 hours, 3 days and 7 days.

According to the results of the cell adhesion, the cell coverage in figure 4.32 demonstrates significantly increased values on the fibronectin and collagen modified surfaces at all investigation times compared to titanium. For titanium comparatively low values of cell coverage were calculated after 24 hours (4%), 3 days (8,8%) and 7 days (12,1%). In contrast to this, for fibronectin modified surfaces values of 44,6% after 24 hours ($p<0,001$), 39,9 % after 3 days ($p<0,05$) and 29,9 % after 7 days ($p<0,05$) can be found. On surfaces that were immobilized with collagen, an increased cell coverage of 48,1 % after 24 hours ($p<0,001$), 35,2 % after 3days ($p< 0,01$) and 42,4 % after 7 days ($p<0,001$) can be observed. On laminin modified surfaces the calculated values of cell coverage at all investigation times are below 1 % and are not mentioned here. In correspondence to the cell pictures of figure 4.31, slightly increased cell coverage

can be observed on osteopontin-modified surfaces with 14,7% after 24 hours compared to the titanium control. After 3 and 7 days no distinct differences between titanium and osteopontin modified surfaces are observable.

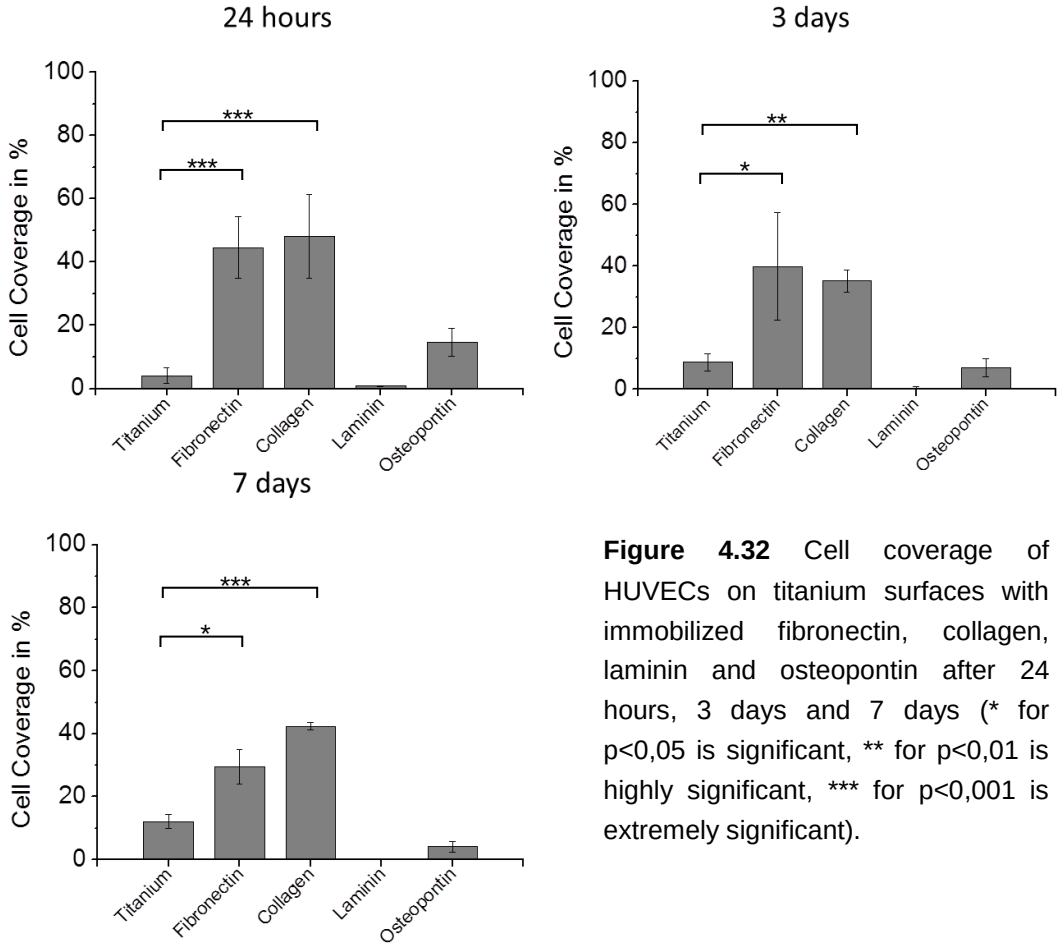

Figure 4.32 Cell coverage of HUVECs on titanium surfaces with immobilized fibronectin, collagen, laminin and osteopontin after 24 hours, 3 days and 7 days (* for p<0,05 is significant, ** for p<0,01 is highly significant, *** for p<0,001 is extremely significant).

4.4.7.2 Cell Adhesion of Osteoblasts

To analyze another clinically relevant cell type in the context of bone implants, human osteoblasts were investigated. Concerning the cell adhesion of human osteoblasts on the different modified titanium samples, it can be seen in figure 4.33, that on all modified samples there is a distinct increase in cell adhesion at all investigation times compared to the titanium control. After 24 hours, on laminin there seems to be an increased formation of cell aggregates compared to the other modified samples on which the cells grow more homogenously. After 3 days on all modified titanium samples there is a homogenous and confluent cell layer and the cell adhesion is distinctly enhanced on the modified samples compared to the titanium control. Apparently, there seems to be no difference of

cell adhesion enhancing effect between the different modified samples. A similar result can be observed after 7 days. The cell adhesion is distinctly enhanced on all modified samples compared to the titanium control.

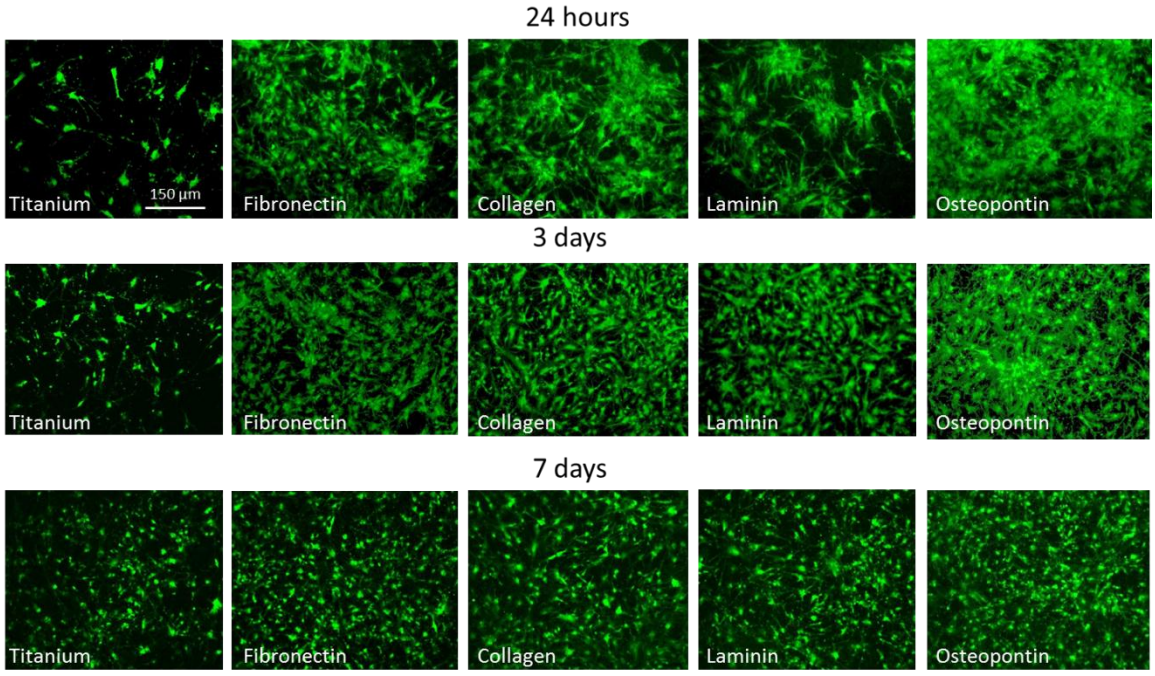

Figure 4.33 Cell adhesion of HOBs on titanium surfaces with immobilized fibronectin, collagen, laminin and osteopontin after 24 hours, 3 days and 7 days.

The quantitative analysis of the cell coverage in 4.34 reveals that at all investigation times and on all modified samples significantly increased cell coverage can be observed compared to titanium. After 24 hours compared to titanium (8,5 %), the densest cell coverage can be observed on modified samples with collagen and a cell coverage of 66,1 % ($p<0,01$) and osteopontin of 66,9 % ($p<0,01$). On modified samples with fibronectin and a cell coverage of 38,5 % ($p<0,05$) and laminin of 40,4 % ($p<0,05$), a less dense cell coverage can be seen. A similar result is found after 3 days with the difference that the cell coverage is in general higher on all samples compared to the results after 24 hours. Here, the highest values for cell coverage can be observed on collagen modified samples with 82,6% ($p<0,001$) and on osteopontin modified surfaces with 76,3 % ($p<0,001$). Lower values can be seen on fibronectin with a cell coverage of 67,1 % ($p<0,01$) and laminin of 71,1 % ($p<0,01$). By far the lowest cell coverage after 3 days was found on titanium (8,7 %). After 7 days the highest cell coverage

of 90,6 % can be observed on collagen (p<0,001) and laminin with 86,5 % (p<0,001). Modified samples with fibronectin and a cell coverage of 76 % (p<0,01) and osteopontin with 71,5 % (p<0,05) show slightly lower values. In agreement with the cell adhesion results of figure 4.33, distinctly lower values for the cell coverage were calculated on titanium (32,3 %).

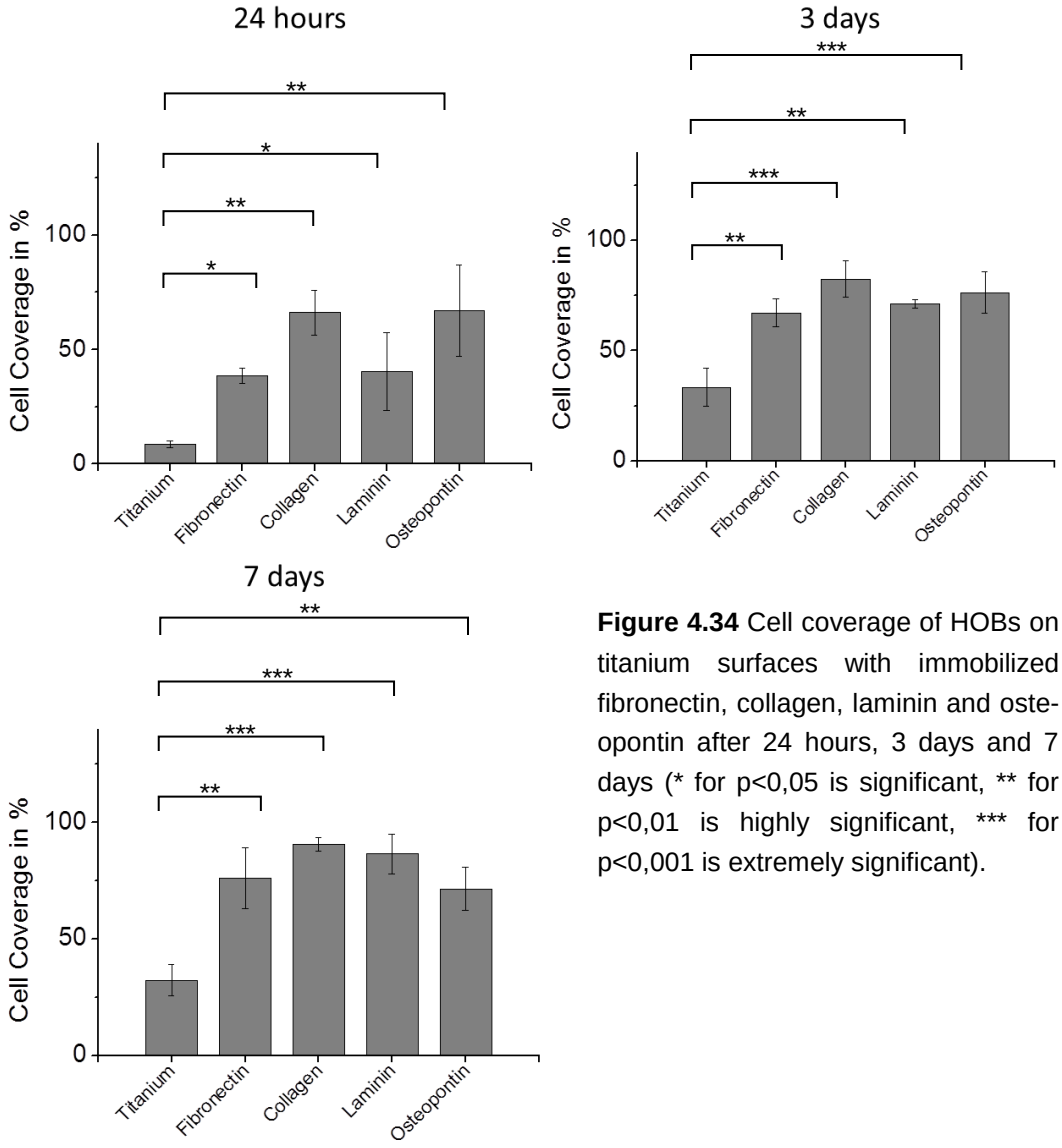

Figure 4.34 Cell coverage of HOBs on titanium surfaces with immobilized fibronectin, collagen, laminin and osteopontin after 24 hours, 3 days and 7 days (* for p<0,05 is significant, ** for p<0,01 is highly significant, *** for p<0,001 is extremely significant).

4.4.8 Animal Experiments

In order to investigate a biological effect of VEGF and RGD/VEGF modified surfaces *in vivo*, osteosynthesis plates were modified and implanted in the tibia of rabbits as described in 3.2.16. The results of the RGD modified implants cannot be shown because the animals carrying the RGD modified implant died unfortunately some days after the implantation. Because of the small number of animals a statistical analysis was not possible. In figure 4.35, the histological bone preparation with the implanted osteosynthesis plates can be seen. The picture of the uncoated plate (4.35 A) reveals that there are areas around the sample at which no dark blue staining can be observed, indicating no new bone formation. Dark blue stained new bone is partly formed at the lower part of the implant (black arrows). In contrast to this the VEGF modified osteosynthesis plate (4.35 B) is completely surrounded by new formed bone tissue, indicated by the dark blue stained bone tissue around the implant. In 4.35 C no dark blue stained tissue can be observed around the implant that was co-immobilized with RGD and VEGF, indicating no new bone formation.

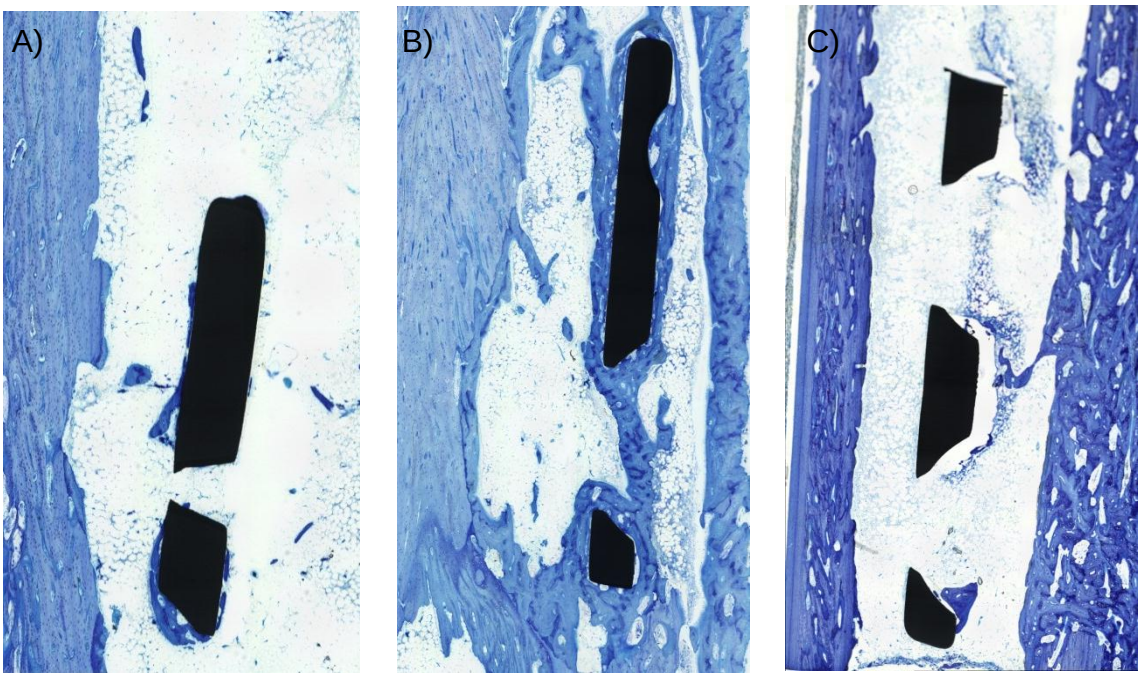

Figure 4.35 Pictures of the osteosynthesis plates integrated in the bone. A) Titanium control, B) VEGF modified, C) RGD/VEGF modified. The dark blue tissue indicates the new formed bone.

5 Discussion

5.1 Characterization of the Titanium Samples

Cellular behavior is influenced by the surface topography and roughness (Anselme et al., 2000). The aim of the titanium sample preparation was the creation of reproducible and defined titanium surfaces regarding to topography and oxide layer composition for the utilization in a reproducible model system for cell experiments. The defined topography was produced by gradual sanding as described in 3.2.1. In addition to this, the samples were acid etched in order to remove the sanding scratches. The reasons for this were observations in preliminary cell experiments that cells orient along the scratches on titanium surfaces.

A natural process that takes place during titanium implant manufacturing steps is the instant oxide layer formation (Kasemo, 1983). In order to fabricate sample surfaces with a reproducible composition of the oxide layer, the titanium samples were oxidized with acidic piranha solution using a constant oxidation time of 1 hour.

Regarding to the topography it can be observed that the titanium preparation steps provide a homogenous surface structure (figure 4.3.). Furthermore, it can be seen that the surface roughness is not influenced by the oxidation step. The oxide layer formation is indicated by the change of color before and after oxidation (figure 4.1) and by the change of wettability (figure 4.2). The reason for the color change can be explained by bulk defects that can occur during titanium oxide layer formation (Diebold, 2003). The decrease in water contact angle is most likely a result of oxygen incorporation during the oxidation process. Due to this, the surface becomes more hydrophilic.

In earlier works it could be shown that comparable titanium samples with defined structure and composition were suitable for the utilization in a model system for cell experiments (Kämmerer et al., 2011).

5.2 Stability and Reactivity of pp-AA Films

Earlier works show that plasma polymerized allylamine films lose material in aqueous solutions (Zhang et al., 2003) and that an increase in plasma process power can increase the stability of plasma polymer films (Chu et al., 2006, Zhang et al., 2003). In agreement with these findings, the results of figure 4.5 show a gradual increase of stability of plasma polymerized allylamine in correlation to higher process powers. After 1 hour of PBS incubation the pp-AA films that were deposited with 80 and 100 W and 0,1 mbar monomer pressure show the highest stability, indicated by the least loss of thickness compared to the pp-AA films that were deposited with lower process powers.

According to results that were found and discussed in earlier works (Förch et al., 2007), also the chemical structure of plasma polymerized allylamine is influenced in aqueous solution. The IR measurements reveal that pp-AA films deposited with lower process power show a more distinct decrease of IR signal intensities at 3300 cm^{-1} and 1630 cm^{-1}, suggesting a loss of amines and amides. At the same time, the signal intensity ratios at 1450 cm^{-1} and 1380 cm^{-1} for hydrocarbons compared to the signal at 1630 cm^{-1} change, suggesting an increased content of hydrocarbons in combination with lower nitrogen content within the films. The smallest changes in signal intensity ratios can be observed for pp-AA films that were deposited with 100 W and 0,1 mbar monomer pressure on gold as well as on titanium oxide. This shows that pp-AA films deposited with these parameters are the most stable, independent from the different used substrates. Since all shown results concerning the loss of thickness and the chemical structure of the investigated pp-AA films indicated the highest stability for the 100 W pp-AA films that were deposited with 0,1 mbar monomer pressure, SPR kinetic measurements were performed to evaluate the stability and behavior in PBS in real-time. As base for the wet chemical immobilization, this investigation was an important step to determine the starting point for the immobilization procedure. The swelling behavior and the stability of plasma polymerized allyamine in solution can be influenced by modulation of plasma polymerization parameters such as process power and monomer pressure (Chu et al., 2006). In the SPR kinetic measurement of figure 4.8 it can be seen that the most distinct decrease of the SPR signal occurs within the first 30 minutes and after 60 minutes there is

almost no change observable. This decrease can be explained by two main events suggested in literature (Chu et al., 2006, Zhang et al., 2003): (1) Uptake of water leads to swelling of the plasma polymer and a decreased polymer network density, which results in a decrease of the refractive index. (2) The dissolution of non-bound material enhances the decrease of polymer network density which ultimately leads to a decrease of layer thickness. According to the found results, it can be suggested that the events that take place during incubation in aqueous solution such as swelling and leaching processes occur within the first 60 minutes. The decrease of the SPR signal is a result of water uptake, swelling, and a decreasing polymer network density, associated with a decreased refractive index and/or layer thickness. After 60 minutes almost no swelling and loss of material occurs, indicated by the stagnating curve. As consequence of the shown results, 100 W pp-AA films were used for the immobilization of biomolecules and incubated at least for one hour before the immobilization procedure was conducted.

The quantitative analysis of primary amines in the different pp-AA films in figure 4.10 indicates a higher amount of primary amines on the plasma polymer layers that were deposited with lower process power. In agreement with earlier works, this phenomenon is based on a higher cross-link density associated with a loss of primary amines during the plasma polymerization process using higher process powers (Förch et al., 2007, Zhang et al., 2003). The results of the quantitative analysis show also a loss of primary amines in the case of the 100 W pp-AA films. Nevertheless, because of the increased stability in PBS, especially regarding to the chemical structure in combination with a calculated amount of 6 primary amines per nm^2, it was suggested that these films are the most suitable for the wet chemical immobilization procedure.

5.3 Immobilization of Biomolecules

5.3.1 Cross-linker Immobilization

For the development of a controllable two step co-immobilization procedure it was necessary to find a suitable cross-linker system. The challenge in this context was the development of an immobilization system that allows the different

cross-linker molecules to react with the primary amines of pp-AA surfaces with the same reaction kinetic in order to ensure an equal distribution for the biomolecule immobilization. At the same time the presence of two different functionalities is necessary for a controllable and separated two-step co-immobilization procedure.

The immobilization of both used cross-linker is indicated by the increase of the SPR signal after cross-linker incubation and rinsing with PBS. This increase can be explained due to the change of refractive index and/or layer thickness as consequence of the conjugated cross-linker molecules. This results can be supported by the IR spectra, in which new peaks are created after cross-linker immobilization.

As described above the electrophilic *N*-hydroxysuccinimide group of both used linker molecules complies with the requirements to react with primary amines on the surface with the same reaction kinetic. Succinimide esters react rapidly in a pH range of 6-9 with protein amine groups, with an optimum between 7 and 8, while the competing hydrolysis has a half-life of 4-5 hours at pH 7,5 (Aslam et al., 1999). Due to this, the immobilization of both cross-linkers was conducted with PBS at pH 7,4. One problem that might occur with bis-*N*-hydroxysuccinimide polyethylene glycol is the formation of loop structures due to the two-sided binding reaction with amines on the pp-AA surface. In order to counteract this formation of loop structures a large excess of cross-linker molecules using a concentration of 5% (w/v) was added to the samples, thus one-sided binding reactions are kinetically favored.

For the co-immobilization procedure it was crucial to figure out a suitable ratio between both used cross-linkers in order to adapt to the different linker lengths and sizes of the used biomolecules RGD and VEGF. Shown in figure 4.15 is the SPR kinetic measurement of the co-immobilization using both cross-linkers with the described ratio of 1:1,5. The increased angle of incidence after PBS rinsing shows the conjugation of the two cross-linkers onto the pp-AA surface. The IR spectra of the co-immobilization are not shown because it was not possible to distinguish the different used cross-linkers via IR due to superposition effects at 1740 and 2900 cm^{-1} of the C=O stretching signals. In former SPR kinetic measurements for the RGD and BSA co-immobilization, a 1:1 ratio of the linker molecules was used for the co-immobilization procedure (data not shown here).

These experiments gave the qualitative evidence for the reproducible co-immobilization procedure. Nevertheless, it was found that this ratio resulted in lower changes of the SPR signal after BSA immobilization compared to the result as shown in 4.18, in which a ratio of 1:1,5 was used. As mentioned in 4.3.3, it was assumed that a more distinct increase of the angle of incidence after BSA immobilization indicates bigger amounts of bound BSA. Due to these findings, a cross-linker ratio of 1:1,5 was considered as more suitable for the co-immobilization procedure.

5.3.2 RGD Immobilization

With respect to the co-immobilization procedure, RGD was immobilized with α-maleinimidohexanoic-ω-*N*-hydroxysuccinimide polyethylene glycol. As discussed in 4.3.1 the reaction of *N*-hydroxysuccinimide has a pH optimum between 7 and 8. The maleimide group contains a double bond activated to nucleophilic attack of the two neighboring carbonyl functions and is therefore capable of undergoing Michael addition reactions (Aslam et al., 1999). It can be used for the reaction with thiols, but depending on the pH it will react also with unprotonated amines. A pH optimum for maleimide reactions with thiols was found to be in the range between 6 and 7 (Aslam et al., 1999). Since the reaction of the *N*-hydroxysuccinimide of both cross-linkers was conducted in PBS with pH 7.4, and due to the fact that this pH is only slightly above the pH optimum of the maleimide-thiol reaction, it was suggested to use the same buffer also for this reaction. The result in figure 4.16 shows the successful immobilization of cysteine-RGD in the SPR kinetic measurement, indicated by the increase of the SPR signal. The reason for the change of the angle of incidence is due to the change of the layer thickness and/or the refractive index as a result of the RGD immobilization. After approximately 30 minutes the adsorption curve ends in a plateau and no change in the SPR signal can be seen anymore. It can be assumed that after 30 minutes all maleimide groups of the used Mal-NHS-linker reacted with the RGD molecules and no further immobilization can be observed. Because of this result the time for the immobilization procedure of RGD as well as for the co-immobilization procedure of RGD and VEGF was set to 60 minutes incubation time. Attempts to quantify RGD over the method of Quartz Crystal

Microbalance (QCM) failed (data not shown). Nevertheless, the qualitative analysis via SPR kinetic measurements gave the qualitative evidence of the immobilization. Furthermore, due to the valuable information of the immobilization time it was possible to reduce the immobilization time to a minimum.
The SPR results can be supported by the change of the water contact angle during the immobilization steps. Although similar water contact angle values of RGD modified surfaces can be found in literature (Jung et al., 2005), changes in wettability are only seen as supportive method and cannot be regarded as scientific evidence for a successful RGD immobilization.

5.3.3 VEGF Immobilization

To evaluate the co-immobilization procedure in a simplified experiment, Bovine Serum Albumin (BSA) was taken as replacement for VEGF to prove the principle of the developed modification system. It was suggested that BSA with 65 KDa (Klajnert et al., 2002) is a suitable protein close to that of $VEGF_{165}$ with 44 KDa (according to the information of Immuno Tools). The results of 4.17 show SPR kinetic measurements in which different concentrations of BSA were investigated for the immobilization procedure using bis-*N*-hydroxysuccinimide polyethylene glycol as cross-linker. The SPR kinetic measurements conducted in this work were not used for quantitative analyses. Since the plasmon shift is approximately proportional to adsorbed amounts of adsorbates as already mentioned above (Laschitsch et al., 2000), differences of the SPR signals during the measurements allow conclusions about immobilized amounts of the used biomolecules. In the SPR kinetic measurements of figure 4.17 the immobilization of BSA can be observed by the increase of the angle of incidence in correlation to different used concentration. Up to a used concentration of 2 mg/ml BSA an increase of the SPR signal compared to the lower concentration of 1 mg/ml was found, suggesting that higher concentrations of BSA result in higher amounts of immobilized BSA. In contrast to this, further increase of the concentrations as seen for 5 mg/ml and 10 mg/ml BSA leads to a comparatively lower increase of the angle of incidence, suggesting a lower amount of immobilized BSA. It can be assumed that the binding reaction of *N*-hydroxysuccinimide and primary amines is kinetically favored up to certain concentrations at which higher amounts of

protein can be immobilized. Exceeding this concentration might result in steric hindrances of the protein molecules in which the interaction between the *N*-hydroxysuccinimide groups and the amines of the protein molecules might be disabled.

In figure 4.18 A and B, it can be observed that the increase of the SPR signal in the case of the passive adsorbed BSA is distinctly higher compared to the covalent immobilized BSA. This observation can be explained by higher amounts of passive adsorbed BSA compared to the amounts that are covalently immobilized.

It was found in earlier works that incubation of pp-AA films in buffer with pH lower than 8 leads to positively charged films, due to protonated amine groups. Accordingly, it could be observed that these positive charges lead to an enhanced binding of negatively charged molecules (Zhang et al., 2003). Due to the used buffer with pH 7,4 in all experiments and the fact that BSA exhibits negative charges at this pH because of its isoelectric point at 5,4 (Shi et al., 2008), it can be assumed that the passive adsorbtion might result in higher amounts of bound BSA compared to the covalent immobilization. Furthermore, the BSA molecules might be able to form a dense protein layer distributed randomly over the whole surface, influencing additionally the refractive index (Vörös, 2004). In contrast to this, the amount of covalently immobilized BSA depends on the amount of cross-linker molecules that are available for the protein conjugation. Since the covalent BSA immobilization is limited to this cross-linker amount, the proteins might form a less dense and more defined layer.

With respect to the covalent immobilization of VEGF, it can be observed that the progression of the BSA adsorption stagnates after approximately 30 minutes. Due to these findings, it can be assumed that after 30 minutes all *N*-hydroxysuccinimide groups of the Di-NHS-linker have reacted with BSA and no further immobilization takes place. As already described for the RGD immobilization, because of the information that was obtained in the SPR kinetic measurements, it was possible to reduce the incubation time of VEGF for the development of the immobilization procedures down to a minimum. The incubation time for VEGF during the single immobilization as well as for the co-immobilization procedure was set to 60 minutes. The results of the water contact angle measurements give hints of the VEGF immobilization, indicated by

the change of the contact angle during the immobilization steps. Similar values of water contact angle measurements of VEGF modified surfaces can be found in literature (Edlund et al., 2011).

5.3.4 RGD/VEGF Co-Immobilization

As described above for the analysis of the VEGF immobilization analysis, also for the co-immobilization analysis BSA was used as replacement for VEGF.
During the development of a controllable and separated co-immobilization procedure, not only the utilization of different coupling chemistries was considered. Because of the different sizes of RGD and VEGF, different cross-linker lengths were used in order to compensate possible steric hindrances during the co-immobilization reactions. It was assumed that in the case of similar linker lengths, VEGF with a size of 44 KDa might cover the maleimide groups after immobilization, thus prevent the RGD interaction and immobilization. The suggestion to compensate this effect was the utilization of a cross-linker for RGD longer than the size of VEGF, in order to ensure that the maleimide group would still be accessible for RGD after the VEGF immobilization. Because of this reason, the size of VEGF was estimated using a 3D model of VEGF-A via PDB code and the software chimera, alpha version 1.7. A diameter of approximately 10 nm for VEGF-A was determined. The theoretical lengths of the linker molecules were calculated considering the binding angles within the polyethylene glycol chains of 109° for C-C bonds and 112° for C-O. The calculated length of the 5000 Dalton α-maleinimidohexanoic-ω-*N*-hydroxysuccinimide polyethylene glycol was approximately 30 nm and for bis-*N*-hydroxysuccinimide polyethylene glycol (2000 Dalton) approximately 16 nm. The difference of 14 nm was assumed to be sufficient for counteracting the described problem of the steric hindrances during the immobilization processes. The SPR kinetic results of the BSA and RGD co-immobilization gave evidence of the functional cross-linker system and the separated and independent two-step co-immobilization.

5.3.5 Surface Characterization via XPS

As additional proof for the immobilization of RGD and VEGF, X-Ray Photoelectron Spectroscopy was used. It was expected that changes in the

content of carbon, nitrogen and oxygen could support the data of the immobilization as shown above. The elemental composition of the polyethylene glycol chain of the used linker molecules considering carbon and oxygen is approximately 2:1. Especially the relative increase in the content of oxygen after cross-linker incubation indicates the immobilization. The low change in the carbon content after the cross-linker incubation can be explained by the fact that the pp-AA film may contribute to the XPS signals. Nevertheless, it can be suggested that the relative decrease of the nitrogen content might indicate that cross-linker molecules are immobilized and nitrogen containing species of the pp-AA are partly covered and cannot be detected. This is the case for the single immobilization of the used cross-linker molecules as well as for the co-immobilization of both cross-linkers. Neither RGD nor RGD/VEGF modified surfaces give distinct signals from that of pp-AA or after linker immobilization. It can be assumed that the relative contents of nitrogen species within the pp-AA films and the biomolecules RGD and VEGF are approximately similar, leading to no distinct changes in the XPS signals.

5.3.6 VEGF Quantification

For the development of a solid phase ELISA it was crucial to create a reliable standard necessary for quantitative analyses. The standard in figure 4.20 shows an increasing adsorption of VEGF on antibody coated titanium samples in correlation to the VEGF concentration. Above the concentration of 5 µg/ml VEGF it seems that the capture antibody coated titanium surfaces are saturated with VEGF and no distinct increase of optical density can be observed. Although this result demonstrated a concentration dependent adsorption of VEGF, there are several reasons why it was not possible to determine the total amount of VEGF on the modified surfaces. One reason is the amount of VEGF that adsorbed on the bottom of the 24 well plates during the immobilization procedure. In order to estimate the amount of adsorbed protein, experiments to determine the amount of VEGF in the supernatant of the protein solution were conducted that was used for the immobilization. Due to too small volumes of protein solution not suitable for the ELISA Kit it was not possible to produce reliable data. Furthermore, the bigger volumes used in the 24 well plates compared to the experiments

conducted in 96 well plates resulted in a dilution of the staining. Trials to calculate and normalize the results failed. Although it was not possible to quantify VEGF on the surface, it can be observed in 4.20 that the modified surfaces lead to an increase of optical density, indicating the presence of VEGF on the surface. Due to this, the obtained results can be understood as further qualitative evidence of the VEGF immobilization on the VEGF and RGD/VEGF surface.

5.4 Cell Experiments

5.4.1 Effect of Immobilized RGD on Cell Adhesion

The results of 4.4.2 demonstrate that the RGD modified samples do not enhance cell adhesion after 24 hours and 3 days. These results correspond with the analysis of the cell coverage as shown in figure 4.22. One possible reason why cells are not stimulated by RGD might be due too low amounts of immobilized RGD, not sufficient to enhance cell adhesion. A decreased density of primary amines in the pp-AA films that were deposited with 100 W and 0,1 mbar monomer pressure as discussed in 5.2 might be the reason for a decreased binding capacity of the pp-AA surfaces, resulting in too low amounts of immobilized RGD.

Another reason for the observed results might be the hydrophilic properties of the polyethylene glycol cross-linker. It is known that pegylated surfaces can have an anti-fouling effect (Wang et al., 2001). In this context one assumption is that the size of the RGD peptide with 450 Dalton (according to the information of Panatecs) is too small to cover the anti-fouling effect and thus cells might have problems to attach to the surface.

Although after 24 hours and 3 days cell adhesion was not enhanced, after 7 days a slightly increased cell adhesion can be observed on the RGD modified surfaces. One possible reason is that a small number of cells might interact with the RGD molecules that are immobilized onto the surface. This might result in a stimulation of the cellular behavior such as proliferation, what can be seen earliest after several days.

5.4.2 Effect of Dissolved VEGF on HUVECs

Before cellular behavior was investigated on the VEGF and RGD/VEGF modified titanium surfaces, first the influence of different concentrations of dissolved VEGF was analyzed. In this context it was additionally tested, whether only VEGF is sufficient for cellular stimulation. In figure 4.23 and 4.24, a distinct concentration dependent effect of dissolved VEGF on cellular adhesion can be observed. The most distinct enhancement of cell adhesion at the highest VEGF concentration, associated with the expanded cell shape in all samples after 24 hours demonstrates the biological activity of VEGF. The analyses of the cell coverage show significantly increased values for the highest concentrations after 24 hours and 3 days. It seems to be obvious that after 24 hours the effect of VEGF is sufficient to stimulate HUVECs in supplement free medium. The results after 3 days demonstrate that cell adhesion is still enhanced by dissolved VEGF in correlation to the concentration. Nevertheless, the rounded shape of the cells in combination with a distinctly decreased cell number compared to the results after 24 hours indicates that only VEGF does not seem to be sufficient for longer cultivation. One explanation for these results might be a decreased VEGF concentration after 3 days due to protein degradation.

5.4.3 Effect of Immobilized VEGF on Cell Adhesion

In order to stimulate cellular behavior of endothelial cells, VEGF was immobilized using different concentrations as described in 3.2.3.2. In accordance to the results of the concentration depending effect of dissolved VEGF as discussed in section 5.4.1, it can be seen in figure 4.25 that also immobilized VEGF shows an effect on HUVEC cell adhesion in correlation to the VEGF concentration that was used for the immobilization. Corresponding to this, significantly increased values of cell coverage were found for samples that were modified with the highest concentration of 20 µg/ml VEGF.

As discussed in 5.3.3, the amount of protein that is immobilized onto a surface depends on the used concentration. In the case of BSA it was demonstrated that up to a certain threshold of protein concentration the amount of immobilized protein seems to increase. According to the described observations of the concentration depending effect of VEGF on HUVECs, in combination with the

found SPR results as mentioned above, it can be assumed that higher VEGF concentrations lead to increased amounts of immobilized VEGF on the surface. Cellular stimulation as reaction on immobilized VEGF seems to occur only after a certain threshold of immobilized VEGF amount is reached.

As already discussed in 5.4.1, an additional explanation for a missing cellular response at lower concentrations of VEGF could be the hydrophilic properties of the used cross-linker associated with an anti-fouling effect. Following the theory of lower immobilized amounts of VEGF at lower used concentrations, it is suggested that a certain amount of immobilized VEGF is necessary to form a homogenous and dense protein layer that is able to cover the anti-fouling effect. If this amount cannot be reached due to too low concentrations, gaps in the protein layer may occur. In this case the hydrophilic linker molecules are not totally covered and may exhibit an anti-fouling effect.

5.4.4 Effect of RGD/VEGF Modified Titanium on Cell Adhesion

The results of 4.4.4 show that after 24 hours there is only a slightly enhanced cell adhesion observable on the surfaces that were co-immobilized with RGD and VEGF using a VEGF concentration of 20 µg/ml. These results can be supported by a significantly increased cell coverage found on these samples compared to the titanium control. Nevertheless, due to the increased cell adhesion on pp-AA samples after 24 hours, it cannot be distinguished whether the observed cellular response on the RGD/VEGF modified surfaces is due to the biological activity of RGD or VEGF.

As already described above, the amount of immobilized RGD might not be sufficient to enhance cell adhesion. On the RGD/ VEGF modified surfaces, the amount of immobilized RGD is most likely additionally decreased due to a reduced amount of α-maleinimidohexanoic-ω-*N*-hydroxysuccinimide polyethylene glycol as result of the co-immobilization with the second cross-linker. In accordance, no additional cell adhesion enhancing effect as seen with RGD was expected. Corresponding to the results of the single immobilization of VEGF, the increase in cell adhesion and cell coverage might be based on the effect of VEGF. The reason for a more distinct cellular response on single modified VEGF surfaces, compared to RGD/VEGF modified surfaces, is most likely due to higher

amounts of bound VEGF. Nevertheless, the conjugated amounts of VEGF co-immobilized with RGD, with a used VEGF concentration of 20 µg/ml, seems to be sufficient to stimulate cellular response.

In contrast to the results after 24 hours, after 3 days a more distinct cellular response of RGD/VEGF modified samples compared to all other surfaces can be observed, indicating the biological functionality of the RGD/VEGF modified surfaces. It seems to be obvious that only on the surfaces that were co-immobilized with RGD and the highest VEGF concentration of 20 µg/ml lead to sufficient amounts of immobilized VEGF that is necessary to stimulate cells.

However, RGD does not enhance cell adhesion in the developed immobilization and co-immobilization systems as expected. Although the biological effect of the RGD/VEGF surfaces was not as high as observed for the VEGF modified surfaces, a biological effect of immobilized VEGF could be observed in both designed immobilization systems.

Concerning the anti-fouling properties of the cross-linker, it might be possible that low concentrations of VEGF and/or RGD could lead to gaps in the protein layer, enabling the anti-fouling properties to show effect as already discussed in 5.4.1 and 5.4.3.

5.4.5 VEGF Receptor Stimulation

In order to investigate the biological functionality of the immobilized VEGF on VEGF and RGD/VEGF surfaces, ELISA measurements were conducted to detect phosphorylated VEGF receptors, thus to give additional evidence for the biological activity. The results of 4.4.5 show that neither the surfaces with immobilized VEGF nor the surfaces with co-immobilized VEGF lead to a measurable increased amount of phosphorylated VEGF receptors. A first conclusion might be a missing interaction of the immobilized VEGF molecules with the VEGF receptors that would be essential for receptor activation. Concerning the observed biological activity of immobilized VEGF in the cell experiments, this assumption is rather unlikely.

An additional explanation might be the sensitivity of the ELISA assay. The used assay is designed to detect phosphorylated VEGF receptors in a recommended amount of 10^7 dissolved cells. For the experiments in this work triplicate

measurements of each surface modification have been performed. For this purpose, 10^5 cells were seeded on each sample and after cell lysis the obtained cell lysates were pooled. Since the cell experiments performed in this work were limited to 1 cm² titanium samples in 24 well plates it was not possible to increase the cell number on the samples and thus to achieve the recommended amount of cells.

Another reason for the missing receptor stimulation might be the cell incubation time of 1 hour that was not sufficient for cell interactions with the immobilized VEGF molecules on the surface. Furthermore, the fact, that the cells had to interact with the conjugated VEGF molecules on the surface, reduced additionally the theoretical possibility of VEGF interactions with the receptors compared to a system in which VEGF diffuses in medium.

5.4.6 Additional Cell Adhesion Molecules

The results of the stimulating effect on HUVECs of RGD modified titanium samples showed that in the context of the developed immobilization technique, RGD did not enhance cell adhesion as distinct as expected. Reasons for this were discussed in section 5.4.1. The aim of this work was the immobilization of two different biomolecules, to create surfaces with the potential to trigger various cellular responses. Since for RGD modified titanium the aim of enhancing cell adhesion could not be achieved, the challenge was to find alternative cell adhesion enhancing molecules. As described above, it could be shown in literature that proteins of the ECM have a promoting effect on the cellular response after immobilization on various substrates. Because of this reason the ECM proteins fibronectin, collagen, laminin and osteopontin were chosen to be immobilized on titanium using bis-*N*-hydroxysuccinimide polyethylene glycol as cross-linker.

The immobilization of the used ECM proteins can be observed in the SPR kinetic measurements of figure 4.30. The increase of the SPR signal in all measurements before and after protein incubation (4.30 A, B, C, D) demonstrates that all used proteins were immobilized successfully. As described in 5.3.3, the SPR kinetic measurements in this work were not used as quantitative method. However, for a complete analysis of the obtained SPR results, the differences of

the SPR signals during and after the immobilization of the used ECM proteins will be discussed concerning the protein size and the immobilized protein amounts.

Differences in the progress of the adsorption curves during the immobilization processes are due to changes in optical properties of the used proteins. The optical properties of protein solutions are influenced by the used buffer, the protein concentration and the molecule size. The density and refractive index of adsorbing protein layers depend on the molecule size, and the fact that smaller proteins form denser protein layers on surfaces, influencing additionally the refractive index (Vörös, 2004). Fibronectin was used with the highest concentration of 1 mg/ml compared to collagen and laminin with 500 µg/ml. Because of the fact that the concentration of osteopontin used for the immobilization was far below the other used protein concentrations, the results for the osteopontin will be discussed separately.

It was expected that the highest protein concentration of fibronectin would lead to the most distinct plasmon shift after incubation. In contrast to this, higher changes of the SPR signal during the protein incubation and after rinsing with PBS were observed for collagen and laminin. As mentioned above, changes of the SPR signal correlate to adsorbed protein amounts associated with changes in layer thickness and/or refractive index. Due to the fact that laminin is with a size of 850 KDa (Maher et al., 1988) the biggest among the investigated proteins it seems to be obvious that the immobilization of laminin leads to the highest increase in layer thickness and/or refractive index and thus to the most distinct change in the angle of incidence.

Considering the sizes of fibronectin with approximately 520 KDa (Nelea et al., 2008) and collagen with approximately 300 KDa (Friess, 1998), it seems surprising that a higher change of the SPR signal during incubation and after immobilization can be observed for collagen. One possible explanation is based on the nature of collagen. Collagen forms many structures in the ECM such as fibrils, networks and transmembrane collagenous domains (Shoulders et al., 2009). It is assumed that the dissolved collagen used in this work contains such fibrils or network-like structures, which might have an impact on the refractive index. According to this, collagen might arrange in a denser protein layer after immobilization, leading to a higher amount of immobilized collagen compared to fibronectin.

For osteopontin the smallest change of the SPR signal can be observed after incubation and immobilization. One possible explanation is the low concentration used for the osteopontin immobilization and the small size in the range between 44 -75 KDa (Denhardt et al., 1993). The low concentration leads most likely to a decreased amount of immobilized protein molecules. The fact that smaller protein sizes lead to denser protein layers and thus an increased refractive index, might be prevented because of the low concentration.

The cell results show a distinctly enhanced cell adhesion of HUVECs on fibronectin and collagen modified surfaces at all investigation times compared to the titanium control. Furthermore, significantly increased cell coverage can be observed. It is known that fibronectin as well as collagen contain the RGD motive and it could be shown in literature that these proteins are able to stimulate integrin mediated cell adhesion as described above.

The results indicate that especially in the case of fibronectin and collagen HUVECs seem to recognize the RGD motive within the proteins and interact with the integrin receptors and thus cellular adhesion is enhanced. For laminin modified surfaces there is no cell adhesion observable. According to literature there are different subfamilies among the integrins due to different combinations of α and β subunits (Hynes, 2002). Various combinations of subunits lead to different ligand specificities, therefore different subfamilies are involved for the interaction with laminin and RGD. Although laminins possess binding sides for integrin receptors (Timpl et al., 1994) it might be possible that the used HUVECs do not express the suitable integrin receptors which are able to interact with laminin. Another reason could be the orientation of the laminin molecules on the surface associated with a decreased accessibility of the integrin binding sites within the laminin protein.

Since osteopontin also contains the RGD sequence (Reinholt et al., 1990) and after 24 hours a slightly enhanced cell adhesion can be observed, it might be possible that the amount of osteopontin is not sufficient to stimulate HUVECs due to the low concentration that was used for the immobilization.

In the context of titanium implants for the medical application in bone, the biological effect of the designed surfaces was also investigated in the case of human osteoblasts. It can be observed in that at all investigation times and on all modified surfaces cell adhesion is distinctly enhanced compared to the titanium

control. These results correlate with significantly increased cell coverage values. It seems to be obvious that HOBs interact with the integrin-binding motives on all modified surfaces, indicated by the increased number of cells in combination with an expanded cell shape. The used HOBs seem to express the integrins that are responsible for the interaction with RGD as well as the integrins that are necessary for laminin interaction. This could be a possible explanation why HOBs show increased cell adhesion on the surfaces with RGD containing proteins such as fibronectin, collagen and osteopontin as well as on laminin modified surfaces. The differences between cell adhesion of HOBs and HUVECs on osteopontin modified surfaces could be explained by the fact that for the stimulation of HOBs a lower amount of osteopontin seems to be sufficient.

5.4.7 Mechanical Stability of pp-AA Films *ex vivo*

With respect to the clinical application in implantation systems such as titanium screws, the mechanical stability of the developed biomimetic surfaces is a crucial issue. Because of this reason, the mechanical stability of pp-AA was investigated *ex vivo*, simulating comparable clinical bearing conditions.

The results of 4.11 demonstrate the mechanical stability of a pp-AA film deposited with 40 W process power and 0,15 mbar monomer pressure. The reason for the different plasma polymerization parameters for the pp-AA deposition in this experiment is due to the fact, that these measurements were conducted in an earlier stage of this work, before the stability tests in aqueous solutions were conducted. Up to this stage, only pp-AA films were used that were deposited with these parameters, because earlier results showed promising properties of these pp-AA films suitable for bio-functionalization (Lotz et al., 2012). Nevertheless, it can be assumed that the effect of shearing forces on pp-AA films deposited with different parameters during the screwing procedure into the bone are most likely similar affected by the screwing procedure and thus are comparable.

Furthermore, it is demonstrated that the shearing forces of the screwing procedure into the bone have a strong effect on the pp-AA film. In 4.11 A it can be seen that especially in the lower part of the screw the shearing forces show the strongest effect. This can be explained due to the fact that the lower part of

the screw enters the pre-drilled hole first, while widening it. As result the shearing forces at the upper part of the screw are not as strong as at the lower part. In the closer view (figure 4.12) it can be observed that the film partly remains on the surface of the screw. This shows that the pp-AA film is partly stable enough to resist the shearing forces of the screwing procedure. Although the shown results give an impression of the shearing force effect on pp-AA films, it will be interesting to investigate the mechanical stability of pp-AA films in the range of micro-, and nanometers. In this context the surface roughness and especially the remain of the pp-AA film in the cavities of the titanium micro- and nano-structure will be an important information.

5.4.8 Animal Experiments

In the *in vitro* experiments it could be demonstrated that even though RGD and RGD/VEGF modified surfaces showed a cellular stimulation, the most distinct biological effect was triggered by single immobilized VEGF. As discussed in 5.3.3 and 5.3.4, the reduced cellular response might be due to too low VEGF concentrations, associated with too low amounts of immobilized VEGF. According to the cell results, also *in vivo* the by far strongest effect on new spongious bone formation could be seen on samples that were modified with VEGF only. However, in contrast to cell culture, a VEGF concentration of only 1 µg/ml for the immobilization seemed to be sufficient to stimulate cells and to initiate bone formation *in vivo.* Although it could be shown that the RGD/VEGF modified surfaces triggered cellular adhesion *in vitro*, on the implants with co-immobilized RGD and VEGF, there was no new bone formation observable. This may seem surprising, but considering the reduced biological activity on the RGD/VEGF surfaces compared to the VEGF surfaces *in vitro*, it was expected that the RGD/VEGF surfaces would exhibit only a reduced biological activity (please see discussion 5.3.2-5.3.4).

In summary, these preliminary *in vivo* results demonstrate in the case of the VEGF modified surfaces a distinct biological effect on the new bone formation. For RGD/VEGF modified implants no biological effect could be observed *in vivo.*

6 Conclusion and Outlook

Biomimetic surfaces for medical applications such as bone implants seem to be one of the most promising scientific approaches to improve side effects that can occur after implantation. Counteracting the foreign body reaction and improving the wound healing situation are some of the goals that could lead to an improvement of long lasting bone implants. Since a good blood vessel supply is essential for a healthy bone formation, especially angiogenic growth factors became the focus of interest in the context of biomimetic surfaces. The Design of multifunctional titanium surfaces in order to enhance cell adhesion as well as cell stimulation of endothelial cells and osteoblasts was the aim of this work. For this purpose, a controllable co-immobilization procedure for the cell adhesion motif RGD and the angiogenic VEGF had to be developed.

Plasma polymerization is a powerful method to functionalize different materials for a further utilization in the context of biomimetic surface modifications. The stability of plasma polymerized allylamine was investigated with infrared spectroscopy, profilometry and SPR kinetic measurements, while the functionality was tested via FITC staining and sulfo-SDTB assay. It was found that the plasma polymerized allylamine films used in this work provided a stable and functional base for the design of a covalent wet chemical immobilization and co-immobilization procedure.

With respect to the development of a controllable co-immobilzation procedure, the used biomolecules RGD and VEGF were first single immobilized and their effect was investigated on the cellular response of HUVECs. For the development of the co-immobilization procedure two different cross-linker molecules were used, in order to provide different coupling chemistries for a controllable and separated two-step co-immobilization procedure. Furthermore, different VEGF concentrations were used for the immobilization and/or co-immobilization. SPR kinetic measurements were conducted to investigate the covalent conjugation of the biomolecules. It could be demonstrated that the developed immobilization and co-immobilization procedures are suitable for single biomolecule conjugation as well as for a separated and controlled co-immobilization. Furthermore, the biological functionality of all immobilized biomolecules using the developed

immobilization and co-immobilization procedures could be demonstrated *in vitro* and in the case of only VEGF modified surfaces also *in vivo.*

Further work would have to include investigations to answer the question how the correlation is between concentration of the used biomolecules and the amounts of immobilized biomolecules. A closer look on the amount of immobilized biomolecules might be valuable in order to obtain more detailed information about thresholds in correlation to the biological effect. In this context, especially the development of the solid phase VEGF ELISA is regarded as crucial step to provide valuable information. Concerning the cellular response it will be necessary to investigate a higher variety of cellular parameters such as proliferation, differentiation and activation and a transfer in more animal models will be crucial to obtain more information about the biological effect *in vivo.* Furthermore, the addition of various coupling chemistries in combination with additional biomolecules such as other growth factors and cytokines will be essential to approach the future goal of the completely biocompatible, tailor-made implant for an accelerated and improved integration in the bone.

7 References

Ahrendt, G., Chickering, D. E., & Ranieri, J. P. (1998). Angiogenic growth factors: a review for tissue engineering. *Tissue Engineering*, **4(2)**, 117-130.

Alberts, B., Johnson, A., Lewis, J., Raff, M., Roberts, K., Walter, P. (2008). *Molecular Biology of the Cell*, 5th Edition, Garland Science, Taylor & Francis Group, New York, Abingdon.

Albrektsson, T., Johansson, C. (2001). Osteoinduction, osteoconduction and osseointegration. *European Spine Journal* **10(2)**, 96-101.

Albrektsson, T., Albrektsson, B. (1987). Osseointegration of bone implants. A review of an alternative mode of fixation. *Acta Orthopaedica Scandinavica* **58(5)**, 567-577.

Albrektsson, T., Brånemark, P.-I., Hansson, H. A., Kasemo, B., Larsson, K., Lundström, I., McQueen, D.H., Skalak, R. (1983). The interface zone of inorganic implants *In vivo*: Titanium implants in bone. *Annals of Biomedical Engineering* **11(1)**, 1-27.

Albrektsson, T., Brånemark, P.-I., Hansson, H. A., & Lindström, J. (1981). Osseointegrated titanium implants: Requirements for ensuring a long-lasting, direct bone-to-implant anchorage in man. *Acta Orthopaedica* **52(2)**, 155-170.

Al-Nawas, B., Brägger, U., Meijer, H. J., Naert, I., Persson, R., Perucchi, A., Perruchi, et al. (2011). A Double-Blind Randomized Controlled Trial (RCT) of Titanium-13Zirconium versus Titanium Grade IV Small-Diameter Bone Level Implants in Edentulous Mandibles–Results from a 1-Year Observation Period.*Clinical Implant Dentistry and Related Research* **14(6)**, 896-904.

Andrade, J. D. (Ed.). (1985). *Surface and Interfacial Aspects of Biomedical Polymers, Volume* 2, New York: Plenum Press.

Anselme, K., Bigerelle, M., Noel, B., Dufresne, E., Judas, D., Iost, A., & Hardouin, P. (2000). Qualitative and quantitative study of human osteoblast adhesion on materials with various surface roughnesses. *Journal of Biomedical Materials Research*, **49(2)**, 155-166.

Aota, S. I., Nagai, T., & Yamada, K. M. (1991). Characterization of regions of fibronectin besides the arginine-glycine-aspartic acid sequence required for adhesive function of the cell-binding domain using site-directed mutagenesis. *Journal of Biological Chemistry* **266(24)**, 15938-15943.

Aslam, M., Dent, A. (1998). *Bioconjugation*, Macmillan Reference LTD, London, Basingstoke.

Backer, M. V., Levashova, Z., Levenson, R., Blankenberg, F. G., & Backer, J. M. (2008). Cysteine-containing fusion tag for site-specific conjugation of therapeutic and imaging agents to targeting proteins. *Methods in Molecular Biology* **494**, 275-294.

Barksdale, J. (1966). Titanium,Its Occurrence. Chemistry, and Technology, 2nd Edition, *Ronald Press Co*., New York.

Bayer, E. A., & Wilchek, M. (1990). Application of avidin-biotin technology to affinity-based separations. *Journal of Chromatography A* **510**, 3-11.

Beck, A. J., Candan, S., Robert, D., Goodyear, A., & Braithwaite, N. S. J. (2001). The role of ions in the plasma polymerization of allylamine. *The Journal of Physical Chemistry B* **105(24)**, 5730-5736.

Beder, O. E., Eade G. (1956). An investigation of tissue tolerance to titanium metal implants in dogs. *Surgery* **39**, 470-473.

Bentz, H., Schroeder, J. A., & Estridge, T. D. (1998). Improved local delivery of TGF-β2 by binding to injectable fibrillar collagen via difunctional polyethylene glycol. *Journal of Biomedical Materials Research* **39(4)**, 539-548.

Bergström, K., Holmberg, K., Safranj, A., Hoffman, A. S., Edgell, M. J., Kozlowski, A., Hovanes, B. A., & Harris, J. M. (1992). Reduction of fibrinogen adsorption on PEG-coated polystyrene surfaces. *Journal of Biomedical Materials Research*,**26(6)**, 779-790.

Berkowitz, D. B., & Webert, D. W. (1981). The inactivation of horseradish peroxidase by a polystyrene surface. *Journal of Immunological Methods* **47(1)**, 121-124.

Bothe, R. T., Beaton, L. E., & Davenport, H. A. (1940). Reaction of bone to multiple metallic implants. *Surg Gynecol Obstet* **71**, 598-602.

Brånemark, P.I., Hansson, B.O., Adell, R., Breine, U., Lindström, J, Hallén, O., Ohman, A. (1977). Osseointegrated implants in the treatment of the edentulous jaw. Experience from a 10-year period. *Scandinavian Journal of Plastic and Reconstructive Surgery* **16**, 1-13.

Brånemark, P.I., Adell, R., Breine, U., Hansson, B.O., Lindström, J., Ohlsson, A. (1969). Intra-osseous anchorage of dental prostheses. I. Experimental studies. *Scandinavian Journal of Plastic and Reconstructive Surgery* **3(2)***,* 81-100.

Butler, J. E., Ni, L., Nessler, R., Joshi, K. S., Suter, M., Rosenberg, B., Chang, J., Brown, W. R., & Cantarero L. A. (1992). The physical and functional behavior of capture antibodies adsorbed on polystyrene. *Journal of Immunological Methods*, **150(1-2)**, 77.

Calderon, J. G., & Timmons, R. B. (1998). Surface molecular tailoring via pulsed plasma-generated acryloyl chloride polymers: Synthesis and reactivity.*Macromolecules* **31(10)**. 3216-3224.

Campbell, N.A., Reece, J.B. (2003). *Biologie*, 6 Auflage, Spektrum Akademischer Verlag, Heidelberg, Berlin, Oxford.

Candan, S., Beck, A. J., OToole, L., & Short, R. D. (1998). Effects of “processing parameters” in plasma deposition: Acrylic acid revisited. *Journal of Vacuum Science & Technology A: Vacuum, Surfaces, and Films* **16(3)**, 1702-1709.

Chen, Q., Förch, R., & Knoll, W. (2004). Characterization of pulsed plasma polymerization allylamine as an adhesion layer for DNA adsorption/hybridization. *Chemistry of Materials*, **16(4)**, 614-620.

Chiu, L. L., Weisel, R. D., Li, R. K., & Radisic, M. (2011). Defining conditions for covalent immobilization of angiogenic growth factors onto scaffolds for tissue engineering. *Journal of Tissue Engineering and Regenerative Medicine* **5(1)**, 69-84.

Chiu, L. L., & Radisic, M. (2010). Scaffolds with covalently immobilized VEGF and Angiopoietin-1 for vascularization of engineered tissues. *Biomaterials* **31(2)**, 226-241.

Chiu, H. C., Zalipsky, S., Kopeckova, P., & Kopecek, J. (1993). Enzymic activity of chymotrypsin and its poly (ethylene glycol) conjugates toward low and high molecular weight substrates. *Bioconjugate Chemistry*, **4(4)**, 290-295.

Choukourov, A., Biederman, H., Slavinska, D., Hanley, L., Grinevich, A., Boldyryeva, H., & Mackova, A. (2005). Mechanistic studies of plasma polymerization of allylamine. *The Journal of Physical Chemistry B* **109(48)**, 23086-23095.

Chu, L. Q., Knoll, W., & Förch, R. (2006). Stabilization of plasma-polymerized allylamine films by ethanol extraction. *Langmuir* **22(13)**, 5548-5551.

d'Angelo, N. (1990). Low-frequency electrostatic waves in dusty plasmas.*Planetary and Space Science* **38(9)**, 1143-1146.

DeHaven, K. E., & Lintner, D. M. (1986). Athletic injuries: comparison by age, sport, and gender. *The American Journal of Sports Medicine*, **14(3)**, 218-224.

Denhardt, D. T., & Guo, X. (1993). Osteopontin: a protein with diverse functions.*The FASEB Journal* **7(15)**, 1475-1482.

Devge, C., Tjellström, A., Nellström, H. (1997). Magnetic resonance imaging in patients with dental implants: a clinical report. *The International Journal of Oral & Maxillofacial Implants* **12(3)**, 354-359.

Diebold, U. (2003). The surface science of titanium dioxide. *Surface Science Reports* **48(5)**, 53-229.

Donachie, M.J.Jr. (1988). Titanium: A Technical Guide*. Metals Park, OH: ASM International*. 11.

Donath, K., & Breuner, G. (1982). A method for the study of undecalcified bones and teeth with attached soft tissues*. *Journal of Oral Pathology & Medicine*, **11(4)**, 318-326.

Donnelly, V. M., Malyshev, M. V., Schabel, M., Kornblit, A., Tai, W., Herman, I. P., & Fuller, N. C. M. (2002). Optical plasma emission spectroscopy of etching plasmas used in Si-based semiconductor processing. *Plasma Sources Science and Technology* **11(3A)**, A26.

Duewelhenke, N., Eysel, P. (2007). Serumfreie Kultivierung von Osteoprogenitorzellen und Osteoblasten zur Testung von Biomaterialien. *Der Ortopäde* **3**, 220-226.

Edlund, U., Sauter, T., & Albertsson, A. C. (2011). Covalent VEGF protein immobilization on resorbable polymeric surfaces. *Polymers for Advanced Technologies*, **22(1)**, 166-171.

Faria, A. C., Rodrigues, R. C., Claro, A. P., da Gloria Chiarello de Mattos, M., Ribeiro, R. F. (2011). Wear resistance of experimental titanium alloys for dental applications. *Journal of the Mechanical Behavior of Biomedical Materials* **4(8)**, 1873-1879.

Ferris, D. M., Moodie, G. D., Dimond, P. M., Giorani, C. W. D., Ehrlich, M. G., & Valentini, R. F. (1999). RGD-coated titanium implants stimulate increased bone formation in vivo. *Biomaterials*, **20(23)**, 2323-2331.

Förch, R., Chifen, A. N., Bousquet, A., Khor, H. L., Jungblut, M., Chu, L-Q., Zhang, Z., Osey-Mensah, I., Sinner, E.-K., & Knoll, W. (2007). Recent and Expected Roles of Plasma-Polymerized Films for Biomedical Applications. *Chemical Vapor Deposition* **13(6-7)**, 280-294.

Friedrich, J. (2011). Mechanisms of Plasma Polymerization–Reviewed from a Chemical Point of View. *Plasma Processes and Polymers* **8(9)**, 783-802.

Friess, W. (1998). Collagen–biomaterial for drug delivery. *European Journal of Pharmaceutics and Biopharmaceutics* **45(2)**, 113-136.

Gaur, R. K., Gupta, K. C. (1989). A Spectrophotometric Method for the Estimation of Amino Groups on Polymer Supports. *Analytical Biochemistry* **180**, 253-258.

Grad, H. (1969). Plasmas. *Physics Today* **22**, 34.

Greenhalgh, D. G. (1996). The role of growth factors in wound healing. *The Journal of Trauma and Acute Care Surgery* **41(1)**, 159-167.

Goodson, R. J., & Katre, N. V. (1990). Site-directed pegylation of recombinant interleukin-2 at its glycosylation site. *Nature Biotechnology*, **8(4)**, 343-346.

Habeeb, A. J., & Hiramoto, R. (1968). Reaction of proteins with glutaraldehyde. *Archives of Biochemistry and Biophysics* **126(1)**, 16.

Habibovic, P., Van der Valk, C. M., Van Blitterswijk, C. A., De Groot, K., & Meijer, G. (2004). Influence of octacalcium phosphate coating on osteoinductive properties of biomaterials. *Journal of Materials Science: Materials in Medicine*,**15(4)**, 373-380.

Hackel, P. O., Zwick, E., Prenzel, N., & Ullrich, A. (1999). Epidermal growth factor receptors: critical mediators of multiple receptor pathways. *Current Opinion in Cell Biology* **11(2)**, 184-189.

Hamerli, P., Weigel, T., Groth, T., & Paul, D. (2003). Surface properties of and cell adhesion onto allylamine-plasma-coated polyethylenterephtalat membranes. *Biomaterials* **24(22)**, 3989-3999.

Harvey, J., Bergdahl, A., Dadafarin, H., Ling, L., Davis, E. C., & Omanovic, S. (2012). An electrochemical method for functionalization of a 316L stainless steel surface being used as a stent in coronary surgery: irreversible immobilization of fibronectin for the enhancement of endothelial cell attachment. *Biotechnology Letters* **34(6)**, 1159-1165.

Horbett, T. A., & Brash, J. L. (1987). Proteins at interfaces: current issues and future prospects. *JL Brash and TA Horbett, Proteins at Interfaces. Physicochemical and Biochemical Studies. Washington DC: ACS Symposium Series* **343**, 1-33.

Hsieh, M. C., Farris, R. J., & McCarthy, T. J. (1997). Surface “priming” for layer-by-layer deposition: Polyelectrolyte multilayer formation on allylamine plasma-modified poly (tetrafluoroethylene). *Macromolecules* **30(26)**, 8453-8458.

Huggins, C. B. (1931). The formation of bone under the influence of epithelium of the urinary tract. *Archives of Surgery* **22(3)**, 377-408.

Huh, J.-B., Lee, J.-Y., Lee, K.-L., Kim, S.-E., Yun, M.-J, Shim, J.-S., Shim, J.-S., and Shin, S.-W. (2011). Effects of the immobilization of heparin and rhPDGF-BB to titanium surfaces for the enhancement of osteoblastic functions and anti-inflammation. *The Journal of Advanced Prosthodontics* **3(3)**, 152-160.

Hynes, R.O. (2002). Integrins: Bidirectional, Allosteric Signaling Machines. *Cell* **110**, 673-687.

Ito, Y. (2007). Covalently immobilized biosignal molecule materials for tissue engineering. *Soft Matter* **4(1)**, 46-56.

Ito, Y., Hasuda, H., Terai, H., & Kitajima, T. (2005). Culture of human umbilical vein endothelial cells on immobilized vascular endothelial growth factor. *Journal of Biomedical Materials Research Part A*, **74(4),** 659-665.

Judet, R., Siguier, M., Brumpt, B., Judet, T.(1978). A noncemented total hip prosthesis. *Clinical Orthopaedics and Related Research* **137**, 76-84.

Jung, H. J., Ahn, K. D., Han, D. K., & Ahn, D. J. (2005). Surface characteristics and fibroblast adhesion behavior of RGD-immobilized biodegradable PLLA films. *Macromolecular Research* **13(5)**, 446-452.

Kämmerer, P. W., Gabriel, M., Al-Nawas, B., Scholz, T., Kirchmaier, C. M., & Klein, M. O. (2012). Early implant healing: promotion of platelet activation and cytokine release by topographical, chemical and biomimetical titanium surface modifications in vitro. *Clinical Oral Implants Research* **23(4)**, 504-510.

Kämmerer, P. W., Heller, M., Brieger, J., Klein, M. O., Al-Nawas, B., & Gabriel, M. (2011). Immobilisation of linear and cyclic RGD-peptides on titanium surfaces and their impact on endothelial cell adhesion and proliferation. *European Cells & Materials* **21**, 364-372.

Kantlehner, M., Schaffner, P., Finsinger, D., Meyer, J., Jonczyk, A., Diefenbach, B., Nies, B., Hölzemann, G., Goodman, S. L., Kessler, H. (2000). Surface Coating with RGD Peptides Stimulates Osteoblast Adhesion and Proliferation as well as Bone Formation. *Chembiochem* **1**, 107-114.

Kasemo, B. (1983). Biocompatibility of titanium implants: surface science aspects. *The Journal of Prosthetic Dentistry* **49(6)**, 832-837.

Klajnert, B., & Bryszewska, M. (2002). Fluorescence studies on PAMAM dendrimers interactions with bovine serum albumin. *Bioelectrochemistry* **55(1)**, 33-35.

Knoll, W. (1998). Interfaces and thin films as seen by bound electromagnetic waves. *Annual Review of Physical Chemistry* **49(1)**, 569-638.

Koch, S., Yao, C., Grieb, G., Prevel, P., Noah, E. M., & Steffens, G. C. (2006). Enhancing angiogenesis in collagen matrices by covalent incorporation of VEGF. *Journal of Materials Science: Materials in Medicine* **17(8)**, 735-741.

Kodama, T. (1989). Study on biocompatibility of titanium alloys [Article in Japanese]. *Kokubyo Gakkai Zasshi The Journal of the Stomatological Society, Japan* **56(2)**, 263-288.

Krishnamurthy, V., Kamel, I. & Wei, Y. (1989). Analysis of plasma polymerization of allylamine by FTIR. *Journal of Polymer Science. Part A. Polymer Chemistry* **27**, 1211-1224.

Kuhl, P. R., & Griffith-Cima, L. G. (1996). Tethered epidermal growth factor as a paradigm for growth factor–induced stimulation from the solid phase. *Nature Medicine* **2(9)**, 1022-1027.

Laschitsch, A., Menges, B., & Johannsmann, D. (2000). Simultaneous determination of optical and acoustic thicknesses of protein layers using surface plasmon resonance spectroscopy and quartz crystal microweighing.*Applied Physics Letters* **77(14)**, 2252-2254.

Lausmaa, J., Kasemo, B. (1990). Surface spectroscopic characterization of titanium implant materials. *Applied Surface Science* **44 (2)**,133–146.

Lausmaa, J., Kasemo, B., Rolander, U., Bjursten, L. M., Ericson, L. E., Rosander, L., & Thomsen, P. (1988). Preparation, surface spectroscopic and electron microscopic characterization of titanium implant materials. *Surface Characterization of Biomaterials. Amsterdam: Elsevier*, 161-174.

Levander, G. (1938). A study of bone regeneration. *Surgery, Gynecology & Obstetrics* **67**, 705-714.

Leventhal, G. S. (1951). Titanium, a metal for surgery. *The Journal of Bone & Joint Surgery* **33A**, 473.

Lieberman, J. R., Daluiski, A., & Einhorn, T. A. (2002). The role of growth factors in the repair of bone biology and clinical applications. *The Journal of Bone & Joint Surgery* **84(6)**, 1032-1044.

Li, D., Ferguson, S. J., Beutler, T., Cochran, D. L., Sittig, C., Hirt, H. P., & Buser, D. (2002). Biomechanical comparison of the sandblasted and acid-etched and the machined and acid-etched titanium surface for dental implants.*Journal of Biomedical Materials Research*, **60(2)**, 325-332.

Lind, M. (1996). Growth factors: Possible new clinical tools: A review. *Acta Orthopaedica* **67(4)**, 407-417.

Liu, X., Chu, P. K., & Ding, C. (2004). Surface modification of titanium, titanium alloys, and related materials for biomedical applications. *Materials Science and Engineering: R: Reports* **47(3)**, 49-121.

Lotz, A., Heller, M., Brieger, J., Gabriel, M., & Förch, R. (2012). Derivatization of Plasma Polymerized Thin Films and Attachment of Biomolecules to Influence HUVEC-Cell Adhesion. *Plasma Processes and Polymers* **9(1)**, 10-16.

Maher, J. J., Friedman, S. L., Roll, F. J., & Bissell, D. M. (1988). Immunolocalization of laminin in normal rat liver and biosynthesis of laminin by hepatic lipocytes in primary culture. *Gastroenterology* **94(4)**, 1053.

Martin, J. Y., Schwartz, Z., Hummert, T. W., Schraub, D. M., Simpson, J., Lankford, J., Dean, D. D., Cochran, D. L., & Boyan, B. D. (2004). Effect of titanium surface roughness on proliferation, differentiation, and protein synthesis of human osteoblast-like cells (MG63). *Journal of Biomedical Materials Research* **29(3)**, 389-401.

Martin, S. M., Ganapathy, R., Kim, T. K., Leach-Scampavia, D., Giachelli, C. M., & Ratner, B. D. (2003). Characterization and analysis of osteopontin-immobilized poly (2-hydroxyethyl methacrylate) surfaces. *Journal of Biomedical Materials Research Part A* **67(1)**, 334-343.

Matsuno, H., Yokoyama, A., Watari, F., Uo, M., Kawasaki, T.(2001). Biocompatibility and osteogenesis of refractory metal implants, titanium, hafnium, niobium, tantalum and rhenium. *Biomaterials* **22(11)**, 1253-1262.

Means, G. E., & Feeney, R. E. (1968). Reductive alkylation of amino groups in proteins. *Biochemistry*, **7(6)**, 2192-2201.

Mustafa, K., Wroblewski, J., Lopez, B. S., Wennerberg, A., Hultenby, K., & Arvidson, K. (2008). Determining optimal surface roughness of TiO2 blasted titanium implant material for attachment, proliferation and differentiation of cells derived from human mandibular alveolar bone. *Clinical Oral Implants Research* **12(5)**, 515-525.

Nelea, V., Nakano, Y., & Kaartinen, M. T. (2008). Size distribution and molecular associations of plasma fibronectin and fibronectin crosslinked by transglutaminase 2. *The Protein Journal* **27(4)**, 223-233.

Niinomi, M. (2003). Recent research and development in titanium alloys for biomedical applications and healthcare goods. *Science and Technology of Advanced Materials* **4(5)**, 445-454.

Pedersen, J. G., Lund, B., Reimann, I. (1983). Depressive effects of acrylic cement components on bone metabolism. Isotope release and phosphatase production studied in vitro. *Acta Orthopaedica Scandinavica* **54(6)**, 796-801.

Philpott, G. W., Kulczycki Jr, A., Grass, E. H., & Parker, C. W. (1980). Selective binding and cytotoxicity of rat basophilic leukemia cells (RBL-1) with immunoglobulin E-biotin and avidin-glucose oxidase conjugates. *The Journal of Immunology* **125(3)**, 1201-1209.

Pierschbacher, M. D., Ruoslahti, E. (1984). Cell attachement activity of fibronectin can be duplicated be small synthetic fragments of the molecule. *Nature* **309**, 30-33.

Pouilleau, J., Devilliers, D., Garrido, F., Durand-Vidal, S., & Mahé, E. (1997). Structure and composition of passive titanium oxide films. *Materials Science and Engineering B* **47(3)**, 235-243.

Puleo, D. A., Nanci, A. (1999). Understanding and controlling the bone-implant interface. *Biomaterials* **20(23-24)**, 2311-2321.

Ratner, B. D., Bryant, S. B. (2004). Biomaterials: Where We Have Been and Where We Are Going. *Annual Review of Biomedical Engineering* **6**, 41-75.

Reinholt, F. P., Hultenby, K., Oldberg, A., & Heinegård, D. (1990). Osteopontin--a possible anchor of osteoclasts to bone. *Proceedings of the National Academy of Sciences* **87(12)**, 4473-4475.

Ring, P. A. (1978). Five to fourteen year interim results of uncemented total hip arthroplasty. *Clinical Orthopaedics and Related Research* **137**, 87-95

Rinsch, C. L., Chen, X., Panchalingam, V., Eberhart, R. C., Wang, J. H., & Timmons, R. B. (1996). Pulsed radio frequency plasma polymerization of allyl alcohol: Controlled deposition of surface hydroxyl groups. *Langmuir* **12(12)**, 2995-3002.

Ritter, H., Dege, U., Kubba, R. (1979). Initial experiences with a total knee prosthesis implanted without bone cement. *Archives of Orthopaedic and Trauma Surgery* **95 (1-2)**, 89-93.

Ruoslahti, E., & Pierschbacher, M. D. (1987). New perspectives in cell adhesion: RGD and integrins. *Science* **238(4826)**, 491.

Salzer, M., Knahr, K., Locke, H., Stärk, N., Matejovsky, Z., Plenk, H. Jr., Punzet, G., Zweymüller, K. (1979). A bioceramic endoprosthesis for the replacement of the proximal humerus. *Archives of Orthopaedic and Trauma Surgery* **93 (3)**, 169-184.

Schliephake, H., Scharnweber, D., Dard, M., Sewing, A., Aref, A., Roessler, S. (2005). Functionalization of dental implant surfaces using adhesion molecules. *Journal of biomedical materials research. Part B, Applied Biomaterials* **73**, 88-96.

Schiegnitz, E., Kämmerer, P. W. (2012). Systemische Erkrankungen als Risiko für die Implantattherapie Eine Übersicht. *Quintessenz* **63(2)**,191–197.

Schiller, S., Hu, J., Jenkins, A. T. A., Timmons, R. B., Sanchez-Estrada, F. S., Knoll, W., & Förch, R. (2002). Chemical structure and properties of plasma-polymerized maleic anhydride films. *Chemistry of Materials* **14(1)**, 235-242.

Shirkhanzadeh, M. (1995). Calcium phosphate coatings prepared by electrocrystallization from aqueous electrolytes. *Journal of Materials Science: Materials in Medicine* **6(2)**, 90-93.

Semlitsch, M. F., Weber, H., Streicher, R. M., Schön, R. (1992). Joint replacement components made of hot-forged and surface-treated Ti-6Al-7Nb alloy. *Biomaterials.* **13(11)**, 781-788.

Semlitsch, M., Staub, F., Weber, H. (1985). Titanium-aluminium-niobium alloy, development for biocompatible, high strength surgical implants. *Biomedizinische Technik. Biomedical Engineering* **30(12)**, 334-339.

Shen, Y. H., Shoichet, M. S., & Radisic, M. (2008). Vascular endothelial growth factor immobilized in collagen scaffold promotes penetration and proliferation of endothelial cells. *Acta Biomaterialia* **4(3)**, 477-489.

Shen, G., Anand, M. F. G., & Levicky, R. (2004). X-ray photoelectron spectroscopy and infrared spectroscopy study of maleimide-activated supports for immobilization of oligodeoxyribonucleotides. *Nucleic Acids Research*, **32(20)**, 5973-5980.

Shi, Q., Zhou, Y., & Sun, Y. (2008). Influence of pH and Ionic Strength on the Steric Mass-Action Model Parameters around the Isoelectric Point of Protein. *Biotechnology Progress*, **21(2)**, 516-523.

Shoulders, M. D., & Raines, R. T. (2009). Collagen structure and stability.*Annual review of biochemistry* **78**, 929.

Sundgren, J. E., Bodö, P., & Lundström, I. (1986). Auger electron spectroscopic studies of the interface between human tissue and implants of titanium and stainless steel. *Journal of Colloid and Interface Science* **110(1)**, 9-20.

Takada, Y., Ye, X., Simon, S. (2007). The Integrins. *Genom Biology* **8**, 215.

Taguchi, T., Kishida, A., Akashi, M., & Maruyama, I. (2000). Immobilization of human vascular endothelial growth factor (VEGF165) onto biomaterials: an evaluation of the biological activity of immobilized VEGF165. *Journal of Bioactive and Compatible Polymers* **15(4)**, 309-320.

Timpl, R., & Brown, J. C. (1994). The laminins. *Matrix Biology*, **14(4)**, 275-281.

Trippel, S. B., Coutts, R. D., Einhorn, T. A., Mundy, G. R., & Rosenfeld, R. G. (1996). Instructional Course Lectures, The American Academy of Orthopaedic Surgeons-Growth Factors as Therapeutic Agents*†. *The Journal of Bone & Joint Surgery* **78(8)**, 1272-86.

Urist, M. R,. & McLean, E, C, (1952). Osteogenic potency and new bone formation by induction in transplants to the anterior chamber of the eye. *The Journal of Bone & Joint surgery* **34(2)**. 443-470.

Van Noort, R. (1987). Titanium: the implant material of today. *Journal of Material Science* **22**, 3801-3811.

Vörös, J. (2004). The density and refractive index of adsorbing protein layers.*Biophysical Journal*, **87(1)**, 553-561.

Vukicevich, S., Luyten, F.P., Kleinman, H.K., Reddi, A.H. (1990). Differentiation of canalicular cell processes in bone cells by basement membrane matrix components: regulation by discrete domains of laminin. *Cell* **63**, 437-445.

Wang, Y., Ke, Y., Ren, L., Wu, G., Chen, X., & Zhao, Q. (2008). Surface engineering of PHBV by covalent collagen immobilization to improve cell compatibility. *Journal of Biomedical Materials Research Part A* **88(3)**, 616-627.

Wang, P., Tan, K. L., Kang, E. T., & Neoh, K. G. (2001). Synthesis, characterization and anti-fouling properties of poly (ethylene glycol) grafted poly (vinylidene fluoride) copolymer membranes. *Journal of Materials Chemistry* **11(3)**, 783-789.

Waterfield, M. D. (1989). Growth factor receptors. *British Medical Bulletin* **45(2)**, 541-553.

Wilson-Hench, J. (1987). Osteoinduction. *Progress in Biomedical Engineering: Definitions in Biomaterials (Williams D, ed), Elsevier, Amsterdam*. 29.

Wissink, M. J. B., Beernink, R., Poot, A. A., Engbers, G. H. M., Beugeling, T., Van Aken, W. G., & Feijen, J. (2000). Improved endothelialization of vascular grafts by local release of growth factor from heparinized collagen matrices. *Journal of Controlled Release* **64(1)**, 103-114.

Wu, Y. J., Timmons, R. B., Jen, J. S., & Molock, F. E. (2000). Non-fouling surfaces produced by gas phase pulsed plasma polymerization of an ultra low molecular weight ethylene oxide containing monomer. *Colloids and Surfaces B: Biointerfaces* **18(3)**, 235-248.

Xu, F. J., Wang, Z. H., & Yang, W. T. (2010). Surface functionalization of polycaprolactone films via surface-initiated atom transfer radical polymerization for covalently coupling cell-adhesive biomolecules. *Biomaterials* **31(12)**, 3139-3147.

Yancopoulos, G. D., Davis, S., Gale, N. W., Rudge, J. S., Wiegand, S. J., & Holash, J. (2000). Vascular-specific growth factors and blood vessel formation. *Nature* **407**, 242-248.

Yang, Z., Wang, J., Luo, R., Maitz, M. F., Jing, F., Sun, H., & Huang, N. (2010). The covalent immobilization of heparin to pulsed-plasma polymeric allylamine films on 316L stainless steel and the resulting effects on hemocompatibility.*Biomaterials* **31(8)**, 2072-2083.

Yang, Z., Wang, X., Wang, J., Yao, Y., Sun, H., & Huang, N. (2009). Pulsed-Plasma Polymeric Allylamine Thin Films. *Plasma Processes and Polymers*,**6(8**), 498-505.

Yasuda, H. (1985). *Plasma polymerization*. Academic Press.

Yasuda, H., & Hirotsu, T. (1977). Some aspects of plasma copolymerization of acetylene with N2 and/or water. *Journal of Polymer Science: Polymer Chemistry Edition* **15(11)**, 2749-2771.

Yoshida, E., Yoshimura, Y., Uo, M., Yoshinari, M., & Hayakawa, T. (2012). Influence of nanometer smoothness and fibronectin immobilization of titanium surface on MC3T3-E1 cell behavior. *Journal of Biomedical Materials Research* **100A(6)**, 1556-1564.

Zhang, Z., Knoll, W., Förch, R., Holcomb, R., & Roitman, D. (2005). DNA hybridization on plasma-polymerized allylamine. *Macromolecules* **38(4)**, 1271-1276.

Zhang, Z., Chen, Q., Knoll, W., Foerch, R., Holcomb, R., & Roitman, D. (2003). Plasma polymer film structure and DNA probe immobilization. *Macromolecules* **36(20)**, 7689-7694.

Zhang, Z., Chen, Q., Knoll, W., & Förch, R. (2003). Effect of aqueous solution on functional plasma polymerized films. *Surface and Coatings Technology* **174**, 588-590.

Zdolsek J., Eaton J. W., Tang, L. (2007). Histamine release and fibrinogen adsorption mediate acute inflammatory responses to biomaterial implants in humans. *Journal of Translational Medicine* **5**, 31.

Ziebart, T., Schnell, A., Walter, C., Kämmerer, P. W., Pabst, A., Lehmann, K. M., Ziebart, J., Klein, M. O., & Al-Nawas, B. (2012). Interactions between endothelial progenitor cells (EPC) and titanium implant surfaces. *Clinical Oral investigations*, 1-9.

Ziebart, T., Yoon, C. H., Trepels, T., Wietelmann, A., Braun, T., Kiessling, F., Stein, S., Grez, M., Ihling, C., Muhly-Reinholz, M., Carmona, G., Urbich, C., Zeiher, A. M., & Dimmeler, S. (2008). Sustained persistence of transplanted proangiogenic cells contributes to neovascularization and cardiac function after ischemia.*Circulation Research* **103(11)**, 1327-1334.

8 Annex

8.1 Original Data Sets

8.1.1 Contact Angle Measurements of Titanium

Table 8.1 Contact angle measurements on differently treated titanium surfaces. Data is based on 3 independent experiments. 3-fold measurements of 3 different titanium batches were performed.

Surface Treatment	**Mean**	**SD**
Acid etched	57	4,7
Acid etched+oxidized	24	4,5

8.1.2 Density of Primary Amines (Sulfo-SDTB)

Table 8.2 Sulfo- SDTB measurements were performed in triplicate of 20-30 nm thick pp-AA films and reproduced 3 times.

Density of primary amines of pp-AA 40 W 0,1 mbar before PBS incubation		**Density of primary amines of pp-AA 40 W 0,1 mbar after 1 hour of PBS incubation**	
Mean	SD	Mean	SD
16,53	5,5	8	2,33
Density of primary amines of pp-AA 60 W 0,1 mbar before PBS incubation		**Density of primary amines of pp-AA 60 W 0,1 mbar after 1 hour of PBS incubation**	
Mean	SD	Mean	SD
13,83	4,96	6,27	1,38
Density of primary amines of pp-AA 80 W 0,1 mbar before PBS incubation		**Density of primary amines of pp-AA 80 W 0,1 mbar after 1 hour of PBS incubation**	
Mean	SD	Mean	SD
8,97	1,78	7,53	2,35
Density of primary amines of pp-AA 100 W 0,1 mbar before PBS incubation		**Density of primary amines of pp-AA 100 W 0,1 mbar after 1 hour of PBS incubation**	
Mean	SD	Mean	SD
8,07	2,203	5,97	1,56

8.1.3 Loss of Thickness of Different pp-AA Films after PBS Incubation

Table 8.3 Loss of thickness of pp-AA films in PBS was determined in 3 independent experiments via step profiler. One silicon wafer for each plasma polymerization parameter was analyzed on 3 different points of interest before and after 1 hour of PBS incubation.

pp-AA 40 W 0,1 mbar after 5 min Deposition before PBS incubation in nm			**pp-AA 40 W 0,1 mbar after 5 min Deposition after 1 hour PBS incubation in nm**		
Mean	SD	Deposition Rate in nm/min	Mean	SD	Loss of Thickness in %
75,3	6,4	≈ 15	25,7	4,1	67 %
pp-AA 60 W 0,1 mbar after 5 min Deposition before PBS incubation in nm			**pp-AA 60 W 0,1 mbar after 5 min Deposition after 1 hour PBS incubation in nm**		
Mean	SD	Deposition Rate in nm/min	Mean	SD	Loss of Thickness in %
87,9	4,5	≈ 17	43,4	12,4	49 %
pp-AA 80 W 0,1 mbar after 5 min Deposition before PBS incubation in nm			**pp-AA 80 W 0,1 mbar after 5 min Deposition after 1 hour PBS incubation in nm**		
Mean	SD	Deposition Rate in nm/min	Mean	SD	Loss of Thickness in %
135,2	12,2	≈ 27	91,6	13,1	32 %
pp-AA 100 W 0,1 mbar after 5 min Deposition before PBS incubation in nm			**pp-AA 100 W 0,1 mbar after 5 min Deposition after 1 hour PBS incubation in nm**		
Mean	SD	Deposition Rate in nm/min	Mean	SD	Loss of Thickness in %
165,6	17,4	≈ 33	114,1	23,2	32 %

8.1.4 Contact Angle Measurements of the Surface Modification Steps

Table 8.4 Data of the contact angle measurements is based on 3 independent experiments. 3-fold measurements of each surface were performed.

Surface	Mean [θ/°]	SD
pp-AA	55	3,9
Di-NHS Linker	36	4
Mal-NHS Linker	23	10,2
Di-NHS/Mal-NHS Linker	29	3,5
RGD	51	5,6
VEGF	50	4,2
RGD/VEGF	54	5,2

8.1.5 Solid Phase VEGF ELISA

Table 8.5 Standard measurement of antibody-coated titanium for the solid phase ELISA.

Amount of VEGF in µg/ml	Optical Density			Mean	SD
0,05	0,321	0,353	0,352	0,342	0,01819341
0,1	0,559	0,696	0,657	0,63733333	0,07058565
0,2	0,835	0,786	0,842	0,821	0,03051229
0,5	0,83	0,978	0,99	0,93266667	0,08911416
1	0,98	1,054	0,87	1,017	0,0925851
5	1,343	1,326	1,463	1,3345	0,07467485
10	1,334	1,393	1,411	1,37933333	0,0402782
20	1,404	1,397	1,434	1,41166667	0,01965536

Table 8.6 Original data sets of 3 independent solid phase ELISA experiments.

1)

Surfaces	Optical Density			Mean	SD
Titanium	0,012	0,035	0,011	0,01933333	0,01357694
VEGF	0,15	0,199	0,184	0,17766667	0,02510644
RGD/VEGF	0,067	0,094	0,057	0,07266667	0,01913984

2)

Surfaces	Optical Density			Mean	SD
Titanium	0,008	0,007	0,007	0,00733333	0,00057735
VEGF	0,017	0,011	0,02	0,016	0,00458258
RGD/VEGF	0,01	0,007	0,009	0,00866667	0,00152753

3)

Surfaces	Optical Density			Mean	SD
Titanium	0,014	0,026	0,014	0,018	0,006928203
VEGF	0,155	0,207	0,236	0,19933333	0,04104063
RGD/VEGF	0,098	0,133	0,083	0,10466667	0,025658007

8.1.6 Cell Coverage of HUVECs on RGD Modified Titanium

Cell coverage calculations are based on 3 representative pictures of each surface. For the statistical analyses of the cell experiments a one-way analysis of variance (ANOVA) with Bonferroni´s multiple comparison test was carried out to compare the groups of titanium, pp-AA and RGD modified surfaces (* for p<0,05 is significant, ** for p<0,01 is highly significant, *** for p<0,001 is extremely significant).

Table 8.7 Cell coverage of HUVECs on RGD modified samples after 24 hours, 3 days and 7 days.

24 hours Cultivation					
Surface	**Cell Coverage in %**			**Mean**	**SD**
Titanium	3,96	6,2	3,8	4,65	1,3418395
pp-AA	16,64	16,4	14,1	15,71	1,4023313
RGD	4,2	8,9	3,94	5,68	2,7916303
3 days Cultivation					
Surface	**Cell Coverage in %**			**Mean**	**SD**
Titanium	10,3	6,2	7,2	7,9	2,1377558
pp-AA	5,4	4,8	7,8	6	1,5874507
RGD	4,1	2,1	4,3	3,5	1,2165525
7 days Cultivation					
Surface	**Cell Coverage in %**			**Mean**	**SD**
Titanium	11,7	14,1	13,3	13,03	1,2220201
pp-AA	18,4	24,8	27	23,4	4,4676615
RGD	18,8	34,2	32,4	28,47	8,4198178

Table 8.8 Statistical analysis of the cell coverage of HUVECs on RGD modified titanium after 24 hours.

Parameter	Value
One-way analysis of variance	
P value	0,0008
P value summary	**
Bonferroni's Multiple Comparison Test	**P value**
titanium vs pp-AA	P < 0,01
titanium vs RGD	P > 0,05
pp-AA vs RGD	P < 0,01

Table 8.9 Statistical analysis of the cell coverage of HUVECs on RGD modified titanium after 3 days.

Parameter	Value
One-way analysis of variance	
P value	0,0505
P value summary	
Bonferroni's Multiple Comparison Test	**P value**
Titanium vs pp-AA	P > 0,05
Titanium vs RGD	P > 0,05
pp-AA vs RGD	P > 0,05

Table 8.10 Statistical analysis of the cell coverage of HUVECs on RGD modified titanium after 7 days.

Parameter	Value
One-way analysis of variance	
P value	0,0367
P value summary	*
Bonferroni's Multiple Comparison Test	**P value**
titanium vs pp-AA	P > 0,05
titanium vs RGD	P < 0,05
pp-AA vs RGD	P > 0,05

8.1.7 Cell Coverage of HUVECs in Different VEGF Concentrations

Cell coverage calculations are based on 3 representative pictures of each surface. For the statistical analyses of the cell experiments a one-way analysis of variance (ANOVA) with Bonferroni´s multiple comparison test was carried out to compare the groups of the VEGF concentrations 1, 10, 20, 50 and 100 ng/ml supplement-free cell medium (* for p<0,05 is significant, ** for p<0,01 is highly significant, *** for p<0,001 is extremely significant).

Table 8.11 Cell coverage of HUVECs in different VEGF concentrations after 24 hours and 3 days.

24 hours Cultivation					
Amount of VEGF in ng/ml	**Cell Coverage in %**			**Mean**	**SD**
1	10,5	11,9	6,8	9,73	2,635020
10	12,16	20,2	21,3	17,89	4,989843
20	20,24	17,14	22,4	19,93	2,643961
50	17,96	21,1	21,49	20,18	1,935312
100	26,94	30,1	36,8	31,28	5,0347989
3 days Cultivation					
Amount of VEGF in ng/ml	**Cell Coverage in %**			**Mean**	**SD**
1	2,4	2	2,5	2,3	0,264575
10	1,3	0,9	3,7	1,97	1,514375
20	7,5	4,5	5,1	5,7	1,587450
50	5,1	3,7	3,8	4,2	0,781024
100	7,05	7,2	5,93	6,73	0,693998

Table 8.12 Statistical analysis of the effect of different VEGF concentrations on HUVECs after 24 hours.

Parameter	Value
One-way analysis of variance	
P value	0,0006
P value summary	
Bonferroni's Multiple Comparison Test	**P value**
1ng vs 10ng	P > 0,05
1ng vs 20ng	P > 0,05
1ng vs 50ng	P > 0,05
1ng vs 100ng	P < 0,001
10ng vs 20ng	P > 0,05
10ng vs 50ng	P > 0,05
10ng vs 100ng	P < 0,05
20ng vs 50ng	P > 0,05
20ng vs 100ng	P < 0,05
50ng vs 100ng	P < 0,05

Table 8.13 Statistical analysis of the effect of different VEGF concentrations on HUVECs after 3 days.

Parameter	Value
One-way analysis of variance	
P value	0,0012
P value summary	
Bonferroni's Multiple Comparison Test	**P value**
1ng vs 10ng	P > 0,05
1ng vs 20ng	P < 0,05
1ng vs 50ng	P > 0,05
1ng vs 100ng	P < 0,01
10ng vs 20ng	P < 0,05
10ng vs 50ng	P > 0,05
10ng vs 100ng	P < 0,01
20ng vs 50ng	P > 0,05
20ng vs 100ng	P > 0,05
50ng vs 100ng	P > 0,05

8.1.8 Cell Coverage of HUVECs on VEGF Modified Titanium

Cell coverage calculations are based on 3 representative pictures of each surface. For the statistical analyses of the cell experiments a one-way analysis of variance (ANOVA) with Bonferroni´s multiple comparison test was carried out to compare the groups of titanium, pp-AA and different VEGF modified surfaces using VEGF concentrations of 1 µg/ml, 10 µg/ml, 20 µg/ml for the immobilization (* for p<0,05 is significant, ** for p<0,01 is highly significant, *** for p<0,001 is extremely significant).

Table 8.14 Cell coverage of HUVECs on VEGF modified titanium after 24 hours and 3 days.

24 hours Cultivation					
Surface	**Cell Coverage in %**			**Mean**	**SD**
Titanium	6,5	8,6	7,1	7,4	1,0816653
pp-AA	15,9	18,2	13,9	16	2,1517434
VEGF (1 µg/ml)	3,8	5,3	7,3	5,47	1,7559422
VEGF (10 µg/ml)	9,4	9,9	7,7	9	1,1532562
VEGF (20 µg/ml)	24,6	39,6	32,6	32,27	7,5055535
3 days Cultivation					
Surface	**Cell Coverage in %**			**Mean**	**SD**
Titanium	7,7	8,7	8,3	8,23	0,5033223
pp-AA	3,5	4,5	7,9	5,3	2,3065125
VEGF (1 µg/ml)	4,2	3,4	3,5	3,7	0,4358898
VEGF (10 µg/ml)	5,2	6,4	6,7	6,1	0,7937253
VEGF (20 µg/ml)	34,3	28,1	24,1	28,83	5,1393903

Table 8.15 Statistical analysis of the cell coverage of HUVECs on VEGF modified titanium after 24 hours.

Parameter	Value
One-way analysis of variance	
P value	P<0,0001
Bonferroni's Multiple Comparison Test	**P value**
titanium vs pp-AA	P > 0,05
titanium vs VEGF 1 µg/ml	P > 0,05
titanium vs VEGF 10 µg/ml	P > 0,05
titanium vs VEGF 20 µg/ml	P < 0,001
pp-AA vs VEGF 1 µg/ml	P > 0,05
pp-AA vs VEGF 10 µg/ml	P > 0,05
pp-AA vs VEGF 20 µg/ml	P < 0,01
VEGF 1 µg/ml vs VEGF 10 µg/ml	P > 0,05
VEGF 1 µg/ml vs VEGF 20 µg/ml	P < 0,001
VEGF 10 µg/ml vs VEGF 20 µg/ml	P < 0,001

Table 8.16 Statistical analysis of the cell coverage of HUVECs on VEGF modified titanium after 3 days.

Parameter	Value
One-way analysis of variance	
P value	P<0,0001
Bonferroni's Multiple Comparison Test	**P value**
titanium vs pp-AA	P > 0,05
titanium vs VEGF 1 µg/ml	P > 0,05
titanium vs VEGF 10 µg/ml	P > 0,05
titanium vs VEGF 20 µg/ml	P < 0,001
pp-AA vs VEGF 1 µg/ml	P > 0,05
pp-AA vs VEGF 10 µg/ml	P > 0,05
pp-AA vs VEGF 20 µg/ml	P < 0,001
VEGF 1 µg/ml vs VEGF 10 µg/ml	P > 0,05
VEGF 1 µg/ml vs VEGF 20 µg/ml	P < 0,001
VEGF 10 µg/ml vs VEGF 20 µg/ml	P < 0,001

8.1.9 Cell Coverage of HUVECs on RGD/VEGF Modified Titanium

Cell coverage calculations are based on 3 representative pictures of each surface. For the statistical analyses of the cell experiments a one-way analysis of variance (ANOVA) with Bonferroni´s multiple comparison test was carried out to compare the groups of titanium, pp-AA and different RGD/VEGF modified surfaces using VEGF concentrations of 1 µg/ml, 10 µg/ml, 20 µg/ml for the immobilization (* for p<0,05 is significant, ** for p<0,01 is highly significant, *** for p<0,001 is extremely significant).

Table 8.17 Cell coverage of HUVECs on RGD/VEGF modified titanium after 24 hours and 3 days.

24 hours Cultivation					
Surface	**Cell Coverage in %**			**Mean**	**SD**
Titanium	7,3	7,6	7,1	7,33	0,2516611
pp-AA	16,6	18,8	17,9	17,77	1,106044
RGD/VEGF (1 µg/ml)	12	11,2	8,1	10,43	2,0599352
RGD/VEGF (10 µg/ml)	7,7	6,1	9	7,6	1,4525839
RGD/VEGF (20 µg/ml)	12,04	15,2	12,48	13,24	1,7116074
3 days Cultivation					
Surface	**Cell Coverage in %**			**Mean**	**SD**
Titanium	7,7	3,5	7,94	6,38	2,4970382
pp-AA	5,4	7,7	4,9	6	1,4933185
RGD/VEGF (1 µg/ml)	3,16	9,9	6,1	6,39	3,3791320
RGD/VEGF (10 µg/ml)	3,2	6,1	5,6	4,97	1,5502687
RGD/VEGF (20 µg/ml)	11,48	15,6	20,34	15,81	4,433614

Table 8.18 Statistical analysis of the cell coverage of HUVECs on RGD/VEGF modified titanium after 24 hours.

Parameter	Value
One-way analysis of variance	
P value	P<0,0001
Bonferroni's Multiple Comparison Test	**P value**
titanium vs pp-AA	P < 0,001
titanium vs RGD/VEGF 1 µg/ml	P > 0,05
titanium vs RGD/VEGF 10 µg/ml	P > 0,05
titanium vs RGD/VEGF 20 µg/ml	P < 0,01
pp-AA vs RGD/VEGF 1 µg/ml	P < 0,01
pp-AA vs RGD/VEGF 10 µg/ml	P < 0,001
pp-AA vs RGD/VEGF 20 µg/ml	P < 0,05
RGD/VEGF 1 µg/ml vs RGD/VEGF 10 µg/ml	P > 0,05
RGD/VEGF 1 µg/ml vs RGD/VEGF 20 µg/ml	P > 0,05
RGD/VEGF 10 µg/ml vs RGD/VEGF 20 µg/ml	P < 0,01

Table 8.19 Statistical analysis of the cell coverage of HUVECs on RGD/VEGF modified titanium after 3 days.

Parameter	Value
One-way analysis of variance	
P value	0,0056
Bonferroni's Multiple Comparison Test	**P value**
titanium vs pp-AA	P > 0,05
titanium vs RGD/VEGF 1 µg/ml	P > 0,05
titanium vs RGD/VEGF 10 µg/ml	P > 0,05
titanium vs RGD/VEGF 20 µg/ml	P < 0,05
pp-AA vs RGD/VEGF 1 µg/ml	P > 0,05
pp-AA vs RGD/VEGF 10 µg/ml	P > 0,05
pp-AA vs RGD/VEGF 20 µg/ml	P < 0,05
RGD/VEGF 1 µg/ml vs RGD/VEGF 10 µg/ml	P > 0,05
RGD/VEGF 1 µg/ml vs RGD/VEGF 20 µg/ml	P < 0,05
RGD/VEGF 10 µg/ml vs RGD/VEGF 20 µg/ml	P < 0,05

8.1.10 VEGF Receptor ELISA

Table 8.20 Representative standard measurement of phosphorylated VEGF receptor.

Amount of phosphorylated VEGF-Receptor in pg	Optical Density			Mean	SD
8000	0,794	0,592	0,619	0,67	0,10966464
4000	0,683	0,622	0,544	0,62	0,06967305
2000	0,384	0,502	0,7	0,53	0,15967884
1000	0,475	0,491	0,382	0,45	0,05885859
250	0,391	0,332	0,439	0,39	0,05359415

Table 8.21 Result of a representative VEGF-receptor ELISA of HUVECs on differently modified titanium.

Surface	Optical Density			Mean	SD
Titanium	0,271	0,252	0,275	0,27	0,01228821
RGD	0,482	0,197	0,24	0,31	0,15364353
VEGF	0,272	0,184	0,288	0,25	0,056
RGD/VEGF	0,19	0,267	0,28	0,25	0,04864497

8.1.11 Cell Coverage of HUVECs on ECM Protein Modified Titanium

Cell coverage calculations are based on 3 representative pictures of each surface. For the statistical analyses of the cell experiments a one-way analysis of variance (ANOVA) with Bonferroni´s multiple comparison test was carried out to compare the groups of titanium and modified titanium with fibronectin, collagen, laminin and osteopontin (* for $p<0,05$ is significant, ** for $p<0,01$ is highly significant, *** for $p<0,001$ is extremely significant).

Table 8.22 Cell coverage of HUVECs on ECM protein modified titanium after 24 hours, 3 days and 7 days.

24 hours Cultivation					
Surface	**Cell Coverage in %**			**Mean**	**SD**
Titanium	1,9	3,5	6,7	4,03	2,4440403
Fibronectin	35,3	43,7	54,7	44,57	9,7289944
Collagen	32,8	55,1	56,4	48,1	13,266122
Laminin	0,8	0,9	0,8	0,83	0,0577350
Osteopontin	13	11,4	19,8	14,73	4,4601943
3 days Cultivation					
Surface	**Cell Coverage in %**			**Mean**	**SD**
Titanium	12,1	7	7,4	8,83	2,8360771
Fibronectin	26	59,5	34,1	39,87	17,478653
Collagen	36,1	31,2	38,3	35,2	3,6345563
Laminin	0,3	0,1	1	0,47	0,4725815
Osteopontin	4,4	6,4	10,2	7	2,946183
7 days Cultivation					
Surface	**Cell Coverage in %**			**Mean**	**SD**
Titanium	9,5	13,6	13,3	12,13	2,2854613
Fibronectin	32,3	33,2	23,3	29,6	5,4744862
Collagen	43,8	41,7	41,6	42,37	1,2423096
Laminin	0,1	0,1	0,2	0,13	0,0577350
Osteopontin	6,2	3,3	2,8	4,1	1,8357559

Table 8.23 Statistical analysis of the cell coverage of HUVECs on ECM protein modified titanium after 24 hours.

Parameter	Value
One-way analysis of variance	
P value	P<0,0001
Bonferroni's Multiple Comparison Test	**P value**
titanium vs fibronectin	P < 0,001
titanium vs collagen	P < 0,001
titanium vs laminin	P > 0,05
titanium vs osteopontin	P > 0,05
fibronectin vs collagen	P > 0,05
fibronectin vs laminin	P < 0,001
fibronectin vs osteopontin	P < 0,01
collagen vs laminin	P < 0,001
collagen vs osteopontin	P < 0,01
laminin vs osteopontin	P > 0,05

Table 8.24 Statistical analysis of the cell coverage of HUVECs on ECM protein modified titanium after 3 days.

Parameter	Value
One-way analysis of variance	
P value	0,0004
Bonferroni's Multiple Comparison Test	**P value**
titanium vs fibronectin	P < 0,01
titanium vs collagen	P < 0,05
titanium vs laminin	P > 0,05
titanium vs osteopontin	P > 0,05
fibronectin vs collagen	P > 0,05
fibronectin vs laminin	P < 0,01
fibronectin vs osteopontin	P < 0,01
collagen vs laminin	P < 0,01
collagen vs osteopontin	P < 0,05
laminin vs osteopontin	P > 0,05

Table 8.25 Statistical analysis of the cell coverage of HUVECs on ECM protein modified titanium after 7 days.

Parameter	Value
One-way analysis of variance	
P value	P<0,0001
Bonferroni's Multiple Comparison Test	**P value**
titanium vs fibronectin	P < 0,001
titanium vs collagen	P < 0,001
titanium vs laminin	P < 0,01
titanium vs osteopontin	P > 0,05
fibronectin vs collagen	P < 0,01
fibronectin vs laminin	P < 0,001
fibronectin vs osteopontin	P < 0,001
collagen vs laminin	P < 0,001
collagen vs osteopontin	P < 0,001
laminin vs osteopontin	P > 0,05

8.1.12 Cell Coverage of HOBs on ECM Protein Modified Titanium

Cell coverage calculations are based on 3 representative pictures of each surface. For the statistical analyses of the cell experiments a one-way analysis of variance (ANOVA) with Bonferroni´s multiple comparison test was carried out to compare the groups of titanium and modified titanium with fibronectin, collagen, laminin and osteopontin (* for p<0,05 is significant, ** for p<0,01 is highly significant, *** for p<0,001 is extremely significant).

Table 8.26 Cell coverage of HOBs on ECM protein modified titanium after 24 hours, 3 days and 7 days.

24 hours Cultivation					
Surface	**Cell Coverage in %**			**Mean**	**SD**
Titanium	10,2	7,2	8,2	8,53	1,5275252
Fibronectin	35,5	42,2	37,8	38,5	3,4044089
Collagen	72,9	70,7	54,8	66,13	9,8764029
Laminin	20,9	52	48,2	40,37	16,965357
Osteopontin	57,1	89,9	53,8	66,93	19,958039
3 days Cultivation					
Surface	**Cell Coverage in %**			**Mean**	**SD**
Titanium	23,4	38,7	38,2	33,43	8,6927173
Fibronectin	59,9	71,7	69,7	67,1	6,3150614
Collagen	85,6	73,3	88,8	82,57	8,1831127
Laminin	71,9	72,5	69	71,13	1,8717194
Osteopontin	65,5	83,3	80,2	76,33	9,5091184
7 days Cultivation					
Surface	**Cell Coverage in %**			**Mean**	**SD**
Titanium	25,1	38,2	33,6	32,3	6,6460515
Fibronectin	65,7	90,7	71,5	75,97	13,084851
Collagen	88,6	89,5	93,8	90,63	2,7790886
Laminin	91,5	91,4	76,7	86,53	8,5160633
Osteopontin	62,9	70,3	81,4	71,53	9,3114625

Table 8.27 Statistical analysis of the cell coverage of HOBs on ECM protein modified titanium after 24 hours.

Parameter	Value
One-way analysis of variance	
P value	0,0011
Bonferroni's Multiple Comparison Test	**P value**
titanium vs fibronectin	P > 0,05
titanium vs collagen	P < 0,01
titanium vs laminin	P > 0,05
titanium vs osteopontin	P < 0,01
fibronectin vs collagen	P > 0,05
fibronectin vs laminin	P > 0,05
fibronectin vs osteopontin	P > 0,05
collagen vs laminin	P > 0,05
collagen vs osteopontin	P > 0,05
laminin vs osteopontin	P > 0,05

Table 8.28 Statistical analysis of the cell coverage of HOBs on ECM protein modified titanium after 3 days.

Parameter	Value
One-way analysis of variance	
P value	P<0,0001
Bonferroni's Multiple Comparison Test	**P value**
titanium vs fibronectin	P < 0,01
titanium vs collagen	P < 0,001
titanium vs laminin	P < 0,01
titanium vs osteopontin	P < 0,001
fibronectin vs collagen	P > 0,05
fibronectin vs laminin	P > 0,05
fibronectin vs osteopontin	P > 0,05
collagen vs laminin	P > 0,05
collagen vs osteopontin	P > 0,05
laminin vs osteopontin	P > 0,05

Table 8.29 Statistical analysis of the cell coverage of HOBs on ECM protein modified titanium after 7 days.

Parameter	Value
One-way analysis of variance	
P value	P<0,0001
Bonferroni's Multiple Comparison Test	**P value**
titanium vs fibronectin	P < 0,01
titanium vs collagen	P < 0,001
titanium vs laminin	P < 0,001
titanium vs osteopontin	P < 0,01
fibronectin vs collagen	P > 0,05
fibronectin vs laminin	P > 0,05
fibronectin vs osteopontin	P > 0,05
collagen vs laminin	P > 0,05
collagen vs osteopontin	P > 0,05
laminin vs osteopontin	P > 0,05

Acknowledgement

Wurde für die Online-Version entfernt.

Curriculum Vitae

Wurde für die Online-Version entfernt.

Wurde für die Online-Version entfernt.

Wurde für die Online-Version entfernt.

Declaration of the Authorship

I hereby declare that I wrote the dissertation submitted without any unauthorized external assistance and used only sources acknowledged in the work. All textual passages which are appropriated verbatim or paraphrased from published and unpublished texts as well as all information obtained from oral sources are duly indicated and listed in accordance with bibliographical rules. In carrying out this research, I complied with the rules of standard scientific practice as formulated in the statutes of Johannes Gutenberg-University Mainz to insure standard scientific practice.

Mainz, den 16.04.2013

Dipl. Biol. Martin Heller

Declaration

Here I declare that the scientific thesis I am handling in has not yet been published at any other German University, or any university abroad, or any comparable institution, with the aim of attaining a scientific degree.

Here I also declare that I have not yet finished any other doctoral PhD or any similar graduation program in any of the subjects represented by the MPGC-JOGU without success.

Mainz, den 16.04.2013

Dipl. Biol. Martin Heller